Characterization of the Essential Role of the *miR-200* family of microRNAs in Mucociliogenesis

by

Jennifer Lauren Cisson

A dissertation submitted in partial satisfaction of the

requirements for the degree of

Doctor of Philosophy

in

Molecular and Cell Biology

in the

Graduate Division

of the

University of California, Berkeley

Committee in charge:
Professor Lin He, Chair
Professor Astar Winoto
Professor Kunxin Luo
Professor Gertrude Buehring
Spring 2016

Abstract

Characterization of the Essential Role of the *miR-200* family of microRNAs in Mucociliogenesis

by

Jennifer Lauren Cisson

Doctor of Philosophy in Molecular and Cell Biology

University of California, Berkeley

Professor Lin He, Chair

MicroRNAs are small, noncoding RNAs that play essential roles in regulation of a variety of processes including development, cellular feedback mechanisms, and reproductive biology. The studies that follow focus on a particularly pleiotropic set of miRNAs: the *miR-200* family. For example, the *miR-200* family is known to be crucial for differentiation and maintenance of specialized epithelial cell types, which corresponds to its role in regulation of Epithelial-Mesenchymal Transition (EMT).[1–4] *miR-200* consists of five homologous members, divided between two distinct genomic loci and can be further segregated into two subfamilies based on seed sequence homology: *miR-200a/141* and *miR-200b/200c/429*. In an effort to discern the importance of the *miR-200* family of miRNAs, we acquired and intercrossed *mir-200b/a/429* ("200ab") and *mir-200c/141* ("200c") heterozygotes to breed single and double knockout mice (a generous gift from the Bradley Lab at the Sanger Institute).[5] I discovered a striking postnatal lethality in *mir-200ab/c* double knockout (DKO) progeny, whereby neonates survive less than 16 hours post parturition. In an effort to characterize the lethal effect of losing *miR-200*, I performed behavioral studies, expression profiling, histopathological analysis, and electron microscopy. Interestingly, DKO pups exhibit no milk spot, and develop labored breathing, along with pale, sticky skin within hours after birth. As expected, epithelial tissues such as the lungs and gastrointestinal tract exhibit the highest expression level of *miR-200* between E18.5 and P0. Although tissue architecture appears relatively normal in DKO epithelial tissues immediately after birth, I observed rapid accumulation of debris and mucus in the large and small airways that correlates with cyanosis. Intriguingly, the phenotypic changes in the lungs, gut, and skin of DKO pups are comparable to human symptoms of cystic fibrosis and asthma, which may provide novel insights into these diseases, where current mouse models fail.[6,7] We have acquired a *mir-200c/141: LacZ* reporter (a generous gift from the McManus Lab, UCSF), and used double immunofluorescence (IF), FACS, and single cell qPCR to determine the cell population expressing *miR-200* is largely motile ciliated cells (MCCs). In addition, we have found that *miR-200* is highly enriched in MCCs during frog development in published datasets.[8] Finally, in single (200ab) knockout males, I observed an infertility defect that correlates with

mislocalized flagella – a structure related to the cilia in MCCs. Future studies include further characterizing the mucociliary defect, and identifying *miR-200* targets. Overall, I have shown that *miR-200* is absolutely essential for the proper function and maintenance of the mucociliary epithelium lining the airways. Loss of *miR-200* leads to excessive mucus secretion into the airway lumen, and correspondingly, respiratory distress culminating in death.

Table of Contents

List of Figures

Chapter One:

Chapter Three:

Supplemental Material:

List of Tables

Chapter Two:

Chapter Three:

Supplemental Material:

Table of Abbreviations

Abbreviation	Term
ncRNA	noncoding RNA
miRNA	microRNA
UTR	Untranslated region
EMT	Epithelial-to-Mesenchymal Transition
MET	Mesenchymal-to-Epithelial Transition
ECM	Extracellular Cellular Matrix
CAF	Cancer Activated Fibroblast
NSCLC	Non-Small Cell Lung Cancer
iPSC	Induced-Pluripotent Stem Cell
MEF	Mouse Embryonic Fibroblast
CSC	Cancer Stem Cell
MCC	Motile Ciliated Cell
AEC-I	Alveolar Epithelial Cell Type I
AEC-II	Alveolar Epithelial Cell Type II
P	Postnatal Day
E	Embryonic Day
CF	Cystic Fibrosis
OVA	Ovalbumin
AHR	Airway Hyperresponsiveness
CFTR	Cystic Fibrosis Transmembrane Conductance Regulator
CC10	Clara Cell 10 kD Protein
ENaC	Epithelial Sodium Channel
ASL	Airway Surface Liquid
MI	Meconium Ileus
DKO	Double Knockout
SKO	Single Knockout
HET KO	Heterozygous Knockout
RISC	RNA-induced Silencing Complex
AGO	Argonaut (RISC Component)
SPC	Surfactant Protein-C
SPA	Surfactant Protein-A
SPB	Surfactant Protein-B
SPD	Surfactant Protein-D
MO	Morpholino
IF	Immunofluorescence
H&E	Hematoxylin & Eosin
PAS	Periodic Acid Schiff
WT	Wildtype
GI	Gastrointestinal Tract
MOE	Main Olfactory Epithelium
IVF	In vitro fertilization

Acknowledgements

I would like to thank my family, friends, labmates and classmates for all of their help and support these past six years. In particular, I want to thank my parents, Mike and Anne Cisson who have raised me up, encouraged me, and always believed in me. I also want to offer a special thank you to my little brother, Philip, and his beautiful wife Lindsey, for all of their love and support. To my best friends: Rachel, Ria, Casey, Megan, and Diane – thank you for the late night talks, hangouts, endless phone dates, and your unwavering faith in me. You ladies are such priceless, precious gifts. To Em and Andrew, who always had a way of offering a much needed, late night in lab, hilarious anecdote, catch phrase, or understanding look – THANK YOU. Thank you to all He-ites, past and present: Margaux, Virginie, Erich, Nobu, Amy, Nico, Yongjin, Paul, Sean, Joe, Rui, Bin, Andrew and Em. Thank you to my hardworking undergrads – past and present: Jessica, Byron, Jason, Alicia, and Wes. It was an absolute pleasure to work with you, to watch you grow in your understanding of science and maturation in experimental planning and design. You have each made me so proud, and I will always remember each of you with fond memories of how you reignited my own passion for science – even on the difficult days. Thank you to Lin, for supporting me these past six years and for teaching me that "we are all standing on the shoulders of giants." And last but never least – thank you to the love of my life, Dave, who has stood by me for the last 3.5 years, and who has shown me so much understanding, strength, and unconditional love. I am the luckiest person in the world to have each and every one of you in my life and I could not have made it through this process without you.

Chapter One
Introduction

Small, Non-coding RNAs

The field of non-coding RNAs (ncRNA) has experienced rapid expansion over the past three decades – illuminating the importance of ncRNAs in development, cellular function, and disease. Researchers are beginning to recognize the significance of the large ratio of non-coding, transcriptionally active sequences, to protein-coding genes in the mammalian genome. Approximately 80% of the human genome is capable of being transcribed into RNA, while less than 2% is protein-coding.[9–11] Intriguingly, there is a positive correlation between increasing ncRNA genomic content and organismal complexity.[11] Thus, a strong argument highlights the meaningful retention and multiple genetic duplications of ncRNAs in higher, more complex organisms. In particular, small, non-coding RNAs, termed miRNAs are a unique subset of ncRNAs that function through posttranscriptional gene regulation, and will be the focus of my studies reported here. miRNAs, unlike transcriptional regulators, offer an additional layer of expression modulation by targeting mRNAs. A functional, mature miRNA exists as a 21-25 nucleotide-long, single stranded RNA that acts upon its targets in the cytoplasm of the cell. The miRNA sequence includes a seed region that spans from nucleotide position 2 through position 8.[12] Seed region complementarity is the basis for the nucleotide-pairing between the miRNA and a seed sequence match in the 3' untranslated region (UTR) of a target mRNA.[13] Importantly, miRNA families are defined by their homology – particularly with respect to their seed sequences, since homologous seed regions will target the same pool of mRNAs, thereby facilitating a synergistic effect when multiple miRNA homologs are present.[14–17] The resulting miRNA-mRNA duplex formed by perfect or imperfect base-pair matching leads to sequestration, cleavage, and degradation of the target mRNA in the cytoplasm.[18,19]

The first functional miRNA and target mRNA pair, *lin-4* and *lin-14* respectively, was described in 1993 as a crucial component of temporal larval development regulation in *Caenorhabditis elegans.*[20] Interestingly, opposing developmental phenotypes were discovered in *lin-4* and *lin-14* mutant worms suggesting a common regulatory pathway. The *lin-4* miRNA is essential for first larval stage (L1) cell division patterning completion – the lack of which leads to repeated inappropriate L1 cell divisions. Alternatively, the *lin-14* gene encodes a nuclear protein necessary for L1 cell fate. Mutants of *lin-14* do not establish L1 cell fates and prematurely progress to the second larval stage (L2). We now know that *lin-14* mRNA is negatively regulated at the posttranscriptional level by *lin-4* miRNA via seven complimentary binding sites in order to generate the necessary downregulation of LIN14 to allow progression into L2. Although *lin-4* and *lin-14* were found to be specific to worms, another functional miRNA, *let7*, and its target mRNAs, *lin-41* and *lin-57*, were described using forward genetics in worms, but were also shown to be conserved in higher organisms seven years later.[21–24] Again, *let-7* miRNA controlled developmental transitions between the fourth larval stage (L4) and the adult stages by binding to the 3'UTRs of its targets to downregulate their expression.[23,25,26] Importantly, *let-7* became the first example of this novel mode of posttranscriptional gene regulation to be evolutionarily conserved across metazoans.[24] The genetic interactions between *lin-4* and *lin-14* and *let-7* with *lin-41* and *lin-57*, led to ignition of an entirely new field in which non-protein coding genetic components were investigated for their power to regulate a myriad of molecular and cellular processes.

MicroRNA Biogenesis

The stepwise processing of miRNAs from transcription through mRNA target-binding is illustrated in Figure 1. MicroRNAs are transcribed by RNA polymerase-III as single or multiple-hairpin loop structures, which make up the primary transcript or "pri-microRNA".[27,28] The pri-microRNA will undergo its first cleavage by the ribonuclease type-III enzyme, Drosha, to remove the ends of the transcript outside the hairpin loops, generating 70-nucleotide precursor intermediates, termed "pre-microRNAs".[28,29] The individual hairpin pre-miRNAs are then translocated from the nucleus to the cytoplasm via the action of Exportin 5, which is a Ran-GTP-dependent dsRNA binding protein.[30] Once in the cytoplasm, the pre-miRNA is further processed by the ribonuclease-III enzyme Dicer, which cleaves the loop, leaving a short, double-stranded RNA fragment, 21-25 nucleotides in length.[28,31–35] One of the strands will act as the mature miRNA, and is incorporated into the RNA-induced-silencing-complex (RISC), which binds target mRNAs, while the remaining miRNA "star-strand" is degraded.[36–38] The miRNA-RISC complex can now use imperfect base pair-matching to locate and bind seed sequences in the 3'UTR of various mRNA transcripts. Once miRNA-RISC binds a target, it represses translation of the mRNA by cleavage-induced degradation or sequestration of the transcript.[36,39]

MicroRNA Genetic Structure

Since the seminal work of Dr. Victor Ambros and Dr. Gary Ruvkun in 1993, miRNA biologists have described more than 24,000 miRNAs in plants, sea urchins, worms, flies, fish, frogs, mice and humans.[14,15,40] If we examine trends in conservation of miRNA across evolutionary time, it is apparent that miRNA family expansion correlates with organismal complexity. *D. melanogaster* and *C. elegans* have between two- and three-hundred annotated miRNAs, whereas mice and humans have close to one thousand and over two thousand, respectively.[15,17,40]

The reason for the duplication and expansion of miRNA family members is perhaps best addressed by considering their genetic structures. In vertebrates, we can observe mono-, di-, or poly-cistronic strands of homologous and paralogous miRNAs. Numerous studies in the miRNA field have shown that deletion of individual miRNAs – with a few exceptions – has little or no effect on development and function of the organism.[41–43] Although it has historically been tempting to dismiss miRNAs as only modest regulators of their targets, a handful of recent studies have demonstrated that knocking out all related miRNA family members simultaneously can have devastating consequences for specialized cell types and in some cases the entire organism.[8,44,45] From such studies, we may infer that the reason for the evolutionary retention and expansion of miRNAs in higher organisms is likely for protection as a compensatory mechanism to ensure that vital processes are executed properly.

In addition to protection, expression of multiple related miRNAs in a single transcript has the added benefits of increasing efficiency, broadening the range of potential targets, and enhancing knockdown potency. For example, the *mir-34/449* family of miRNAs are comprised of six members spread across three distinct genomic loci. Loss of the single *mir-34a* locus or the *mir-34a* plus *mir-34b/c* loci do not readily display developmental deficiencies.[45] However, loss of the third locus, *mir-449* leads to severe motile ciliated cell defects and lethality in triple

knockout mice.[45] Similarly, *miR-133a-1* and *miR-133a-2* are two homologous miRNAs encoded at two separate loci. Loss of one of these miRNAs fails to generate a specific phenotype, whereas double knockout animals develop a lethal ventricular-septal defect.[46] Alternatively, some miRNA families exhibit dominant functionality at a particular locus. The *mir-17-92* family exists at three distinct loci: *mir-17-92, mir-106a-363,* and *mir-106b-25*; however, loss of the *mir-17-92* locus alone affects normal development. In fact, mice deficient for *mir-17-92* exhibit postnatal lethality, pulmonary hypoplasia, skeletal defects, apoptosis, and defective B cell development.[47,48]

In addition to redundant miRNA loci encoding extra copies of homologous microRNAs, individual microRNAs within a di- or polycistronic transcript may function synergistically to down regulate targets of the same pathway, thereby enhancing a cellular phenotype. For instance, in the EuMyc/+ Burkitt Lymphoma mouse model, a member of the *mir-17-92* cluster, miR-19b, can be overexpressed and demonstrate the same oncogenic capacity as overexpression of miR-17/18a/19a/20a/19b miRNAs altogether.[49–51] The miR-19a and miR-19b miRNAs when over expressed function to suppress apoptosis in tumor cells at least in part by targeting the tumor suppressor PTEN for degradation.[51] Alternatively, one or more members of a given polycistronic transcript may antagonize the activity of the other family members by targeting components of a different pathway. Again, the *mir-17-92* cluster is an intriguing example of complexity within a single polycistronic transcript. Although overexpression of *mir-17-92* in the EuMyc/+ model causes accelerated lymphomagenesis, overexpression of *mir-17-19b* with a *miR-92* deletion causes an even more enhanced phenotype.[49,51] Intriguingly, *miR-92* antagonizes the oncogenic activity of the other family members by enhancing apoptosis of tumorigenic cells.[52] In this way, the number of homologous and paralogous miRNAs in the transcript, their stability and turnover rates, can act to skew the balance between one cellular readout and another – especially in pathological versus healthy conditions.

Introduction to *miR-200*

The *miR-200* family of microRNAs consists of five members, which exist at two distinct genomic loci: *mir-200b/a/429* on murine chromosome four (chromosome one in humans) and *mir-200c/141* on murine chromosome six (chromosome twelve in humans). MicroRNAs are widely conserved across metazoans and display a tendency to undergo multiple duplication events in higher, more complex organisms (Figure 2). The invertebrates *D. melanogaster* (fly) and *C. elegans* (worm) possess a single copy of the *miR-200* ortholog *miR-8* or *miR-236*, respectively, while *X. laevis* (frog), and *D. rerio* (zebrafish) have the same five *miR-200* members annotated in mice and humans.[40] The positive correlation between noncoding genome complexity and organismal hierarchy supports the notion that *miR-200* miRNAs have expanded their target repertoire and become essential to higher order organismal development and function. Such homologous and paralogous miRNA family members further extend their functional flexibility by arrangement at separate loci, under distinct transcriptional control. Thus, the genomic structure of *miR-200* as di- and polycistronic miRNA transcripts facilitates their overlapping and unique functions that are specific to cellular and disease context.

The *mir-200* family can be further sub-divided to reveal two sets of homologous family members based on seed-sequence matching: *mir-200a/141* and *mir-200b/c/429* (Figure 2). Despite their presence on two distinct chromosomes, all *miR-200s* are similarly enriched in epithelial tissues. The *miR-200* family first became intensively studied due to its role in a classic reciprocal negative feedback loop regulating Epithelial to Mesenchymal Transition (EMT) and Mesenchymal to Epithelial Transition (MET) – two essential processes in tumor metastasis as well as in development.[53,54] Multiple studies at the time showed compelling evidence that *miR-200* acts by directly targeting *Zeb1/2* mRNAs for degradation, thereby upregulating the target of Zeb factor transcriptional repression: *E-cadherin*, a major component of adherens junctions essential to formation of epithelial sheets.[53,55,56] Thus, while overexpression of *miR-200* down-regulates *Zeb* expression while upregulating *E-cadherin* and epithelial fate; overexpression of *Zeb* leads to transcriptional repression of both *miR-200* loci, and *E-cadherin*, thus promoting mesenchymal fate and corresponding metastatic capacity (Figure 3).

miR-200 in Cancer

Over nearly a decade, evidence has accrued to support the concept that *miR-200* may function as both a tumor suppressive and an oncogenic miRNA, depending on the cellular and disease-stage. Like many miRNA families, *miR-200* has multiple genomic loci under the transcriptional control of unique promoters allowing for diversification and expansion of their functions in different cellular contexts. At least one member of the two sub-groups of *miR-200*: *miR-200a/141* and *miR-200b/c/429*, exists at each locus, thereby expanding the pool of putative targets. Different loci of a single miRNA family can exhibit differential expression that changes between cell types, during development, or at baseline verses stressed conditions. The presence of both *miR-200* sub-group homologs at each locus may facilitate adaptive targeting of different mRNAs, since they bind to their targets by imperfect base pairing. The process of tumorigenesis is an extremely dysregulated series of events during which molecular signaling imbalances or subtle changes can confer or inhibit a selective advantage for a tumor cell. It is perhaps not surprising that miRNAs are so dysregulated and easily made to exert a tumor suppressive or oncogenic effect on so many different cancer types.[57]

In cancer, it is typically not the primary tumor that causes symptoms or complications that affect quality of life and survival in patients rather, it is metastases in distal tissues. For this reason, much of the cancer field focuses on the mechanism through which a primary tumor cell becomes metastatic. In solid tumors of epithelial origin, the process of epithelial to mesenchymal transition (EMT) and the reverse process of mesenchymal to epithelial transition (MET) describe the changes a tumor cell undergoes when leaving the primary tumor site and seeding a new tissue, respectively. In order to detach from the primary tumor, a cell must down-regulate expression of components of intercellular attachments such as Epithelial-cadherin (E-cadherin) thereby breaking down adherens junctions that compose epithelial sheets. The cell is thus, no longer attached to the epithelial mass and adopts a spindle-like or mesenchymal shape, which is conducive to migration and invasion of adjacent or distal tissues. Correspondingly, the reverse order of events must be orchestrated for a metastatic, 'mesenchyme-like' cell to attach to another epithelial tissue and effectively initiate formation of a micrometastasis. Among the many signaling and cell-polarization changes that ensue, is the

necessary upregulation of E-cadherin to re-establish intercellular contacts in the form of adherens junctions to successfully engraft in the new niche. The highly controlled balance between EMT and MET first highlighted the *miR-200* family as a key regulator of epithelial cell fate.

The *miR-200* family was first identified through a screen of over 240 miRNAs in sixty cancer cell lines from the National Cancer Institute as correlating with E-cadherin^{+} tumor cells.[4,57] High expression levels of *miR-200* were observed in breast, lung, colon and ovarian epithelial tumor cell lines and not in mesenchymal, Vimentin^{+} tumors. Furthermore, knockdown of *miR-200* led to loss of *E-cadherin* expression, intercellular attachments, and adoption of a spindle-like morphology indicative of mesenchymal cell fate. Importantly, key EMT transcriptional regulators *Zeb1* and *Zeb2,* through target prediction, showed five *miR-200b/c/429* binding sites in their 3'UTRs, and three or two *miR-200a/141* sites, respectively. Through gain and loss of function studies in breast, colon, and ovarian cell lines, Park et al. illustrated a negative feedback loop in which the Zeb proteins suppress transcription of *E-cadherin* to promote mesenchymal fate, but overexpression of *miR-200* leads to suppression of *Zeb* translation, allowing *E-cadherin* expression and promoting epithelial fate. Thus *miR-200* inhibits EMT and promotes MET through modulation of the Zeb proteins, and by extension, E-cadherin, thereby promoting establishment and maintenance of epithelial tissue.

More recent studies sought to further examine the activity of *miR-200* in solid tumor models and metastasis to address the question of its tumor suppressive verses oncogenic function. For instance, in a non-small-cell lung cancer (NSCLC) mouse model, *K-ras* and mutant *p53* drive development of metastatic lung adenocarcinoma; but forced expression of *miR-200* abrogates EMT and metastatic competency, thus functioning in a tumor suppressive capacity.[58] Furthermore, upon induction of EMT in NSCLC cell lines by treatment with Transforming Growth Factor-b (TGFb) or by injection of tumor cells into mice, *miR-200* levels significantly decrease.[58] Loss of *miR-200* thus leads to tumor cells with depolarized, mesenchymal characteristics and a propensity to migrate and invade distant tissues. The ability of *miR-200* to suppress tumorigenesis, metastatic capacity and invasiveness is further upheld by clinical correlations between lower levels of *mir-200* in patients with drug-resistant malignancies and with shorter overall survival in certain cancers.[58–60]

However, in addition to *miR-200* actively suppressing EMT, it can also promote MET – the process by which metastatic cells invade and engraft to generate micrometastases. Clinical cohort studies examining the levels of miRNA in stage I and stage IV, NSCLC tumors from resected patients showed a reduced overall survival when *miR-200c* and *miR-141* levels were high, suggesting an oncogenic role.[61] There is also evidence of *miR-200* oncogenic activity in gastric cancer, in which high expression of *miR-200c* in peripheral blood of patients is used as prognostic marker correlating with a poor prognosis.[62] Interestingly, in addition to promoting MET, overexpression of *miR-141* causes down-regulation of *Klf6*, an angiogenesis regulator, leading to an increase in angiogenic factor *VegfA* transcription, and increased angiogenesis.[61] The capacity of a tumor to induce angiogenesis is oncogenic and thus dangerous because vascularization of the tumor provides the nutrients and waste removal pipelines necessary to

efficiently increase its size. Importantly, cancer cell type appears to contribute to conflicting reports regarding the *miR-200* family and regulating angiogenesis. Other groups have shown that *miR-200* family members are protective against angiogenesis and enhance overall survival by targeting pro-angiogenic factors for degradation and affecting endothelial cell responses, thereby suppressing tumor growth in certain breast and renal cancer types.[60,63]

Increasing evidence suggests that cellular environment such as hypoxic conditions or extracellular matrix rigidity and immune cell interactions can also alter transcription of miRNAs that can lead to tumor suppressive or oncogenic effects.[61,63–67] In breast cancer *miR-200* is believed to promote production and release of an oncogenic secretome that enhances metastatic tendency by directly targeting the vesicle-trafficking protein, *Sec23a.*[64] Under hypoxic conditions, *miR-200* can act to enhance or subvert angiogenesis, depending on the tumor cell of origin. Studies focused on collagenous density of extracellular matrix have shown that under normal conditions, breast epithelial cells in a compliant, flexible matrix express *miR-200*, which suppresses the activity of Fli-1 and TCF-12 – two factors associated with cancer activated fibroblasts (CAFs) and extracellular matrix (ECM) remodeling.[65,67] Under fibrotic conditions, the matrix is more stiff, which activates focal adhesion kinases (FAKs) and PI3K and AKT pathways that suppress *miR-200* and induces mesenchymal cellular characteristics, proliferation and metastasis.[66,67] Importantly, the overexpression of *miR-200* was shown to suppress the ability of cancer cells to activate normal fibroblasts and initiate ECM re-modeling, suggesting that *miR-200* is an important facilitator of cancer cell phenotypic flexibility in response to its environment.

Interestingly, immune evasion is another hallmark of cancer whereby the tumor must subvert the activating signals of the immune system by dampening immune signals to avoid being killed. Typically, *miR-200* has been overlooked in terms of its connection to immune cells due to their mesenchymal nature, but surprisingly, *miR-200* is highly expressed in myeloid and lymphoid lineage cells (data not shown). Correspondingly, one such mechanism for immunosuppression that is regulated by *miR-200* is the expression of programmed-death ligand-1 (PDL-1), which binds to cognate receptor PD-1 on immune cells to suppress anti-cancer immunity.[68] *miR-200* directly targets *PDL-1* to suppress its expression, thereby enhancing tumor suppressive immunity, however, in later-stage metastatic cells, *miR-200* expression is suppressed or lost, leading to *PDL-1* expression and immune evasion.[68,69] Interestingly, although *miR-200* is considered tumor suppressive in solely solid tumor models, we have generated evidence that *miR-200* is protective in the non-solid tumor model, EuMyc/+, which emulates Burkitt Lymphoma (unpublished). Taken altogether, *miR-200* can act as a potent regulator of several hallmarks of tumorigenesis that can generate varying tumor suppressive and oncogenic effects, dependent on the cell type of origin and disease state.

<u>*miR-200* in Stem Cells</u>

The induction and maintenance of stem cells in development and disease have been characterized based on required signaling pathways and marker expression profiles, but we have only begun to examine the role of ncRNAs in these processes. Recently, however, the importance of regulation by miRNAs – particularly *miR-200* – has been highlighted by multiple

groups studying induced pluripotent stem cells (iPSCs).[70,71] During the early stages of reprogramming, mouse embryonic fibroblasts (MEFs), which are mesenchymal in nature, must undergo mesenchymal to epithelial transition (MET) – a process promoted by *miR-200*. In fact, two of the key reprogramming factors, Oct4 and Sox2, bind to the promoters at both *miR-200* loci and induce expression.[70] Furthermore, suppression of *miR-200* inhibited MET and iPSC generation, while overexpression enhanced these processes, highlighting the crucial nature of *miR-200* function in establishment of reprogrammed stem cells.

Similar to the multipotency and renewal-capacity of normal stem cells, cancer stem cells (CSCs) have been isolated and studied from a variety of tissues including breast, prostate, colon and ovary. CSCs are tumor cells that can self-renew and differentiate into a tumor, which if left behind after surgical resection, can lead to relapse and metastasis. Also, a single CSC injected into a recipient mouse will establish a tumor and can be re-isolated, and CSCs purified and re-injected into additional recipients to form tumors.[72] CSCs are also credited with providing resistance to chemotherapies since many anti-tumor therapeutics target the rapidly proliferating cells of the tumor. Thus it is necessary to understand the regulation of the signaling pathways involved in establishing and maintaining a pool of CSCs in order to design therapies to effectively eradicate the tumor.

Studies over the last decade have recognized the potential for miRNA-mediated CSC regulation, but so far only a handful of miRNAs have been assigned a mechanism of action in CSCs. However, *miR-200* was one of the first miRNAs recognized as one of the most dysregulated miRNAs in CSCs.[73] *miR-200a/c* suppresses the formation of cancer stem cells in colon cancers by targeting *Sox2*, which suppresses AKT signaling and suppresses mesenchymal, stem-like cell markers.[73,74] In addition, another study showed that down-regulation of *miR-141* by progesterone enhances stemness of breast CSCs by enhancing mammary stem cell markers, while overexpression of *miR-141* directly targets *Stat5a*, a progesterone-regulated gene that expands the luminal mammary progenitor population.[73,75] Thus, *miR-200* acts as an essential regulatory component of normal and transformed stem cell phenotypic flexibility.

miR-200 in Development

A logical extension between EMT and MET in metastasis, is that these same processes are necessary during embryonic patterning and development. For instance, the *miR-200* family regulates the process by which the hard palate is formed by augmenting EMT, proliferation and migration. In order to regulate the various processes involved in palatogenesis, *miR-200* suppresses the TGFb pathway by directly targeting *Smad2* and *Snail.*[76] The *miR-200b*-mediated regulation of TGFb signaling functions to balance apoptosis and proliferation of the medial edge epithelium and mesenchymal palate in the midline fusion region.[76] Loss of *miR-200* during this process can lead to defects in fusion and cleft palate in mice (unpublished observation).

In addition, *miR-200* has been shown to be essential for differentiation and survival of main olfactory neuroepithelium in mice and zebrafish.[1] Additionally, *mir-200c/141* is a potent regulator of BMP signaling by directly targeting BMP inhibitor *Bmpr* and enhancing ameloblast differentiation.[3] *Mir-200c/141*-deficient animals exhibit poor tooth enamel formation,

decreased E-cadherin and decreased BMP signaling, reinforcing *miR-200* as a major component in tooth development.[3]

Since *miR-200* is classically considered a driving force in epithelial cell fate, a logical extension of this concept is that this miRNA family is important for development and maintenance of epithelial tissues. However, specific roles for *miR-200* activity during development of major epithelial tissues such as the lungs and gastrointestinal tract, to our knowledge have not been described. By analyzing *miR-200* null mouse histology and RNA, it is clear that E-cadherin levels are comparable with wildtype animals and single knockout littermates, yet I will show that *miR-200* null mice have defective pulmonary and gut epithelia. The loss of this single miRNA family is sufficient to cause such severe deficiencies in these epithelial tissues, that the effects prove lethal, shortly after birth.

A Brief Introduction to the Pulmonary System

The mammalian lungs fulfill the essential role of providing a means for gas exchange to support life *ex utero*, and the transition to breathing air autonomously invites numerous hurtles such as airborne pathogens, irritants, and dehydration of the tissue.[77] To combat these challenges, the mammalian lung has evolved as a complex tubular network with resident innate immune cells, lubricating secretory cells, flow-inducing motile ciliated cells, and specialized alveolar epithelia to maintain surface tension and facilitate gas exchange.[78–80] The murine lungs are comprised of four right side-derived lobes, and one left lobe.[79] The airways are lined with specialized epithelial cells that coordinate these processes and also maintain fluid and electrolyte transport into and out of the airway lumen. Club cells ($CC10^+$) are secretory cells located in the bronchi and bronchioles, that release glycosaminoglycans to lubricate and protect the airway from noxious chemicals and mechanical damage. Goblet cells ($Muc5^+$) are mucus secreting cells that also line the small and large airways, but provide mucus to emulsify debris and airborne pathogens for clearance by the motile ciliated cells or MCCs ($Acetyl\text{-}a\text{-}tubulin^+$), which also line the large and small airways. The extensive airway network terminates in the functional units of the lung: the alveoli. Each alveolus hosts alveolar type I cells (AEC-I; $T1a^+$) which are thin and stretch to allow gas exchange, and alveolar type II cells (AEC-IIs; SPC^+) which secrete lubricating surfactant to retain surface tension in the inflated alveoli. Resident macrophages can also be found in the alveoli lumen, prepared to mount an innate immune response upon pathogenic insult.

At the time of birth, amniotic fluid must be removed from the lungs to expose the airways, a slowing in this process leads to cyanosis and death, but mechanical removal of this fluid can often rectify the problem. Studies have shown that in addition to fluid being pushed out of the airways as a result of vaginal delivery, significant absorption of this liquid is achieved through the pulmonary epithelium.[81] In addition, studies propose that the earliest evidence of directional fluid flow in the airway is not before postnatal day 7 (P7), whereas we and others have evidence that suggests flow initiation can be observed as early at P0 or P1 (unpublished observation).[82] Thus, the transition between *in utero* and *ex utero* pulmonary function is drastic, abrupt, and essential, for if it fails in one aspect, the consequence can be as severe as perinatal lethality, or have chronic implications such as asthma or Cystic Fibrosis.

Airway Deficiencies and Disease

There are many types of respiratory ailments that stem from airway obstruction and inefficient gas exchange. In particular, asthma and cystic fibrosis (CF) patients suffer from a number of complaints including excessive mucus production, inappropriate mucus viscosity, and ensuing respiratory distress due to mucus or debris plugs that preclude adequate gas exchange. Unfortunately, mouse models of airway diseases have been difficult to define as sufficiently comparable to human pulmonary disorders.[6,7]

Over 18.7 million people in the United States alone currently suffer from asthma, but due to the complexity and heterogeneity of the disease, a singular animal model is lacking.[7,83] Mouse models of asthma classically center on the immunological OVA-model, as the basis for mechanistic and pharmacologic intervention studies. In the OVA model, mice are intra-peritoneally (i.p.) injected with ovalbumin, to serve as the allergen, and an adjuvant such as aluminum hydroxide, to enhance OVA immunogenicity, and thus increase the Th2 immune response. Ten days later, a second booster i.p. injection is administered to complete the primed immune response. The mouse can then be challenged with OVA delivered to the airways by aerosol or intratracheally to elicit an acute inflammatory response and airway hyperresponsiveness (AHR), phenotypically resembling an asthmatic attack.[7,84] The OVA model is considered the gold-standard despite the fact that only half of asthmatic patients present with immune cell-mediated symptoms.[7,83,85] Patients with asthma present with episodes termed 'exacerbations' involving airway hyperresponsiveness manifesting in airway constriction, mucus secretion, and shortness of breath. There are a myriad of studies focused on immunological drivers of these events, but few parallels are drawn to inherent developmental defects in the respiratory epithelium.[7] Since the current immunological model does not provide translatable mechanistic and pharmacologic understanding of human asthma, further investigation of a new model is needed.

Cystic fibrosis is a less common disorder and largely affects individuals of Caucasian decent, 1 in every 2,500 Caucasian infants, 1: 17,000 African Americans, and 1: 31,000 Asian Americans.[86–89] Cystic Fibrosis is characterized by mutations in either the cystic fibrosis transmembrane conductance regulator (CFTR) gene, which encodes a receptor channel that secretes chloride into the airway lumen. The inability to control the ion flux across the airway epithelium can lead to a lower concentration of ions in the air-liquid-space preventing the appropriate amount of water to be released into the lumen and leading to increased mucus viscosity and a propensity to develop mucus plugs and chronic airway infections.[6,90,91] Water is necessary to hydrate the large mucin molecules in the airway in order to make fluid mucus. In the absence of airway surface liquid fluidity, the mucus meant to protect the airway and to aid in the debris emulsification process, effectively forms a thick and sticky coating, preventing mucociliary flow and causing airway obstruction. Similarly, mucus secretion abnormalities can be observed in the intestines of CF patients as infants and as adults. Approximately 36% of infants that are later diagnosed with CF, present with a condition called meconium ileus in which the mucus of their intestines is so thick that it precludes the passage of waste accumulated during development *in utero.*[86] In addition, CF patients exhibit sticky sweat due to an inappropriate

ion concentration on their skin, a fact that is indicative of a defect in these ion channels and could be a precursory phenotype to respiratory defects later in infants.[87,92]

In order to model Cystic Fibrosis mouse models were employed to examine the loss of functional CFTR because it was the most commonly mutated gene in CF patients. Unfortunately, these knockout models failed to completely recapitulate the pulmonary defects of human CF disease, suggesting other factors were involved in airway transepithelial potential, mucus production and secretion regulation.[6,93–95] Interestingly, however, the mouse models displayed severe intestinal pathology, similar to that of human patients.[93–95] CF-model mice exhibited intestinal meconium ileus, accumulation of mucus in the crypts, and significant lethality within the first few weeks of life, making it useful for study of certain aspects of CF disease.[6] In addition to CFTR regulating chloride ion flow into the airway lumen, it also promotes sodium absorption through the epithelial sodium channel, (ENaC). Importantly, over the last decade studies have examined the effects of accelerated sodium transport out of the airway by overexpression of ENaC in airway epithelium.[96] Overexpression of ENaC in mice led to severe air surface liquid depletion, increased mucus concentration and adhesion to the airways comparable to CF.[96,97] Importantly, however, the pulmonary defects in ENaC overexpressing mice yield incomplete penetrance of lethality, with 50% of animals surviving past two months and additional studies show with additional knockdown in immune regulation, a modest increase in lethality is achieved, though incomplete.[96,97] It is therefore intriguing to consider additional modes of airway development and function regulation that may have been previously overlooked.

For instance, in addition to ion flow regulation, recent studies have highlighted genes associated with mucus production and goblet cell metaplasia – both important features of asthma and CF.[98,99] Mucociliary clearance and air surface liquid thickness are critical aspects of airway health and function and require careful coordination of goblet cell and motile ciliated cell activity. Of the seventeen mucin genes, Muc5AC and 5B are the most highly expressed polymeric mucins secreted in the airways and an imbalance of either can lead to compromised airway clearance.[99–102] Interestingly, asthma patients exhibit higher levels of MUC5AC within their goblet cells compared with healthy individuals, while MUC5B production remains constant or increases.[85,100] In respiratory disorders such as asthma and CF, the airway surface liquid (ASL), which is the space occupied by mucus and cilia of motile ciliated cells, is too thick.[103] In healthy individuals, ciliated cells and goblet cells work together to produce directed flow and clear debris from the airway. In asthma and CF patients however, an excess of dehydrated mucin is released and the resultant mucus becomes too thick to achieve mucociliary flow.[102,103] Accumulation of such mucus, if left untreated, leads to morbidity and mortality of asthma and CF patients.

An important aspect of airway surface protection that has only recently been appreciated is the nucleotide and nucleoside-based control of the innate defense mechanisms addressed above. The actions and concentration of nucleotides and nucleosides in the airway lumen serve to regulated air surface liquid and mucociliary clearance.[104–106] Over the past decade exploration of the relationship between purine and purine-sensing receptors on goblet cells have shown

that basal levels of purines are constitutively present in the airways, but stress leads to increased levels of purines, receptor activation, and increased mucus secretion. Interestingly, it has been suggested that motile ciliated cells may be a source of purines that then act in a paracrine fashion on goblet cells to induce mucus release, however a direct mechanistic relationship has not been shown.[105–107] Therefore, in order to better understand the mechanism behind mucus secretion and accumulation, it is necessary to understand the mode of secretory induction. I propose here, that examining the role of miRNA in the development and regulation of mucociliary function may illuminate new avenues for asthma and CF disease intervention.

Project Summary

I will show that *mir-200ab-/-; c-/-* "DKO" mice are 100% perinatally lethal and exhibit severe respiratory distress at terminal stages. DKO mice exhibit an inability to clear debris and mucus from their airways and the ensuing alveolar collapse leads to death within 16 hours of birth. Furthermore, these DKO animals manifest with sustained meconium ileus (MI) – a paralysis of the intestine that precludes peristalsis and passage of meconium waste. Interestingly, nearly all infant cases of meconium ileus are later diagnosed with cystic fibrosis. In cases of MI, the mucus the body produces is thicker and stickier than normal, leading to blockages in the intestine (Seattle Children's Hospital). Also, I see a misregulation of ENAC in the lungs of my DKO mice compared with littermates. Additionally, DKO animals exhibit increased stickiness of their skin, by virtue of bedding and nestlet debris adhering to the skin surface for hours after birth, suggesting a comparable effect to the sticky sweat in CF patients.

Cystic Fibrosis is a disease of the lungs that is predicated on a misregulation of the ion-exchange in the lungs and intestines. In pulmonary epithelium, CF patients produce surfactant and/ or mucus with an irregular consistency. These lubricating fluids cannot be too thick, but must also be viscous enough to provide adequate surface tension (surfactant) in the alveoli for gas exchange to be able to occur efficiently, and mucus must be able to provide a thick enough barrier to trap and emulsify debris or aerosol toxins to prevent pulmonary epithelial injury. If one or both of these secretions are not properly formulated the patient may exhibit chronic respiratory infections, fibrosis, and poor respiration. Similarly, the DKO pups display accumulation of mucus in their small airways with corresponding alveolar collapse. I propose here, that *miR-200* double knockout mice have defective mucociliary epithelium (MCCs and goblet cells) in the lungs, which phenotypically resembles the human disease, Cystic Fibrosis. Traditionally mouse models have not been able to accurately or completely recapitulate human CF disease, but this system shows shocking similarities in a very narrow window of time. It is likely that using conditional knockouts in the future and therapeutic interventions, that we may prolong the life of these DKO mice. Such findings would not only be translatable to CF but also to non-specific perinatal pulmonary distress in humans. Importantly, *miR-200* has also been shown to regulate cytokine responses associated with asthmatic attacks. The deficiencies present in *miR-200* DKO animals thus have intriguing significance for future applications in human respiratory diseases such as asthma, and cystic fibrosis.

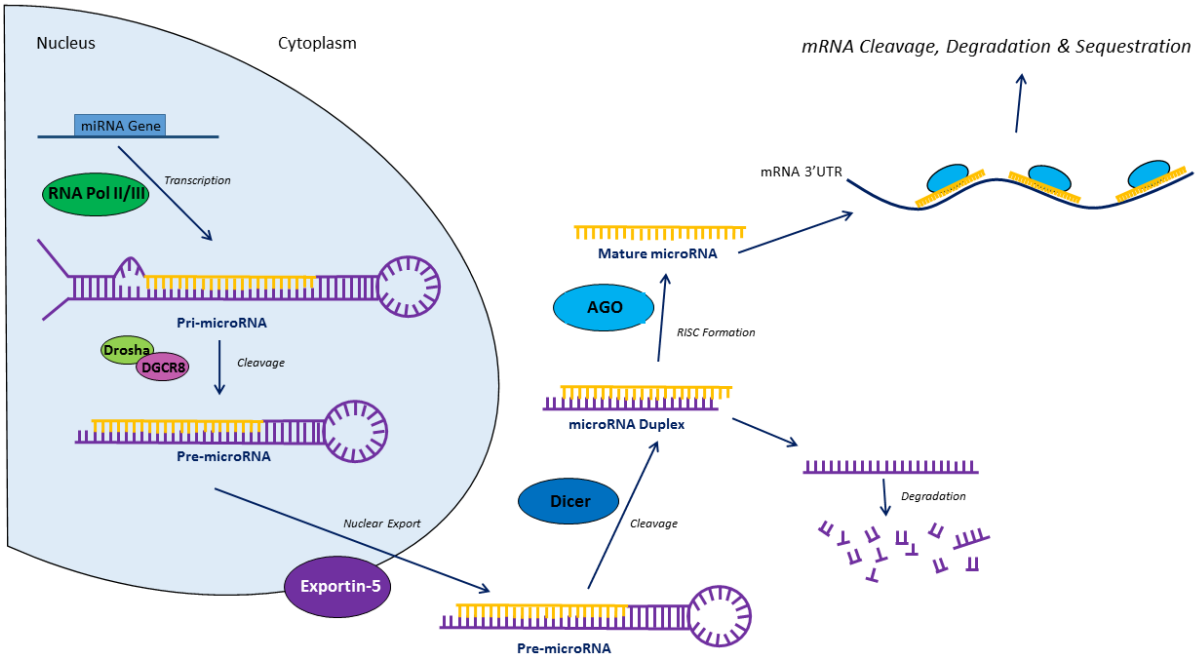

Figure 1. A model of miRNA biogenesis and ensuing posttranscriptional gene silencing. A nascent transcript of a miRNA gene, the "pri-microRNA", is cleaved by Drosha and DGCR8 to generate a stem-loop precursor, the "pre-microRNA", which is then exported from the nucleus by Exportin-5 and subsequently processed by Dicer to produce a mature miRNA duplex. One strand of the duplex is incorporated into the RNA-induced-silencing-complex (RISC), which recognizes and binds to target mRNA with imperfect base pairing to induce posttranscriptional silencing by cleavage, degradation, or sequestration of the mRNA. The other miRNA strand, termed the "star-strand" is also degraded.

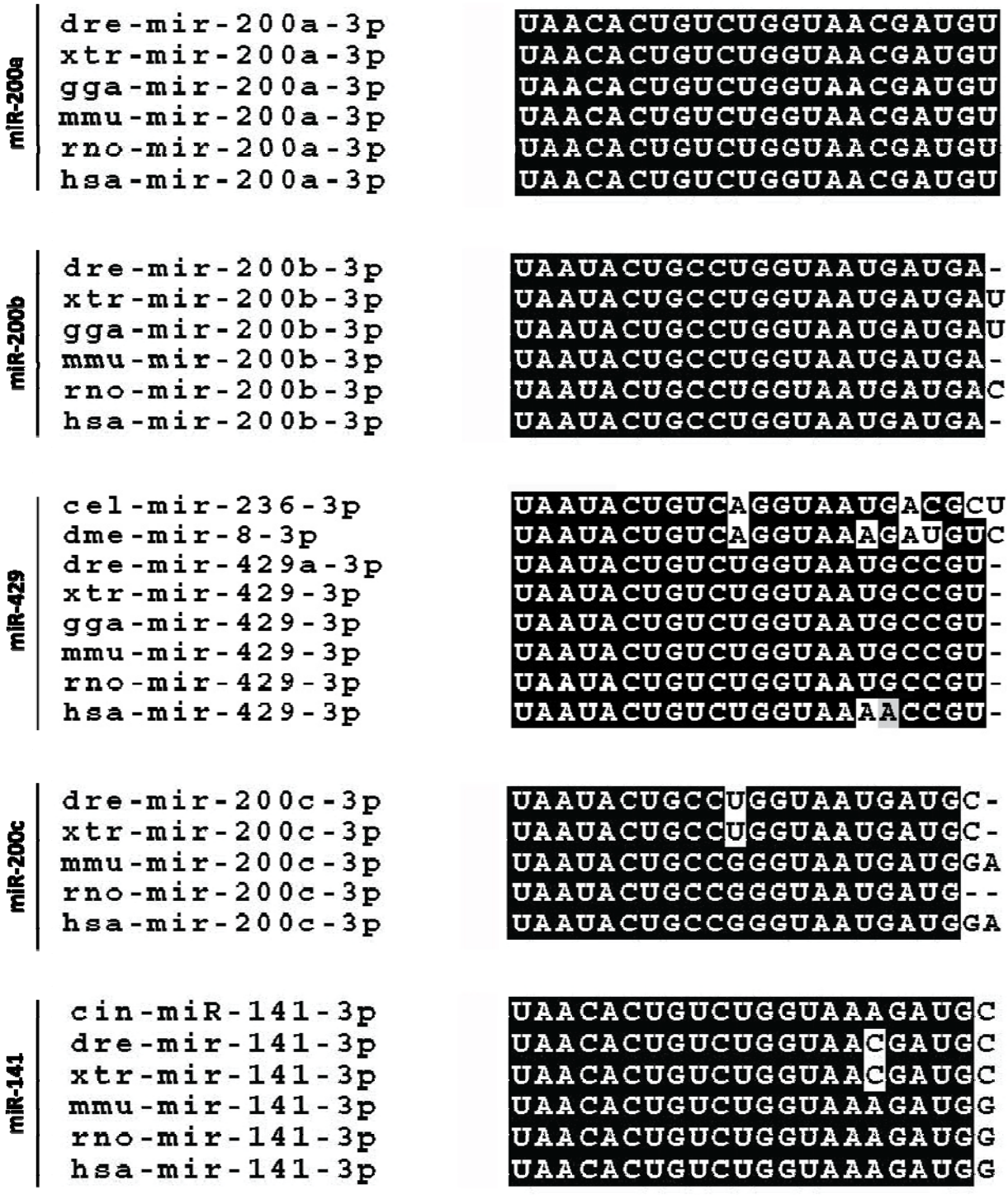

Figure 2. Multi-species alignment depicts miR-200 conservation. The miR-200 family is highly conserved across evolutionary time. miR-429 is the most ancient member of the miR-200 family observed in mammals. miR-200 displays impressive homology with invertebrates such as ascidians (cin), worms (cel), flies (dme), and vertebrates such as zebrafish (dre), frogs (xtr), mice (mmu), rats (rno), and humans (hsa).

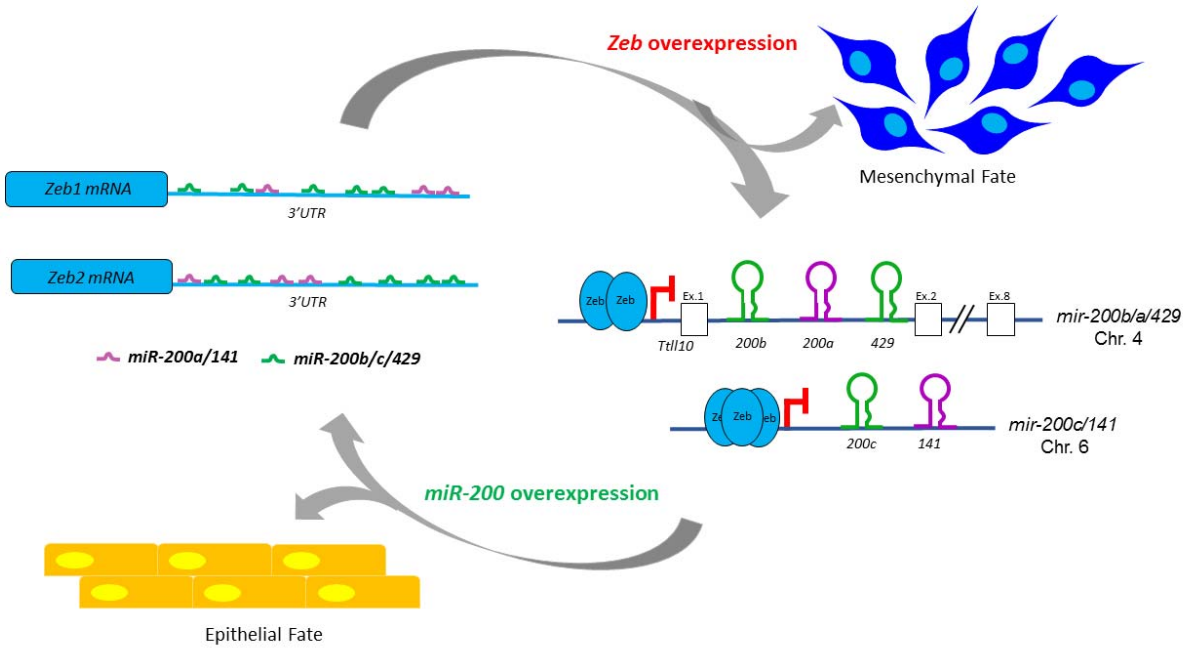

Figure 3. The *Zeb-miR-200* double-negative feedback loop. The balance between Zeb and miR-200 levels regulates transition between epithelial to mesenchymal (EMT) and mesenchymal to epithelial (MET) fate. The 3' untranslated regions (UTRs) of both *Zeb 1* and *Zeb 2* mRNAs contain eight and nine regions of seed sequence homology for miR-200 binding, respectively. Overexpression of miR-200 has been shown to suppress translation of the *Zeb* mRNAs and to promote *E-cadherin* expression and epithelial fate. Cognately, the Zeb proteins are potent transcriptional regulators that have two binding sites upstream of the *mir-200b/a/429* locus, and three binding sites upstream of the *mir-200c/141* locus, which effectively suppresses *miR-200* transcription. In the presence of overexpressed Zeb factors, *miR-200* and *E-cadherin* (not shown) expression is abrogated, and mesenchymal cell fate is adopted.

Chapter 2
Methodology

Methods

Mouse Husbandry

mir-200ab$^{+/-}$; *c*$^{-/-}$ mice were set up in intercross matings to generate *mir-200ab/c* double knockout (DKO) animals. DKO mice were made on a C57BL/6 background. All mice were housed in a non-barrier vivarium facility at UC Berkeley. The following primers were used for genotyping with parenthetical values to indicate to PCR product size: *mir-200ab*-For ACTATTTGACCCTTCAAAGTCCTCAC, *mir-200ab*-WT-Rev CCCATATCGCCAAGGCTAAC, and *mir-200ab*-Mut-Rev TCACTGGCCGTCGTTTTACA (WT band 700bp; KO band 450bp). *mir-200c*-For GATAGTAGAGGCTACAGAAAGCTGGTT *mir-200c*-R GGTTAAAGGTCAGAGGCTGTTGG (WT band 700bp; KO band 400bp). Pregnant females were monitored daily, and between E18.5 and E21, females were checked four times a day, in order to capture the precise time of birth. Neonate pups, upon birth, were processed to assess weight, outward appearance (skin color), behavior (response to stimuli), presence of milk spot, and genotype. In addition, 23% of full term pregnancies ended in requisite cesarean section due to an apparent, partially penetrant defect in labor induction and delivery in *mir-200ab*$^{+/-}$; *c*$^{-/-}$ females. Pups born naturally or delivered by cesarean were monitored throughout the first 18 hours after birth, and sacrificed for histology, RNA, and functional studies at 0-4 hours (pre-terminal stage) and 4-16 hours (terminal stage).

Histopathology

Tissues were dissected and fixed overnight in 10% neutral buffered formalin, pH 7.4 (NBF, Fisher Scientific, #SF100-4), processed by standard procedures including dehydration of the tissues and embedded into paraffin wax (Fisher Scientific, #AC41677-0020) blocks. All blocks were sectioned at 6um, and slides were stained for hematoxylin and eosin (H&E) (Fisher Scientific, 7211 and 7111), periodic acid Schiff (PA Sigma 10450-60-9; Schiff Sigma 3952016), and Trichrome.

qRT-PCR

Total RNA was isolated using TRIzol (Invitrogen, #15596) from various organs per the manufacturer's protocol and treated with DNase I to remove DNA contamination (Invitrogen, #18068). In order to quantitate mRNAs, TRIzol-isolated RNA was reverse-transcribed to make cDNA using Superscript III reverse transcriptase (Invitrogen, #18080) using random primers. qPCR was then performed on the cDNA template, using Sybrgreen (SsoAdvanced #1725270). Actin transcript was used as a control for each qPCR. The following qPCR primers were used with parenthetical values indicating product size: [put all primers in a table]. Samples from 5 separate DKO, SKO, HetKO, and age-matched WT pups were collected and tested. For *Xenopus laevis* studies, samples were generated from total RNA extracts from epidermis explants using iScript reverse transcriptase supermix (BioRad, #170-8840). qPCR studies were all performed on a BioRadCFX96 System C1000 Touch (BioRad).

For miRNA quantitation, TaqMan microRNA assays were used to measure the level of mature miRNA (Applied Biosystems, *miR-200a/b/c/429/141*) and the level of primary transcript, "pri-miRNA" (Applied Biosystems, *mir-200a/b/429* and *mir-200c/141*). U6 snoRNA (ABI, #4427975) was used as a normalization control for all TaqMan miRNA studies.

Single Cell qPCR

Neonate trachea and bronchi were digested using dispase and collagenase IV (Stem Cell Technologies #07923; Life Technologies #17104-019) for 1 hour at 37 degrees C, and DNase I (Invitrogen 18068015) to remove residual genomic DNA. Cells were then filtered through a 40um mesh and diluted 1:2000 in PBS. Individual cells were aspirated and transferred to PCR strip tubes, and processed per manufacturer instructions (Life Technologies #4458237). In short: Cells are lysed, reverse transcribed into cDNA and then undergo a pre-amplification step using endogenous control and experimental primers to increase the concentration of cDNA. Next the pre-amplified cDNA can be used as template in qPCR reactions using the same Sybrgreen-based primers as those used for the pre-amplification step, and reactions are run using SsoAdvanced Sybr Green Supermix (BioRad #172-5274) on a BioRadCFX96 System C1000 Touch (BioRad).

Visualization of Mucociliary and Flagellar Movement and Mucociliary Flow

For mucociliary analyses: Tracheas from adult and neonate mice were cut into 3 mm X 5 mm pieces using a dissection microscope. Trachea pieces were then transferred to chambers made using 0.5mm sticky spacer (BioRad #SLF-1201) on glass slides. The chamber was filled with 100uL M199 Hank's balanced salt medium (Invitrogen #12350-039) mixed with 1uL of red fluorescent 0.5um beads (Invitrogen #F8812), and then a coverslips was placed over the media and sticky spacer to seal the chamber and flatten the curved trachea pieces. Live images of the airway epithelium were recorded with a high-speed GX-1 Memrecam camera (NAC Image Technology) attached to an Olympus IX71 microscope. The DIC channel was used to record ciliary beating, and the red fluorescent channel recorded mucociliary flow. Videos were recorded at 250 frames per second for 8 seconds, and are played at 250 FPS. ImageJ was used to process and analyze raw images.

For flagellar analyses: Testes from WT and *mir-200a/b/429* KO adult males were dissected and isolated by the "swim up" method, as previously described.[108] Live images of the sperm were recorded with a high-speed GX-1 Memrecam camera (NAC Image Technology) attached to an Olympus IX71 microscope. The DIC channel was used to record flagellar beating, and videos were recorded at 500 frames per second for 8 seconds, and are played at 250 FPS. ImageJ was used to process and analyze raw images

Immunofluorescence staining & Confocal Imaging

For immunofluorescence staining on paraffin sections, 6um sections were deparaffinized and rehydrated in graded alcohols prior to antigen retrieval using Trilogy Buffer (Cell Marque #920P-09) in a vegetable steamer (Cuisinart). Primary antibodies against Beta-galactosidase (1:500; Abcam AB9361), CC10, (1:500; Santa Cruz Biotechnology SC-25555), SPC (1:500; Santa Cruz Biotechnology SC-7706), Muc5ac (1:400; a generous gift from Richard Harland, UC Berkeley), Muc5b (1: 10,000; a generous gift from Chris Evans, UC Denver), Acetylated-a-tubulin (1:1000; Sigma T6793), Foxj1 (1:400; Sigma HPA005714), Caspase-3 (1:500; R&D Systems AF835), E-cadherin (1:500; Fisher #610181) were incubated with the sections overnight at 4C. Slides were then washed 3X in PBST (0.1% Triton-X 100 in PBS) and incubated for 2 hours at room temperature in secondary antibody (1:500 AlexaFluor 594 donkey anti-rabbit (Invitrogen

21207) or goat anti-mouse (Invitrogen A11005) or 1:500 AlexaFluor 488 goat anti-mouse (Invitrogen A11034) or Alexafluor 488 goat anti-chicken (Fisher A11039). Slides were then washed 3X in PBST, counter stained with DAPI (Sigma D9564) and mounted using Prolong Antifade Mountant (Invitrogen P36930). Images were taken with a Zeiss LSM 710 AxioObserver inverted confocal microscope and analyzed using ZEN software.

For *X. laevis* immunofluorescence staining, IF was performed on whole-mount embryos fixed at stage 32 in 4% paraformaldehyde for 1-2 hours at room temperature. Embryos were processed according to the standards of the field and morphological analysis performed as described.[109] Primary antibody mouse monoclonal Acetylated-a-tubulin (1:700; Sigma T6793), and secondary antibody (1:250) AlexaFluor 488 goat anti-mouse antibody (Invitrogen A11001). Actin staining was performed by 30-60-minute incubation at room temperature AlexaFluor-594-labelled Phalloidin (1:40, Molecular Probes A12381). Imaging was performed with a Zeiss LSM 700, Z-stack analysis and processing were completed using ImageJ and Zeiss ZEN software.

For Mouse sperm immunofluorescence staining, IF was performed on WT or KO sperm harvested as previously described, on 10mm X 10mm glass coverslips. Incubation with primary antibody Acetylated-a-tubulin (1:1000; Sigma T6793) was performed overnight at 4C. Samples were washed 3X in PBST and incubated for 1 hour at room temperature with secondary antibody AlexaFluor 594 goat anti-mouse (Invitrogen A11005), counter stained with DAPI (Sigma D9564) and mounted using Prolong Antifade Mountant (Invitrogen P36930). Images were taken with a Zeiss LSM 710 AxioObserver inverted confocal microscope and analyzed using ZEN software.

Transmission Electron Microscopy (TEM) Studies

Neonate trachea and lobe tissue was fixed using Karnovsky's fixative in 0.1M sodium phosphate buffer (Sorenson's), washed with Sorenson's sodium phosphate buffer and post-fixed using 1%OsO4 in Sorenson's for 1 hour as described previously.[45] After rinsing in double-distilled water (DDW), the tissue was incubated for 30 minutes at room temperature in 0.1% tannic acid, rinsed again in DDW, and incubated for 1 hour in 1% uranyl acetate in DDW. Tissue was dehydrated by passaging through a graded series of acetone solutions, then infiltrated and embedded in an epoxy resin mixture. Survey thick sections were cut, and ultra-thin sections of the selected areas were generated with a diamond knife (Diatome). The thin sections were picked up on copper grids and stained with uranyl acetate and lead citrate before viewing on a Philips CM120 Biotin. Micrographs were taken with a Gatan MegaScanModel 794/20 digital camera. TEM analyses with longitudinal and trans- verse sections were performed in the electron microscopy facility of the University of California at Davis. The criteria for classifying MCCs was the presence of basal bodies. ImageJ was used for image analysis and quantitation.

For sperm TEM, samples were pelleted in fixative and processed as described for neonate airway. Imaging and processing were performed also as described for the airway. Criteria for abnormal head-neck attachment was the transverse nature of the axoneme cross section in the same field as a longitudinal section through the sperm head meaning the two structures were perpendicular to one another instead of linear, as in WT sperm.

Manipulation of Xenopus laevis embryos and skin explants

X. laevis eggs were procured as previously described.[110] Embryos were injected with morpholino nucleotides (MOs, Gene Tools) at the eight-cell stage using a PicoSpritzer setup in 1/33modified frog Ringer's solution(MR) with 2.5% Ficoll PM400 (GEHealthcare 17-0300-50), and then were transferred into 1/33MR containing gentamycin after injection.[110] Drop size was calibrated to about 7–8 nl per injection. Rhodamine-B dextran (0.5– 1.0mg/ml; Invitrogen D1841) was co-injected and used as lineage tracer. MO (Gene Tools) doses were administered as follows: a total dose of 20 ng miR-200b/429 MOs; 10 ng each for xtr-mir-200a MO (59-ACATCGTTACCAGACAGTGTTAGAA-39), xtr-mir-429 MO (59-ACGGCATTACCAGACAGTATTAGAC-39), or 20ng of a miR-control MO (59-TGCACGTTTCAATACAGACCGT-39). Analysis of morphant tadpole epidermis was performed at stage 32 for MCC maturation, by IF.

Xenopus skin explants were generated from animal caps, dissected in modified Barth's saline from stage 9 embryos, which were un-injected (time course experiment).[110] Explants were cultured in 0.53 modified Barth's saline until un-manipulated control embryos reached appropriate stage.[110] In the time course experiment, stage 10, 26 and 32 explants represented ciliation state of MCCs for qPCR analysis to detect level of miR-200 expression.

Quantification of Lobe Collapse and Luminal Mucus

For lobe collapse quantitation, three different depths of each lung were taken and stained by H&E and imaged. The number of lobes with collapse were quantified using ImageJ for analysis. PAS stained sections were used to quantitate luminal mucus volume. The basement membrane and the diameter of the airway were measured and multiplied to determine volume.

In vitro Fertilization

32 WT females were super ovulated and oocytes harvested as described previously.[108] Sperm from three WT males and three *mir-200ab* KO males were harvested as in Flagellar imaging section. IVF was performed in the Lishko Lab at UC Berkeley according to established protocols.[108] Images of blastocyst embryos and sperm were analyzed using ImageJ.

Table 1: q-PCR Primer Sequences

Sybr Green Primer	Sequence
pri-2ab-F	TGGTAATGCCGTCCATCCAC
pri-2ab-R	GGCTTGATGAACCCAGCTCT
pri-2c-141-F	CACCCAGTGGAAGACACAGT
pri-2c-141-R	CCCCGGGTTTTGTTTATGGC
Xtr-mir-200a	TAACACTGTCTGGTAACGATGT
Xtr-mir-200b	TAATACTGCCTGGTAATGATGAT
Xtr-mir-429	TAATACTGTCTGGTAATGCCGT
Actin F2	GATCTGGCACCACACCTTCT
Actin R2	GGGGTGTTGAAGGTCTCAAA
Ecad2F	GCACTCTTCTCCTGGTCCTG
Ecad2R	GTTGACCGTCCCTTCACAGT
Zeb1 F	GCCAGCAGTCATGATGAAAA
Zeb1 R	GGAGCAGCTGAAGTTGTCCT
Foxj1 F	ACCAAGATCACTCTGTCGGC
Foxj1 R	CTTCTCCCGAGGCACTTTGA
Cc10 F	CGCCATCACAATCACTGTGGTC
Cc10 R	GCCCGCATTTTGCAGGTCT
T1a For1	TGACCCCAGGTACAGGAGAC
T1a Rev1	CCTCTAAGGGAGGCTTCGTC
SPC For1	CAGCTCCAGGAACCTACTGC
SPC Rev1	TCGGACTCGGAACCAGTATC
Muc5ac-F	ATCAGATGGGCTGTGTTCCTG
Muc5ac-R	CAGAACATGTGTTGGTGCAG
Muc5b F	CCTCTCCTGTCCACCCACTA
Muc5b R	GTCCATGCGTGAGTTGAAGA
ENaC F	ACCCCGTGAGTCTCAACATC
ENaC R	CCTGGCGAGTGTAGGAAGAG
Cftr F	AAGCCGCGTTCTTGATAAAA
Cftr R	CAGAGAAGCCCCATCAGAAG
MCSF F	TTCAAGCTCTTTCTGAACCGTGTA
MCSF R	GCCTTGTTTTGTGCCATTAAGAAG
MCSF-R F	CATCCACGCTGCGTGAAG
MCSF-R R	GGGATTCGGTGTCGCAATAT

Chapter Three

"miR-200 miRNAs play essential roles in mucociliary development and function in perinatal mice"

Introduction

MiRNAs are a class of small, noncoding RNAs that function as posttranscriptional regulators of gene expression. Interestingly, miRNAs are highly conserved across metazoans and exhibit significant redundancy that correlates with increased organismal complexity. Although mice and humans have over 1,000 annotated miRNAs, many are homologs or paralogs of one another, organized into discrete mono-, di-, or polycistronic transcripts spread across the genome. Due to the inherent redundancy of miRNA families, loss of a single miRNA or an entire locus may not exhibit a clear phenotypic defect due to the compensatory action of other family members. In addition, many homologous miRNAs are highly enriched in specialized tissues at essential stages of developmental transition. In order to illuminate the functional significance of this robust expression, it is necessary to remove all members of a given miRNA family to identify phenotypic defects.

The *mir-200* family of microRNAs is comprised of five members, spread across two genomic loci, and is broadly conserved across phyla (Supplemental Figure 1). The *mir-200b/a/429* locus (termed "200ab") forms a single transcript with three hairpin loops (encoding *miR-200a, 200b, 429*), and the *mir-200c/141* locus (termed "200c") forms a disistronic transcript with two hairpin loops (encoding *miR-200c*, and *miR-141*). Although they span two separate chromosomes, homologous miR-200 family members exist at each locus and can be divided into two sub-groups: *miR-200a/141* and *miR-200b/c/429*, based on seed sequence homology, shown in pink and green, respectively (Figure 1A & B).

Although miR-200 has classically been cited as an important modulator of epithelial-mesenchymal transition (EMT) by promoting *E-cadherin* expression in tumor models, little is known about its importance during normal development and epithelialization. Interestingly, miR-200 expression was particularly enriched in mucociliary epithelium in lung tissue and in the intestinal epithelium at perinatal stages of development. Following parturition, neonate pups are subject to a battery of onslaughts to their senses, homeostasis, and perhaps most essential: an abrupt requirement to breathe autonomously. In respiratory diseases such as asthma and Cystic Fibrosis (CF), excessive mucus accumulation and an inability to efficiently clear debris can lead to respiratory distress, chronic infections and death. The purpose of the investigations reported here is to characterize the complex set of phenotypic defects exhibited by miR-200 double-knockout "DKO" neonates as they compare to respiratory disorders such as asthma and cystic fibrosis.

Methods

Mouse Husbandry

mir-200ab$^{+/-}$*; c*$^{-/-}$ mice were set up in intercross matings to generate *mir-200ab/c* double knockout (DKO) animals. DKO mice were made on a C57BL/6 background. All mice were housed in a non-barrier vivarium facility at UC Berkeley. The following primers were used for genotyping with parenthetical values to indicate to PCR product size: *mir-200ab*-For

ACTATTTGACCCTTCAAAGTCCTCAC, *mir-200ab*-WT-Rev CCCATATCGCCAAGGCTAAC, and *mir-200ab*-Mut-Rev TCACTGGCCGTCGTTTTACA (WT band 700bp; KO band 450bp). *mir-200c*-For GATAGTAGAGGCTACAGAAAGCTGGTT *mir-200c*-R GGTTAAAGGTCAGAGGCTGTTGG (WT band 700bp; KO band 400bp). Pregnant females were monitored daily, and between E18.5 and E21, females were checked four times a day, in order to capture the precise time of birth. Neonate pups, upon birth, were processed to assess weight, outward appearance (skin color), behavior (response to stimuli), presence of milk spot, and genotype. In addition, 23% of full term pregnancies ended in requisite cesarean section due to an apparent, partially penetrant defect in labor induction and delivery in *mir-200ab*$^{+/-}$; *c*$^{-/-}$ females. Pups born naturally or delivered by cesarean were monitored throughout the first 18 hours after birth, and sacrificed for histology, RNA, and functional studies at 0-4 hours (pre-terminal stage) and 4-16 hours (terminal stage).

Histopathology

Tissues were dissected and fixed overnight in 10% neutral buffered formalin, pH 7.4 (NBF, Fisher Scientific, #SF100-4), processed by standard procedures including dehydration of the tissues and embedded into paraffin wax (Fisher Scientific, #AC41677-0020) blocks. All blocks were sectioned at 6um, and slides were stained for hematoxylin and eosin (H&E) (Fisher Scientific, 7211 and 7111), periodic acid Schiff (PA Sigma 10450-60-9; Schiff Sigma 3952016), and Trichrome.

qRT-PCR

Total RNA was isolated using TRIzol (Invitrogen, #15596) from various organs per the manufacturer's protocol and treated with DNase I to remove DNA contamination (Invitrogen, #18068). In order to quantitate mRNAs, TRIzol-isolated RNA was reverse-transcribed to make cDNA using Superscript III reverse transcriptase (Invitrogen, #18080) using random primers. qPCR was then performed on the cDNA template, using Sybrgreen (SsoAdvanced #1725270). Actin transcript was used as a control for each qPCR. The following qPCR primers were used with parenthetical values indicating product size: [put all primers in a table]. Samples from 5 separate DKO, SKO, HetKO, and age-matched WT pups were collected and tested. For *Xenopus laevis* studies, samples were generated from total RNA extracts from epidermis explants using iScript reverse transcriptase supermix (BioRad, #170-8840). qPCR studies were all performed on a BioRadCFX96 System C1000 Touch (BioRad).

For miRNA quantitation, TaqMan microRNA assays were used to measure the level of mature miRNA (Applied Biosystems, *miR-200a/b/c/429/141*) and the level of primary transcript, "pri-miRNA" (Applied Biosystems, *mir-200a/b/429* and *mir-200c/141*). U6 snoRNA (ABI, #4427975) was used as a normalization control for all TaqMan miRNA studies.

Single Cell qPCR

Neonate trachea and bronchi were digested using dispase and collagenase IV (Stem Cell Technologies #07923; Life Technologies #17104-019) for 1 hour at 37 degrees C, and DNase I (Invitrogen 18068015) to remove residual genomic DNA. Cells were then filtered through a 40um mesh and diluted 1:2000 in PBS. Individual cells were aspirated and transferred to PCR strip tubes, and processed per manufacturer instructions (Life Technologies #4458237). In

short: Cells are lysed, reverse transcribed into cDNA and then undergo a pre-amplification step using endogenous control and experimental primers to increase the concentration of cDNA. Next the pre-amplified cDNA can be used as template in qPCR reactions using the same Sybrgreen-based primers as those used for the pre-amplification step, and reactions are run using SsoAdvanced Sybr Green Supermix (BioRad #172-5274) on a BioRadCFX96 System C1000 Touch (BioRad).

Immunofluorescence staining & Confocal Imaging

For immunofluorescence staining on paraffin sections, 6um sections were deparaffinized and rehydrated in graded alcohols prior to antigen retrieval using Trilogy Buffer (Cell Marque #920P-09) in a vegetable steamer (Cuisinart). Primary antibodies against Beta-galactosidase (1:500; Abcam AB9361), CC10, (1:500; Santa Cruz Biotechnology SC-25555), SPC (1:500; Santa Cruz Biotechnology SC-7706), Muc5ac (1:400; a generous gift from Richard Harland, UC Berkeley), Muc5b (1: 10,000; a generous gift from Chris Evans, UC Denver), Acetylated-a-tubulin (1:1000; Sigma T6793), Foxj1 (1:400; Sigma HPA005714), Caspase-3 (1:500; R&D Systems AF835), E-cadherin (1:500; Fisher #610181) were incubated with the sections overnight at 4C. Slides were then washed 3X in PBST (0.1% Triton-X 100 in PBS) and incubated for 2 hours at room temperature in secondary antibody (1:500 AlexaFluor 594 donkey anti-rabbit (Invitrogen 21207) or goat anti-mouse (Invitrogen A11005) or 1:500 AlexaFluor 488 goat anti-mouse (Invitrogen A11034) or Alexafluor 488 goat anti-chicken (Fisher A11039). Slides were then washed 3X in PBST, counter stained with DAPI (Sigma D9564) and mounted using Prolong Antifade Mountant (Invitrogen P36930). Images were taken with a Zeiss LSM 710 AxioObserver inverted confocal microscope and analyzed using ZEN software.

For *X. laevis* immunofluorescence staining, IF was performed on whole-mount embryos fixed at stage 32 in 4% paraformaldehyde for 1-2 hours at room temperature. Embryos were processed according to the standards of the field and morphological analysis performed as described.[109] Primary antibody mouse monoclonal Acetylated-a-tubulin (1:700; Sigma T6793), and secondary antibody (1:250) AlexaFluor 488 goat anti-mouse antibody (Invitrogen A11001). Actin staining was performed by 30-60-minute incubation at room temperature AlexaFluor-594-labelled Phalloidin (1:40, Molecular Probes A12381). Imaging was performed with a Zeiss LSM 700, Z-stack analysis and processing were completed using ImageJ and Zeiss ZEN software.

For Mouse sperm immunofluorescence staining, IF was performed on WT or KO sperm harvested as previously described, on 10mm X 10mm glass coverslips. Incubation with primary antibody Acetylated-a-tubulin (1:1000; Sigma T6793) was performed overnight at 4C. Samples were washed 3X in PBST and incubated for 1 hour at room temperature with secondary antibody AlexaFluor 594 goat anti-mouse (Invitrogen A11005), counter stained with DAPI (Sigma D9564) and mounted using Prolong Antifade Mountant (Invitrogen P36930). Images were taken with a Zeiss LSM 710 AxioObserver inverted confocal microscope and analyzed using ZEN software.

Transmission Electron Microscopy (TEM) Studies

Neonate trachea and lobe tissue was fixed using Karnovsky's fixative in 0.1M sodium phosphate buffer (Sorenson's), washed with Sorenson's sodium phosphate buffer and post-fixed using 1%OsO4 in Sorenson's for 1 hour as described previously.[45] After rinsing in double-distilled water (DDW), the tissue was incubated for 30 minutes at room temperature in 0.1% tannic acid, rinsed again in DDW, and incubated for 1 hour in 1% uranyl acetate in DDW. Tissue was dehydrated by passaging through a graded series of acetone solutions, then infiltrated and embedded in an epoxy resin mixture. Survey thick sections were cut, and ultra-thin sections of the selected areas were generated with a diamond knife (Diatome). The thin sections were picked up on copper grids and stained with uranyl acetate and lead citrate before viewing on a Philips CM120 Biotin. Micrographs were taken with a Gatan MegaScanModel 794/20 digital camera. TEM analyses with longitudinal and trans- verse sections were performed in the electron microscopy facility of the University of California at Davis. The criteria for classifying MCCs was the presence of basal bodies. ImageJ was used for image analysis and quantitation.

For sperm TEM, samples were pelleted in fixative and processed as described for neonate airway. Imaging and processing were performed also as described for the airway. Criteria for abnormal head-neck attachment was the transverse nature of the axoneme cross section in the same field as a longitudinal section through the sperm head meaning the two structures were perpendicular to one another instead of linear, as in WT sperm.

Manipulation of Xenopus laevis embryos and skin explants

X. laevis eggs were procured as previously described.[110] Embryos were injected with morpholino nucleotides (MOs, Gene Tools) at the eight-cell stage using a PicoSpritzer setup in 1/33modified frog Ringer's solution(MR) with 2.5% Ficoll PM400 (GEHealthcare 17-0300-50), and then were transferred into 1/33MR containing gentamycin after injection.[110] Drop size was calibrated to about 7–8 nl per injection. Rhodamine-B dextran (0.5– 1.0mg/ml; Invitrogen D1841) was co-injected and used as lineage tracer. MO (Gene Tools) doses were administered as follows: a total dose of 20 ng miR-200b/429 MOs; 10 ng each for xtr-mir-200a MO (59-ACATCGTTACCAGACAGTGTTAGAA-39), xtr-mir-429 MO (59-ACGGCATTACCAGACAGTATTAGAC-39), or 20ng of a miR-control MO (59-TGCACGTTTCAATACAGACCGT-39). Analysis of morphant tadpole epidermis was performed at stage 32 for MCC maturation, by IF.

Xenopus skin explants were generated from animal caps, dissected in modified Barth's saline from stage 9 embryos, which were un-injected (time course experiment).[110] Explants were cultured in 0.53 modified Barth's saline until un-manipulated control embryos reached appropriate stage.[110] In the time course experiment, stage 10, 26 and 32 explants represented ciliation state of MCCs for qPCR analysis to detect level of miR-200 expression.

Quantification of Lobe Collapse and Luminal Mucus

For lobe collapse quantitation, three different depths of each lung were taken and stained by H&E and imaged. The number of lobes with collapse were quantified using ImageJ for analysis. PAS stained sections were used to quantitate luminal mucus volume. The basement membrane and the diameter of the airway were measured and multiplied to determine volume.

Results

The miR-200 family is enriched in perinatal epithelia

Since the miR-200 miRNAs exist at two distinct genomic loci and are thus controlled by separate promoters, they have the ability to exhibit unique expression profiles depending on cellular, developmental, and disease context. In order to determine when and where miR-200 is expressed during embryonic development, q-PCR studies were designed to provide a comprehensive picture of wildtype (WT) expression at E14.5, E16.5, E18.5, (Embryonic day) and P0 (Postnatal day). Impressively, all five miR-200s exhibited an appreciable degree of tissue specificity, showing high enrichment in lung, stomach, and intestinal epithelium, particularly in the perinatal E18.5 and P0 neonate timepoints (Figure 1E-I). Expression analyses on adult tissues demonstrated comparable enrichment of miR-200s in mucosal, mucociliary, and secretory epithelial tissues (Supplemental Figure 2). Importantly, the mature forms of *miR-200* were not detectable in knockout animal tissues (Supplemental Figure 4). Levels of the primary *mir-200* transcripts, termed "*pri-mir-200b/a/429*" and "*pri-mir-200c/141*", were also enriched in lung and gut, compared with liver (Supplemental Figure 5). Since the levels of both primary transcripts were modest, but the mature forms were highly abundant in the epithelial tissues assayed, it is likely that *mir-200* is highly expressed and rapidly processed through the miRNA biogenesis pathway in these tissues.

mir-200c/141 is highly expressed in mucociliary epithelium in neonates

In order to determine miR-200 expression specificity at greater resolution, *mir-200c/141: LacZ* functional reporter mice (a generous gift from the McManus Lab at UCSF) were used. The *mir-200c/141: LacZ* mice (from now on referred to as "200c/LacZ") allowed investigation into which cell type expresses miR-200 within a given tissue (Figure 1C-D). I observed based on double immunofluorescence staining with anti-B-galactosidase, that 200c/LacZ is co-expressed with acetylated a-tubulin, and to a lesser extent, with Muc5ac in P0 and P3 neonates (Figure 2A-F). Co-expression of acetylated-a-tubulin and *miR-200c/141* suggests that the miR-200 family may play an important role in the development or function of motile ciliated cells (MCCs) that has not been previously known. However, fluorescence staining in goblet cells was less robust than in MCCs, suggesting that miR-200 may play a less important role in goblet cell biology (Muc5ac/b) (Figure 2E-F). Alternatively, miR-200 may function through MCCs in a non-cell autonomous fashion that affects other airway epithelial cells. Importantly, I did not observe co-staining with secretory Club cell marker CC10, suggesting that this secretory cell type may not require *miR-200* expression (Figure 2G-H). Similarly, no detectable B-gal signal exists in the alveoli with Pro-SPC in alveolar epithelial type II cells (AEC-IIs) or AEC type I (data not shown). Absence of *miR-200c/141* in AEC type I and type II cells at P0 and P3 suggests that the alveoli, – the functional unit of the lung necessary for gas exchange, – may also develop and function independently of *miR-200* expression.

Severe defects in pulmonary development and function are catastrophic for mammals. The proper transition between E18.5 and P0 in the airway epithelium is essential for the neonate to remove amniotic fluid from its airways, fill alveoli for gas exchange, generate protective secretions, and provide airway clearance by movement of fluid and debris.[81,82] Infants and

children with severe asthma or CF exhibit difficulties with adequate gas exchange, often due to debris and thick mucus accumulation that obstructs the airways. Thus, understanding the role of miR-200 in the proper development, regulation and maintenance of this complex tissue is imperative.

miR-200 DKO mice exhibit respiratory distress & perinatal lethality

Although deletion of individual miRNAs has not revealed many overt phenotypic deficiencies, recent studies have shown that failure to remove all homologous miRNAs allows functional compensation to mask the true importance of a given miRNA family.[3,41,45,111,112] Due to this inherent genetic redundancy, large miRNA families with two or more members at multiple loci may play essential roles in development and function in a myriad or biological contexts.[1,42,45] For instance, loss of *miR-200b* and *miR-429* leads to female infertility caused by a failure to produce the luteinizing hormone necessary to induce ovulation, while male knockouts retain their fertility.[112] However, there are still three members of the miR-200 family that are capable of compensating for loss of *miR-200b/429*. In order to assess the importance of the entire miR-200 family of miRNAs, I intercrossed *mir-200b/a/429*$^{+/-}$*; mir-200c/141*$^{-/-}$ animals to breed *mir-200 null* mice (knockout strategy shown in Figure 3E & F).

Strikingly, I observed that *mir-200ab/c* double knockout ("DKO") neonates displayed perinatal lethality with 100% penetrance compared to littermates who survived to adulthood and reproduced (Figure 3A). DKO neonates were born at expected Mendelian ratios with *mir-200ab*$^{+/+}$*; mir-200c*$^{-/-}$ single knockout (SKO) and *mir-200ab*$^{+/-}$*; mir-200c*$^{-/-}$ heterozygous knockout (HetKO) siblings (Supplemental Table 1). All littermates exhibited comparable weight, initial pink color, and cognitive behavior (pups can roll over and respond to probe stimuli) (Supplemental Figure 6 and data not shown). An anatomical difference of note is that DKO pups never exhibited a milk spot, – indicating a lack of milk in the stomach and failure to nurse, – while siblings develop milk spots of increasing size over the first 6 hours-post-parturition (hpp) (Supplemental Figure 7A). It is unlikely that starvation is the cause of this rapid death since neonates are capable of self-sustaining for 24 hours after birth by induction of the autophagy pathway, whereas DKOs die within 16 hpp.[113] Furthermore, DKO pups were capable of latching onto an anesthetized mother's nipple, demonstrating attachment capacity (Data not shown). In addition, while all pups appear normal initially, in the hours following birth, I observed an increase in labored breathing and cyanotic behavior specific to DKOs (Figure 3B; Supplemental Figure 8).

Interestingly, histology at E18.5 and immediately after birth (0hpp) appear normal in DKOs compared with their siblings (Supplemental Figure 9). The delay of the DKO phenotype suggests there may be a defect in airway clearance either by excess fluid, lack of flow, or another factor of airway homeostasis. Unfortunately, MCCs are not believed to have directed flow produced until P7.[82] However, we and one other group examined flow using fluorescent beads on tracheas from adults and neonates and found directed flow – though not robust – initiates as early as P0, which may be crucial in the neonate (Personal communication with Harland Lab, UC Berkeley).[82] Thus, it is not possible to rule out a defect in motility of DKO cilia

in MCCs. These data suggest that the clogging of the airways in DKOs may, at least in part, be due to compromised mucociliary movement capacity in DKO cilia.

Beginning as early as 4 hpp, DKO pups showed visible signs of respiratory distress; for this reason, I divided the DKO and sibling pairs into pre-terminal (0-4 hpp) and terminal-stage groups (>4 hpp-15 hpp) for assessment. The terminal DKOs appeared to gasp, become pale or even blue, indicating cyanosis, just before death. Upon dissection, terminal DKOs exhibited severe mucus and collagenous debris clogging in the small and large airways, which correlates with lobe collapse (Figure 3C, G-I; Supplemental Figure 10). Impressively, terminal DKO pups developed on average, collapse of two entire lobes out of five (Figure 3I; n=9). By H&E staining and whole lung analysis, a range of hyperinflation in the remaining, non-collapsed lobes was also visible, which may be due to a compensatory need to make up for the lost surface area for gas exchange (Figure 3G-H; Supplemental Figure 10). Such hyperinflation can also explain the labored breathing and gasping observed in terminal animals, but is likely a secondary effect to the airway clogging.

In addition to the visible collapse of entire lobes in the lung, DKOs also consistently exhibited a dark black material in their intestines that persisted for hours after birth, and after death (Figure 3D; Supplemental Figure 7B-D). The material is removable upon dissection, and visible in gut H&E sections as the contents within fully intact, pink and healthy intestinal villi, indicating that it is not necrotic tissue, but rather luminal contents, or meconium. The meconium has a distinct black color and sticky texture due to its origin and having accumulated *in utero* from the embryo swallowing amniotic fluid with dead cells and debris during development. Since the meconium has not passed from the DKO gut, but is rapidly lost from WT and littermate guts, I propose that this is evidence of a condition known as meconium ileus: the failure of a neonate to pass luminal contents due to excessive, sticky mucus – which is a trait seen in 36% of CF infant patients.[86] It is also worth noting, that *mir-200ab*$^{-/-}$*; c*$^{+/-}$ mice are 30% smaller than their siblings at P9, and exhibit hypertrophic goblet cells (data not shown). It may be that excessive mucus production prevents adequate absorption of nutrients for growth, which is an additional trait seen in CF patients.

DKOs succumb to respiratory distress comparable with Cystic Fibrosis and Asthma

The short-lived nature of this airway obstruction phenotype precludes development of infection or an excessive inflammatory response – levels of *MCSF* and *MCSF-R* remained constant in DKOs and siblings (Supplemental Figure 12). However, in acute episodes of respiratory distress seen in CF or asthma patients, airway obstruction caused by excessive, sticky mucus can be fatal without medical intervention. Importantly, recent studies performed by others show that during an asthmatic attack, cytokines such as IL-13 are released causing airway constriction and mucus release, which correlates with down-regulation of *miR-200* levels in goblet cell metaplasia samples[85,114] (and unpublished, Prescott Lab, UCSF collaboration).

The severity of the mucus plugs and the collapse of the alveoli in DKOs is ultimately catastrophic for the requisite gas exchange necessary for survival. In order to quantify the volume of mucus accumulating in terminal DKOs, Periodic-Acid-Schiff (PAS) staining was

performed (Figure 4A-D). As expected, copious amounts of mucus can be seen in the luminal airways of DKOs but not WT or sibling controls showing a significant correlation between mucus accumulation, lobe collapse, and DKO lethality (Figure 4 and personal communication with Woodruff Lab at UCSF). Furthermore, DKO pups present with apparent meconium ileus (MI), which is a clog in the intestine due to inappropriate, sticky mucus production in the intestines, which further supports the notion of a mucosal defect.

Also, infants whose parents are carriers are tested for chloride imbalances in their sweat shortly after birth, since CF patients exhibit sticky sweat secretions in addition to their pulmonary and GI tract symptoms. DKO pups appear to exhibit a stickiness on their skin by virtue of the fibrous pieces of bedding that adhere to their skin, but not to their siblings' even hours after birth (Figure 3B). Thus, the complete loss of miR-200 generates defects in the gut and skin comparable with human Cystic Fibrosis, as well as mucociliary defects consistent with pulmonary deficiencies observed in both CF and asthma.

Loss of miR-200 imposes defects on lung tissue integrity and cellular composition

In order to further dissect the mechanism by which DKO lung tissue is failing, it was necessary to assess epithelial layer integrity as well as major cell type ratios and organization. Since miR-200 is classically tied into a well-characterized, negative feedback loop involving the transcription factors Zeb1 and Zeb2, and by extension, to the epithelial marker E-cadherin, I began my assessment of the pulmonary tissue by examining the levels of these factors. If loss of miR-200 correlates with defects in epithelial fate or tissue integrity, one would expect a reduction in E-cadherin levels with concomitant increases in the Zeb proteins, which inhibit E-cadherin transcription[4,115]. However, qPCR performed on WT, sibling and DKO tissues showed only modest or no differences in *E-cadherin* and *Zeb1* levels (Figure 5A & B). The lack of appreciable decrease in *E-cadherin* suggests that it is not dependent on miR-200-mediated suppression of *Zeb*. Moreover, the unimpressive increases in levels of *Zeb1* suggest that miR-200-mediated suppression is not the only mechanism in place to down-regulate *Zeb* expression and prevent adoption of mesenchymal fate.

I next examined E-cadherin by immunofluorescence (IF) to determine if there was a difference in abundance or localization of E-cadherin in DKO epithelial tissues, despite the unaltered *E-cadherin* mRNA levels. Interestingly, E-cadherin appears to stain more intensively in the DKO tissues compared with siblings, and appears as a mislocalized haze at cell junctions and in the cytoplasm (Figure 5C-H). Although there is some mislocalization, E-cadherin appears to make adherens junctions required for epithelial sheet formation, so this increase and disorganization of E-cadherin may play a contributory role to additional defects in the respiratory and gut epithelium.

Based on these studies, it is possible that the pulmonary pathology I observed may be due, at least in part, to reduced epithelial tissue integrity. However, the effect of miR-200 loss does not follow the classical model of *miR-200* and *Zeb* regulation. In fact, there was little effect on E-cadherin levels, which suggests there is likely an additional mechanistic defect or defects contributing to this lethality. Due to this unexpected result, I consulted two mouse histologists

from the UC Davis Mouse Biology Program: Dr. Denise Imai and Dr. Stephen Griffey, as well as a mouse lung expert: Dr. Astrid Gillich from Stanford University; and none could detect any major differences in the gut and lung epithelial architecture of DKOs compared with siblings and WT. Thus, due to the severe pathology I observed in the lungs of terminal mice, I elected to perform a more in-depth analysis of this tissue and its major cell types.

First, I examined the major cell types that make up the lung by investigating expression profiles by q-PCR and localization of the different cell type markers by immunofluorescence (IF not shown). Surprisingly, expression of secretory cell type markers CC10 (Club Cells), Muc5b (Goblet cells), and Surfactant Protein-C (Alveolar type II cells) showed consistent expression in WT, siblings, and DKO lungs (Figure 6A-C). Also, motile ciliated cell-marker, Foxj1 levels were virtually unchanged in DKOs (Figure 6D). Interestingly, T1a, a marker of Alveolar type I cells showed a 50% decrease of expression in both sibling controls and DKO compared with WT (Figure 6E). Since AEC-Is are the site of gas exchange in the lungs, this is a crucial cell type for alveolar function; however, since siblings and DKOs exhibit the same reduction in T1a, and miR-200 is not expressed in AEC-I cells, it is unlikely to be the cause of respiratory distress that leads to DKO lethality.

Since miRNAs act to suppress mRNA translation of their targets, I also examined cell type localization by protein detection in tissue sections. Neonate, (P0) lungs showed normal localization, organization, and ratios of $CC10^+$ Club cells and $SP\text{-}C^+$ AEC-IIs (not shown). However, there was an intriguing difference in $Muc5b^+$ goblet cells and $Acetylated\text{-}a\text{-}tubulin^+$ motile ciliated cells (MCCs) in the large airways (Figure 7 and 8). Consistent with the PAS staining, I observed significant pooling of $Muc5b^+$ material in the airways and in collapsed alveoli (Figure 7E-F & K-L). Correspondingly, there was a significant reduction $Muc5b^+$ (and PAS^+) cells in the airways of DKOs, and cells that are positive have less $Muc5b^+$ staining within their cells than their siblings, possibly from excessive secretion (Figure 7A-F). It was unclear however, whether the mucus was stimulated by debris or by inappropriate, dysregulated release. Indeed, fresh neonates taken within 0-3 hpp showed expected numbers of PAS^+ cells in their airways, whereas terminal pups showed a marked reduction that correlated with mucus plugs and lobe collapse (Personal communication with Woodruff Lab, UCSF).

In addition to abundant mucus in the airways, DKOs exhibited a subtle increase in abnormal-ciliated and non-ciliated MCCs based on high-power, confocal imaging of acetylated-a-tubulin IF (Figure 8A-E). Impaired ciliogenesis, or "ciliopathies" have been previously described to yield impaired mucus and debris clearance, chronic infections, and in some cases death.[45,78,116,117]
Since we have demonstrated that directed flow by cilia initiates as early as the first two days post parturition, the structure and beating of the cilia on MCCs in DKOs is likely an important contributor to the clogged airway phenotype. Comprehensive IF studies using acetylated-a-tubulin (cilia), Foxj1 (MCC transcription factor), and g-tubulin (basal body marker) were performed on WT, siblings and DKO lungs. $Foxj1^+$ cells were present in expected ratios (not shown), and g-tubulin staining proved ineffectual due to the delicate nature of the DKO neonate airway (not shown). However, by acetyl-a-tubulin staining, there was a trend of abnormal, short cilia in DKOs compared with controls (Figure 8E). Although this abnormality

could be due to a developmental retardation, it is clear that there is a higher degree of frequency of MCCs that will be ineffective at providing fluid flow in DKO pups. Transmission electron microscopy (TEM) provided additional insights into the ultrastructure of ciliated MCCs at P0. WT and control siblings showed more cilia that were apically anchored, with basal bodies perpendicular to the plane of the cell surface, allowing axoneme outgrowth in the same perpendicular trajectory (Figure 8F-H). On the other hand, DKO MCCs had more frequent basal bodies that appeared parallel to the apical surface, some with cilia which then display a transverse section through the axoneme structure, indicating the cilia are parallel to the cell surface, rather than perpendicular (Figure 8I-L). These data suggest that an increased abnormal ciliation of MCCs is occurring in DKO airways and may in part contribute to the defective clearance of debris and mucus that precipitates lethality. In essence, the combinatorial effects of excessive mucus, impaired ciliogenesis, and weakened tissue integrity may provide the perfect 'storm' to induce rapid morbidity in DKO pups due to respiratory failure.

miR-200 deficiency affects male and female fertility

Since mucociliary defects were present in the pulmonary system, it follows that tissues with similar structures might also exhibit deficiencies. Due to the early-stage lethality of DKO animals, assessment of testis or fallopian tubes was impossible. However, during the course of breeding single locus knockouts for miR-200, I observed a distinctive loss of fertility in *mir-200a/b/429* knockout but not *mir-200c/141* knockout males and females. Another group of investigators partially corroborated this observation by demonstrating that mere loss of *miR-200b* and *miR-429* but not *miR-200a* leads to a defect in luteinizing hormone production and consequently, a failure to ovulate, making female knockout mice infertile.[112] Interestingly, this group also reported the *miR-200b/429* KO males retained their fertility, and that complementation of luteinizing hormone to *miR-200b/429* KO females allowed ovulation to resume and fertility to be restored. In contrast I observed an apparently more severe fertility defect in my *mir-200a/b/429* knockout females and males. Of the *mir-200a/b/429* knockout males set up with wildtype females, 0/9 successfully impregnated females; whereas females set up with *mir-200a/b/429*$^{+/-}$ or wildtype males, became pregnant (n=22/22; Table 1). Similarly, none of the *mir-200a/b/429* knockout females set up with wildtype males, became pregnant (n=5; Table 2).

In addition to the breeding deficiencies in *mir-200a/b/429* KO animals, I also noticed that *mir-200a/b/429*$^{+/-}$*; mir-200c*$^{-/-}$ (KO Het) females exhibited difficulties in breeding. KO Het females were intercrossed with KO Het males to produce DKO pups, and although pregnancy frequency was relatively regular, a number of females had miscarriages wherein embryos were resorbed, pups died inside the mother and had to be removed by cesarean section, or females had long bloody labors that required cesarean section for pups to be rescued (Table 3). In comparison to other laboratory strains, the frequency of these miscarriages and failed labor induction is highly increased. In addition, according to Jackson Laboratories, the rate of mouse miscarriages in their wildtype colonies is close to zero, whereas KO Hets have a 23% frequency (unpublished observations).

Intriguingly, studies of the miRNome of endometriosis biopsies from human uterine walls had highly upregulated levels of *miR-200a*, *200b*, and *141* compared with healthy tissue, suggesting that imbalance of miR-200 levels could correspond to increased lesions.[118] Since endometriosis is a painful overgrowth of endometrium that can hinder fertility, this may account for the reduced litter size observed in *mir-200ab*$^{+/-}$*; c*$^{-/-}$ females, which is not observed in *mir-200ab*$^{+/-}$*; c*$^{+/+}$ females, perhaps due to compensation by *miR-200c* (Table 3).

Since the male fertility deficiency was not previously described, I investigated the reason for this defect more closely. Surprisingly, *in vitro* fertilization experiments performed with collaborators in the Lishko Lab revealed that 2 out of 3 *mir-200a/b/429* knockout males generated sperm that were capable of fertilization at the wildtype frequency of 80% (Personal communication with Lishko Lab, UC Berkeley). This suggests that the sperm in *mir-200a/b/429* knockout males is not defective when placed directly on top of an oocyte, however, in natural matings, when they must swim up the birth canal, they fail. Indeed, by imaging the *mir-200a/b/429* KO sperm, it is clear that there is a structural defect in the attachment of the axoneme (Figure 9A-C). I performed IF with Acetyl-a-tubulin in order to better assess the unusual head-axoneme attachment but found the composition of the axoneme comparable with WT (Figure 9D-F). However, similar to what was shown in the bright field images, the attachment of the axoneme appeared abnormal in 200ab KO males compared with WT (Figure 9G). Moreover, when imaged live, the swimming phase of the flagellum in 200ab KO sperm is highly irregular and precludes efficient forward motion, which could explain the infertility in natural matings (not shown).

In order to further evaluate this structural defect, I performed transmission electron microscopy (TEM) to visualize the ultrastructure of the *mir-200a/b/429* KO sperm compared to wildtype. Similar to the phenomenon in the MCCs, the TEM revealed the perpendicular attachment of the axoneme and sperm head, but failed to offer additional information. It is clear from these studies that, similar to the apparent ciliogenesis phenotype in the lungs of DKO pups, *mir-200a/b/429* KO sperm show defects in the axoneme – a structure closely related to the cilia in motile ciliated cells, and required for movement of or through – viscous fluid.

Loss of miR-200 in Xenopus laevis yields abnormal Mucociliary Epithelium

Mammalian and amphibian miR-200 miRNAs are conserved at the mature sequence and seed region levels, and display similar enrichment in differentiating mucociliary epithelium (Figure 10, 11 and Supplemental Figure 3).[8] Since *X. laevis* embryonic epidermis is similar to mammalian airway epithelium, it represents a highly useful tool to explore conserved modes of miRNA regulation in motile ciliated cells and goblet-like cells. In order to discern developmental and functional differences in miR-200 deficient frog epidermis, I designed and co-injected *miR-200b* and *miR-429* morpholinos (MOs) alongside a control scrambled MO into 8-cell *stage X. laevis* embryos (Figure 12A). If miR-200 is important for ciliogenesis in frogs, one would expect a comparable reduction in cilia number and organization in *miR-200* MO injected verses Control MO injected embryos. Surprisingly, I observed a significant increase in MCC number in mature mucociliary epithelium (Figure 12C-F). Since the experiment was repeated and the results confirmed, it is possible that there is a compensatory response to the defect in

miR-200-deficient MCCs that is masking the effect of miR-200 loss. However, we also allowed injected and uninjected embryos to develop further into swimming larvae, in order to look for skin infections that might implicate defective mucociliary development or function. Unfortunately, no infections were observed.

Discussion

The miR-200ab/c family of miRNA represents the first family of noncoding RNA whose deficiency leads to manifestations of a severe, asthma or cystic fibrosis-like disease in mice. The effect of germline *mir-200ab/c* deficiency has never been described, and our results showed a 100% penetrant, lethal pulmonary defect in mir-200 DKO pups within 16 hours after birth. Classically, mir-200 overexpression is associated with increased levels of E-cadherin and epithelialization, whereas loss of this miRNA correlates with down-regulation of E-cadherin-mediated adherens junctions and adoption of mesenchymal cell traits.[4] Surprisingly, we observed minimal changes in E-cadherin levels and no gross tissue morphological changes that suggested major effects on epithelialization or tissue integrity.

We have confirmed the enriched expression of mir-200 in epithelial tissues – particularly in the lungs and gut, described previously in adult mice and mucociliary epidermis in frogs.[8] However, we demonstrated that mir-200 is essential during perinatal stages of development, between E18.5 and P0, a fact not previously known. We further showed that mir-200 is specifically expressed in motile ciliated cells and goblet cells; cell types whose microRNA expression profiles are not currently defined at the single cell level. We also quantitatively illustrated the increased mucus volume in the airways and the decreased number of functional ciliated MCCs in terminal DKO pups. Our data clearly show that DKO pups have defective mucociliary epithelium due to excessive, rapid mucus secretion from goblet cells and failed motile ciliary clearance of the airways resulting in lobe collapse and death.

Our studies cannot currently distinguish between a developmental delay in MCC cilia maturation and intrinsic ciliary structural defects that preclude functional mucociliary clearance. Such ciliopathies are usually not perinatally lethal, but much remains unknown regarding the functional interplay between MCCs and goblet cells.[105,119] Genetic lesions that affect cilia formation and function typically cause defects in the nasal and pulmonary airways, ventricles in the brain, the oviduct, and testes.[45] Indeed our findings suggest that loss of mir-200 causes defects in the docking and orienting of the basal body and projection of the axoneme structure in MCCs of DKOs as well as the flagella of spermatozoa in mir-200ab KO adult males. However, we did not observe defects in the brain or oviduct (data not shown). It would be interesting to further dissect the question of developmental delay verses true structural defect by using conditional double knockouts in order to have enough tissue material from adult airways for *in vitro* assays, but these studies are not currently possible.

Importantly, we find enrichment of expression of mir-200 in the olfactory epithelium in neonate and adult mice, which support previous findings in human tissue (Supplemental Figure 3).[1,8] Moreover, we demonstrated directly that loss of just the mir-200 family in mice leads to

substantial cell death of progenitors in the main olfactory neuroepithelium (MOE) in the nasal cavities of DKO pups but not in heterozygous knockout, or *mir-200c/141* single knockout MOE (Supplemental Figure 16). Our findings are in agreement with previous work which showed a similar effect in zebrafish olfactory neurogenesis by morpholino knockdown of mir-200, again highlighting the conserved nature of the mir-200 family.[1] Also, this group used an MOE-specific Dicer knockout mouse to inhibit production of all miRNAs and effectively recapitulated the cell death in the olfactory epithelium seen in fish.[1] Importantly, the cell death in neonate neuroepithelium may contribute to our collectively lethal DKO phenotype by virtue of compromised airway function, but this must be verified with additional studies.

Our data also suggest that mir-200 DKO pups suffer from either an excess production of mucus or inappropriate secretion of mucus into their airways and gut. Since the expression levels of mucin genes remain consistent across WT, littermate, and DKO samples, we propose that the defect resides in the secretion of mucin into the airway lumen. However, when considering secretion of mucus, one must also consider water content, because goblet cells secrete mucin molecules, which are highly branched, enormous glycoproteins that must be hydrated to form mucus.[6,90,91,105] Importantly, imbalances in ion and osmotic flow across the airway epithelial barrier will change the volume and viscosity of mucus.[105] Respiratory disorders such as cystic fibrosis are ultimately fatal because of the thick, sticky mucus resulting from insufficient hydration of mucins in their airways.[97,99,120] Our terminal DKO histopathology is consistent with other models of cystic fibrosis with the added benefit of displaying respiratory, gut, and reproductive manifestations of CF, while other models exhibit either respiratory or gut defects.[6] Additional studies are required, however, to further dissect the mechanistic underpinnings of the defect in DKO goblet cells.

In addition to the essential regulation of ion and osmotic flow, we must consider function and activity of purinergic receptors such as P2X and P2Y family members, which can contribute to misregulation and function of mucociliary epithelium in mir-200 DKOs. Importantly, MCCs are capable of secreting purines that can act on goblet cells to promote mucus secretion.[104,105,107] Our future studies will assess the putative role of mir-200 in regulating the expression or activity of these receptors and channels as they may pertain to our excessive mucus secretion phenotype in DKO pups.

Similar to the viscous fluids in the lungs of CF patients, thick, sticky secretions in the gut, pancreas, and sweat also are known to be comorbid effects in CF patients.[87–89] Due to the ion imbalance in epithelial tissues, CF patients exhibit difficulties with digestion caused by thick pancreatic secretions and mucus that prevent effective breakdown of food and extraction of nutrients.[88,89] Ineffective digestion and corresponding trouble with weight gain and nutrition is common in CF.[87,88] Moreover, excess mucus secretions from intestinal goblet cells that hinder nutrient absorption, weight gain, and peristalsis also contribute to CF symptoms. Correspondingly, we have shown that DKO neonates exhibit meconium ileus, an effect observed in other CF mouse models as well as in 36% of human infants with CF.[6,86] Importantly, our preliminary studies in mir-200ab knockout; mir-200c heterozygous animals displayed a 30% reduction in size and weight between P10 and through 6 weeks of age (n=6), and 3/6 of these

animals had to be sacrificed by 3 weeks of age due to severe emaciation and necrosis in the intestines, which is similar to what is observed in gut-specific CF mouse models (Supplemental Figure 19 and not shown).[6] Our future studies include acquiring increased numbers and further investigating into the gut phenotype of mir-200ab KO; c HET animals, but the implications that this may tie into our CF-like disease model are intriguing.

Due to the common goblet cell type between lung and intestine, paired with purinergic receptor regulation of mucus secretion in both tissues, we are very interested to investigate the putative role of mir-200 in mucociliary and mucosal epithelium function and maintenance. It is our hope that mir-200 DKO animals may provide unique insights into cystic fibrosis and asthma since this – to our knowledge – is the first example of a miRNA deficient mouse model that recapitulates both respiratory and gut defects seen in patients with CF.

Summary

The miR-200 family of miRNAs are highly pleiotropic, with required function in highly specialized tissues such as the ameloblast for tooth formation, olfactory epithelium (Supplemental Figures 14, 15 & 16), and pituitary gland for LH production and ovulation.[1,3,112] Based on the data presented here, we may also add pulmonary mucociliary epithelium, intestinal epithelium, and spermatogenesis. miR-200 is essential for the proper development and function of motile-ciliated cells which may directly or indirectly effect goblet cells. The data suggest that miR-200 DKO pups somehow secrete excessive amounts of mucus in a short amount of time, and either by viscosity or mechanical deficiency, the cilia fail to clear it. Similarly, the gut epithelium of the DKO neonates exhibits meconium ileus and excessive amounts of mucus accumulation. Further testing is needed to assess the composition of this mucus, but the implications are that MI in these pups is in part caused by excess mucus secretion. Sticky mucus accumulation in the airways is a hallmark of both asthma and cystic fibrosis, and thus, the mir-200 DKO mouse may provide invaluable insights into these diseases not currently modeled in existing experimental systems. Moreover, the combination of pulmonary and gut mucociliary defects comparable to human CF, is a novel observation, and to our knowledge, the only model to encompass such severe effects simultaneously. Aside from the mucus production, it is clear that cilia and related structures such as the sperm flagella exhibit defects in their attachment and orientation. Abnormal cilia orientation in the airways may lead to compromised ciliary beating and directional flow, but further imaging studies must be performed to confirm this hypothesis. Indeed, the perpendicular orientation of the sperm flagella precludes normal wave motion, which will hinder the ability of the sperm to swim through the viscous fluid in the birth canal, and thus prevents fertilization in natural matings. Lastly, further studies using the frog model are necessary to confirm the efficacy of MO knockdown, and to assess the characteristics of these miR-200-deficient MCCs and goblet-like cells. It will also be interesting to consider alternative molecular regulators downstream of miR-200 targets such as purinoreceptors and purine channels. Purines can be released by MCCs into the airways, and an excess of this signaling molecule will actively promote mucus secretion from goblet cells in a non-cell autonomous fashion.[105] The miR-200 DKO mice represent a complex, yet intriguing and highly informative system from which we may glean unique insights into the biology of mucociliary epithelium and potentially illuminate alternative pathways for intervention in asthma and CF disease.

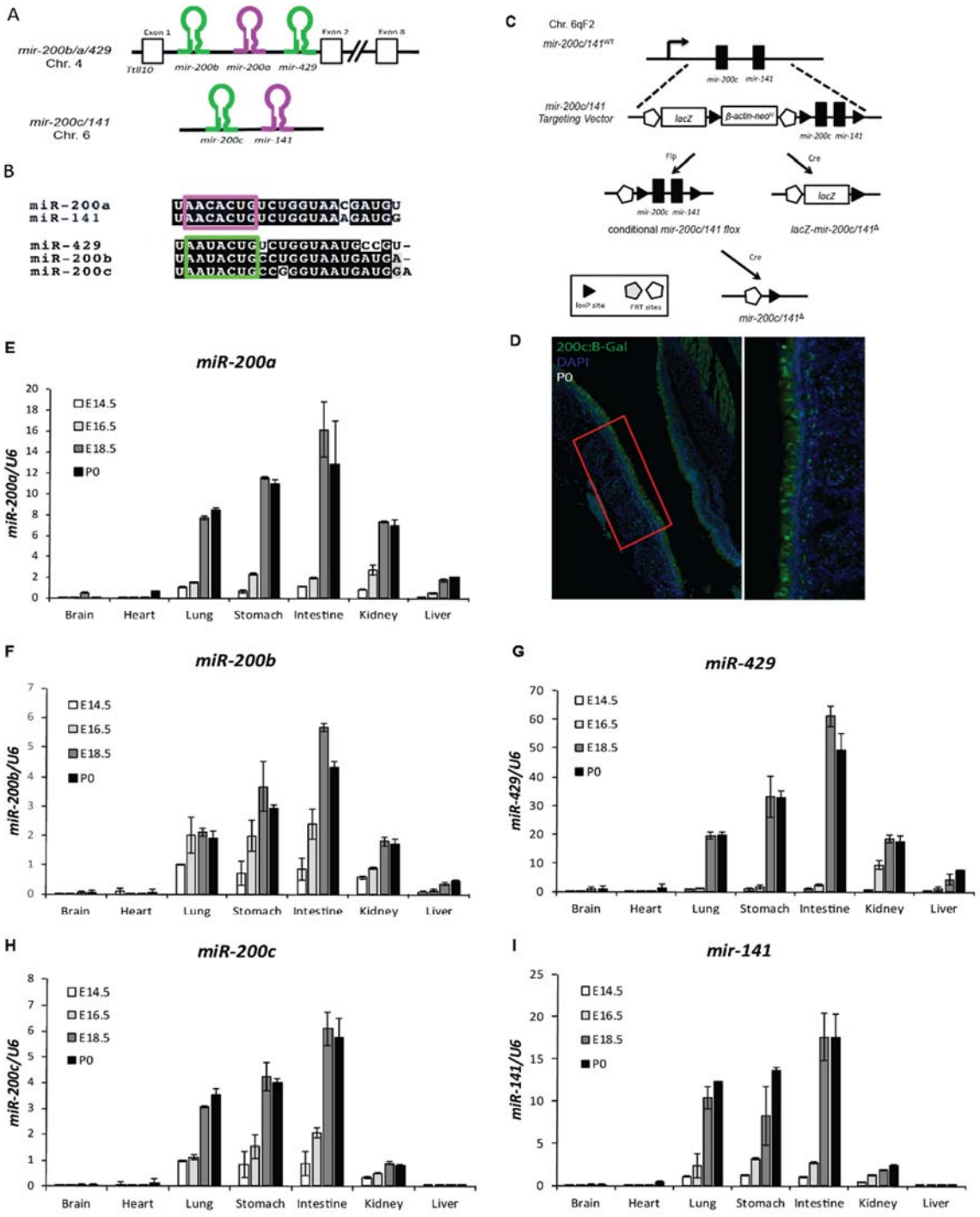

Figure 1: Genomic structure of the *miR-200* family and expression profile. The miR-200 family exists at 2 distinct genomic loci: *mir-200b/a/429* and *mir-200c/141* (A). The family is divided into sub-groups based on seed sequence homology highlighted in pink and green (B). A *mir-200c/141: LacZ* reporter genomic locus (C) and immunofluorescence staining of B-galactosidase in the broncho-pulmonary epithelium at P0 (D). Expression of all five members of the miR-200 family is enriched in epithelial tissues, peaking in P0, neonates (E-I); qPCR based on two pools from four individuals per pool, per timepoint, performed in triplicate (E14.5-E18.5, Embryonic Day).

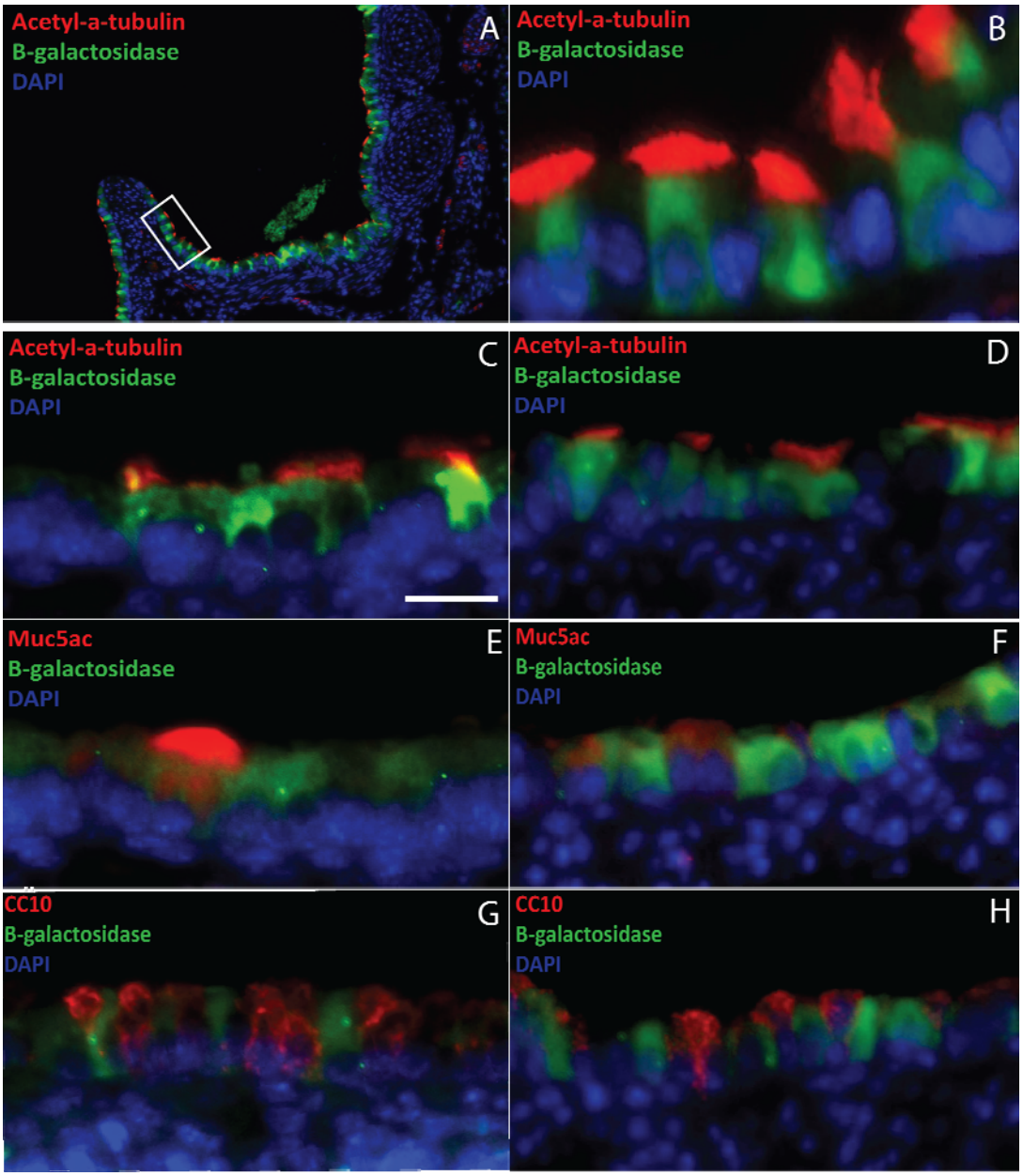

Figure 2. *miR-200* expression is enriched in mucociliary epithelium in neonate airways. Immunofluorescence detecting a *mir-200c*-driven B-galactosidase with Acetyl-a-tubulin (MCCs) A-D; Muc5ac (Goblet Cells) E & F, CC10 (Club Cells) G & H is shown at P0 (C, E, G) and P3 (A, B, D, F, H) timepoints. Colocalization of B-gal and Ac-a-tubulin and Muc5ac but not CC10 at P0 suggest an important role for *miR-200* in MCCs and Goblet cells. No B-gal signal was detected in the alveoli, suggesting AEC-I and -II cells do not express miR-200 (data not shown). Scale bar 10um.

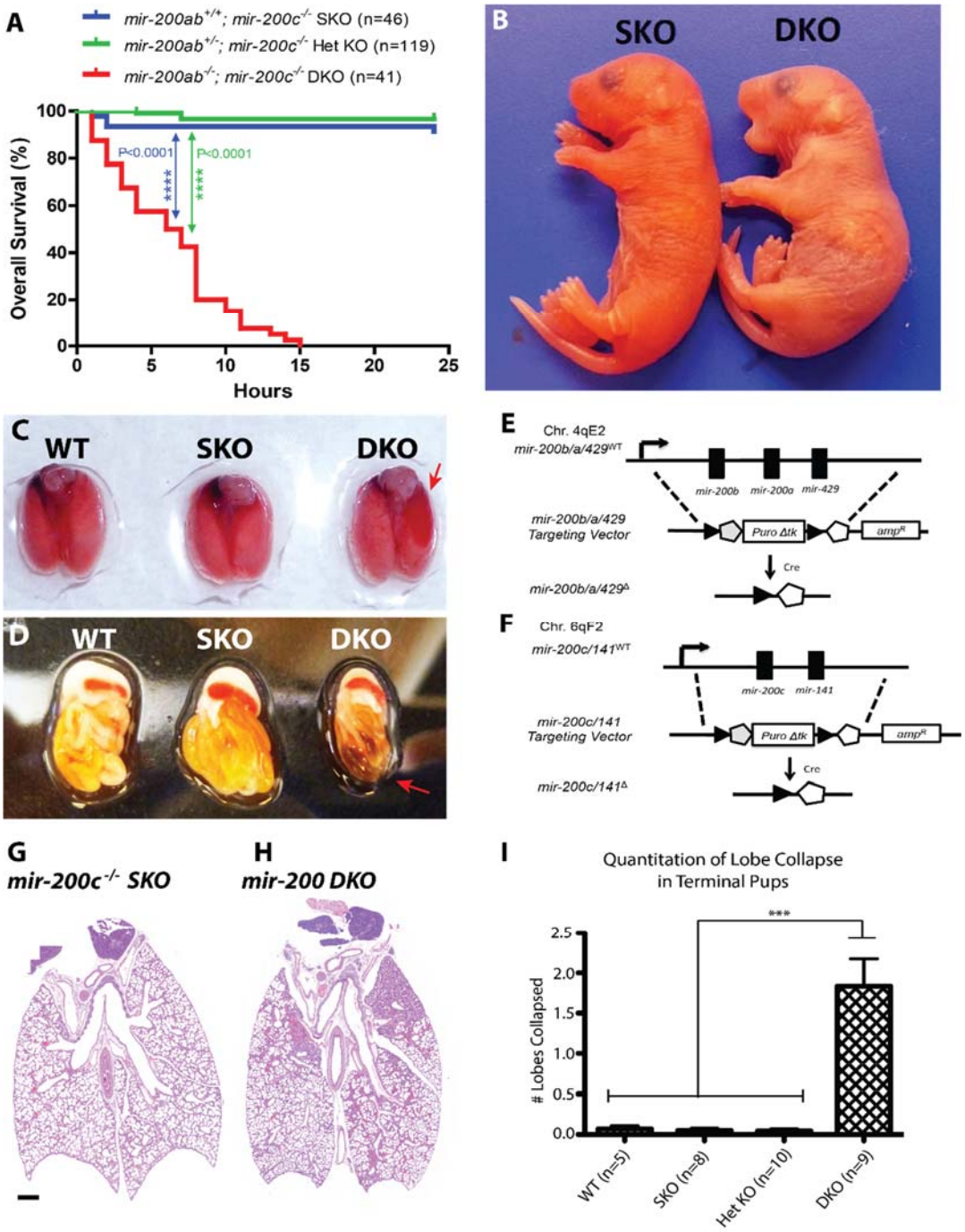

Figure 3: The *miR-200* family is essential to mucociliary development and survival. All pups deficient in *miR-200* (double knockouts, "DKOs") die within 16 hours after birth while siblings (single and heterozygous knockout, "SKO" and "Het KO") survive to adulthood (A). Terminal DKO pups present with cyanotic behavior indicative of respiratory distress (B); upon dissection, collapsed lobes are apparent (C, red arrow). DKO pups also exhibit meconium ileus (failure to pass waste through the GI tract, D). The knockout strategy for the *mir-200b/a/429* and *mir-200c/141* loci (E & F). Histology (H&E stain) illustrates a representative degree of lobe collapse in a 6hpp SKO and DKO littermate pair (G & H). Semi-quantitative analysis of DKO, littermates and WT pups in I, summarizes the degree of lobe collapse per individual, with an average of two lobes being completely collapsed in terminal DKOs.

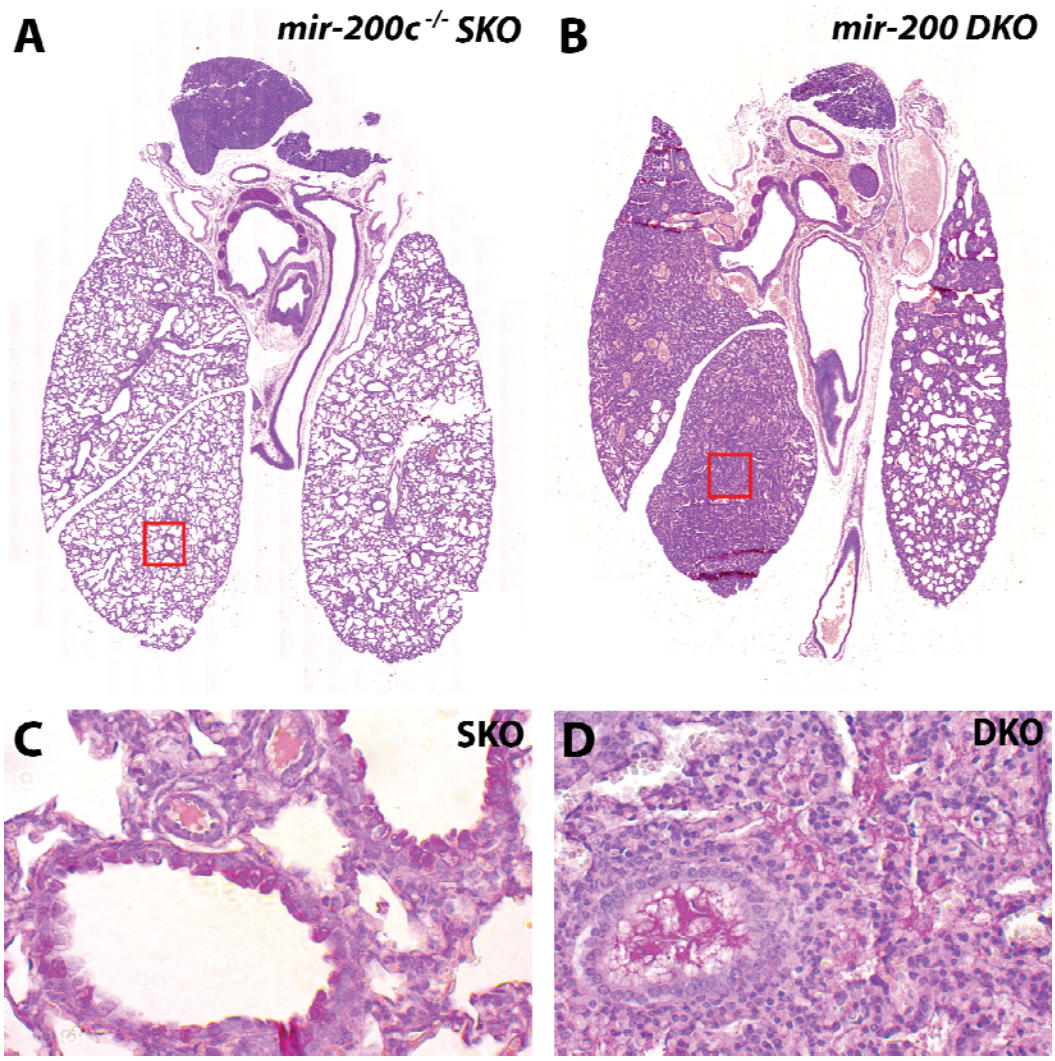

Figure 4: Mucus Accumulation in the Airways Leads to Severe Lobe Collapse and Lethality.
Panels A and B show wholemount lung sections from SKO and DKO siblings stained with Periodic Acid Schiff (PAS) stain to detect mucin in goblet cells and mucus in the airways (dark pink); C and D show higher magnification of SKO and DKO (red boxes). Quantitation of the volume of mucus obstructing the airways in our samples was significant ($p<0.0001$) between DKO (n=5) and WT (n=4), Het KO (n=5), and SKO (n=5) (personal communication with a collaborator in the Woodruff Lab at UCSF).

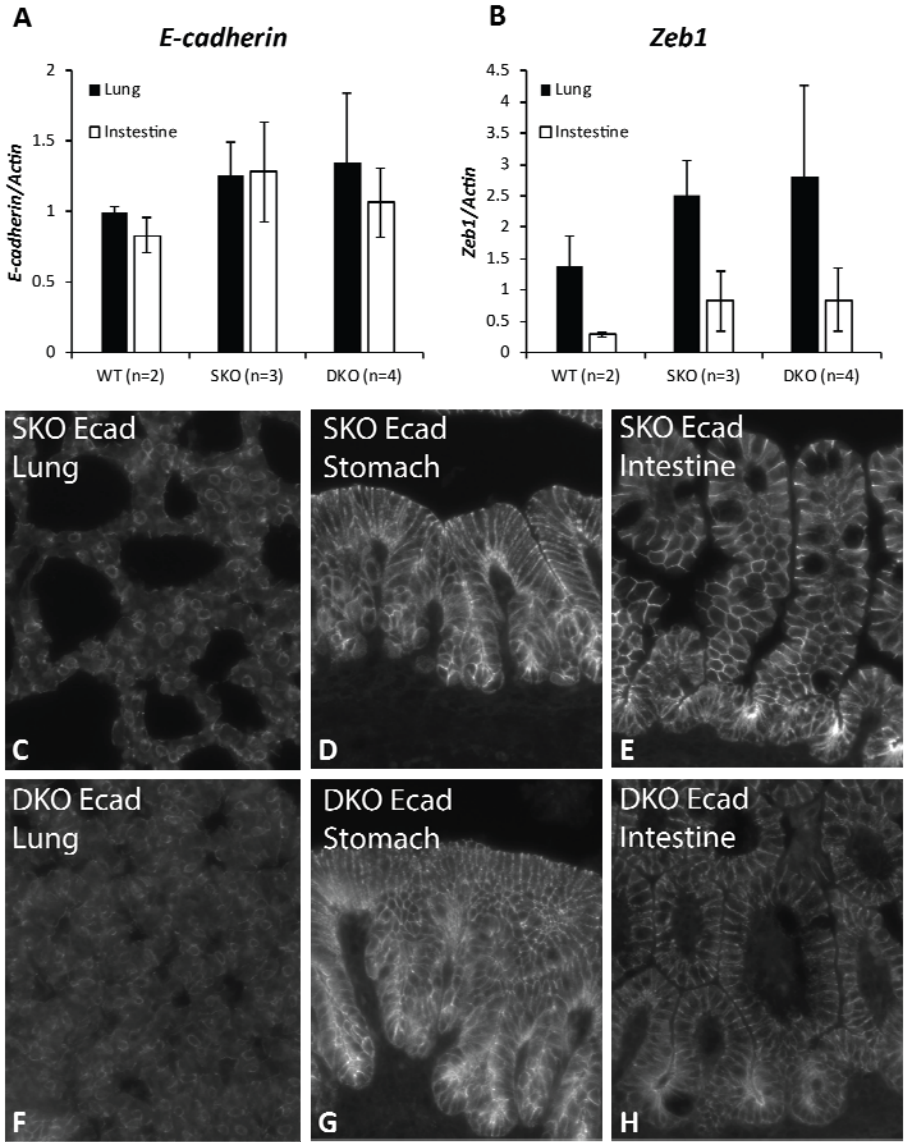

Figure 5. E-cadherin and Zeb1 expression in epithelial tissues in DKO and SKO littermates. *E-cadherin* (A) and *Zeb1* (B) expression is comparable between WT and single KO and double KO siblings. However, levels of E-cadherin by IF appear more crisp and defined in SKO tissues (C-E), while E-cadherin may be slightly increased and mislocalized in the DKO lung (F), stomach (G) and intestine (H), leading to a more hazy signal.

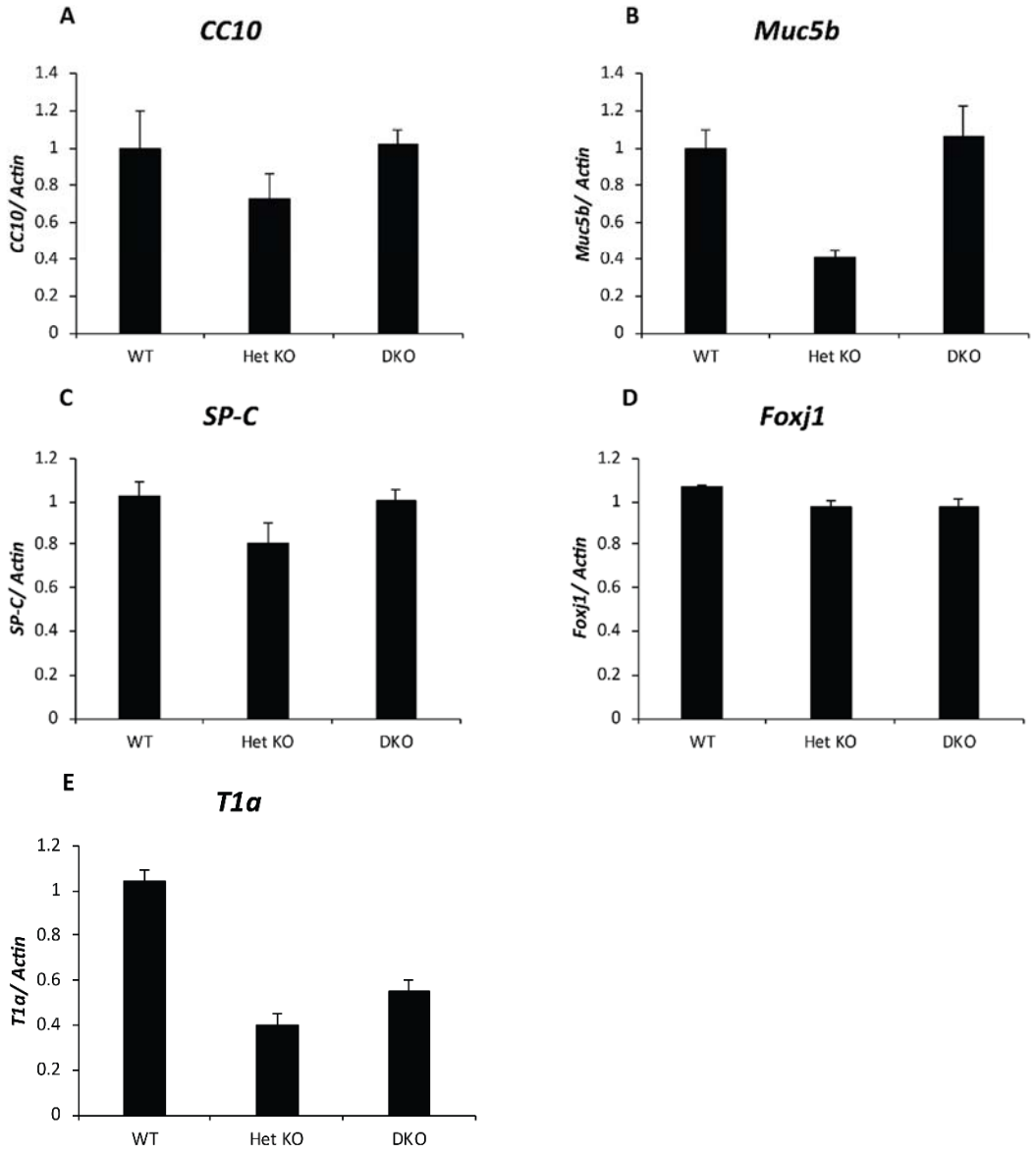

Figure 6: q-PCR markers for pulmonary tissue cellular subsets show modest differences. CC10 marks Club cells, a secretory club cell which shows no changes at the mRNA level (A), and similar numbers of CC10+ cells by IF in DKOs and siblings (data not shown). Muc5b marks mucus secreting goblet cells (B), SPC marks surfactant producing AEC-II cells (C), and Foxj1 is specific for ciliated MCCs, which all show similar mRNA levels and cell numbers (IF not shown). AEC-I cells responsible for gas exchange show a marked reduction at the mRNA level in littermates and DKOs (E), but no gross differences in alveoli cell number are apparent in DKOs (not shown).

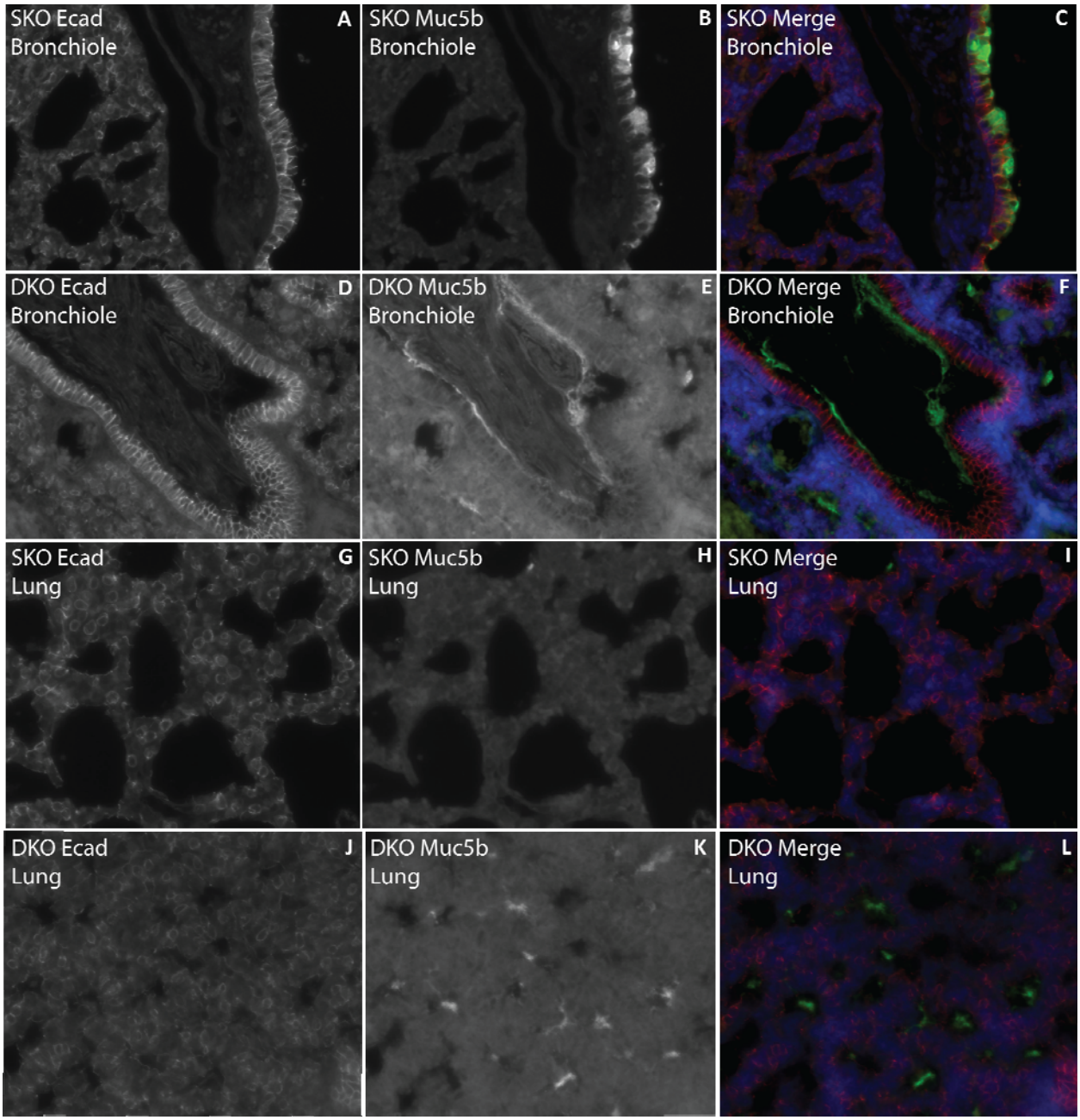

Figure 7: Expression and localization of Muc5b^{+} cells and mucus in DKOs. Mucus is stored in the form of mucin prior to release from goblet cells and intensive intracellular Muc5b staining is evident in the bronchi of SKO animals, but severely reduced or absent from the goblet cells of terminal DKOs (A-F). DKO has a large plug coated with mucus (E & F), and mucus is also observed coating the alveoli throughout the DKO lungs (even in those distant from plugs), whereas no such staining is seen in siblings (n=4 per genotype).

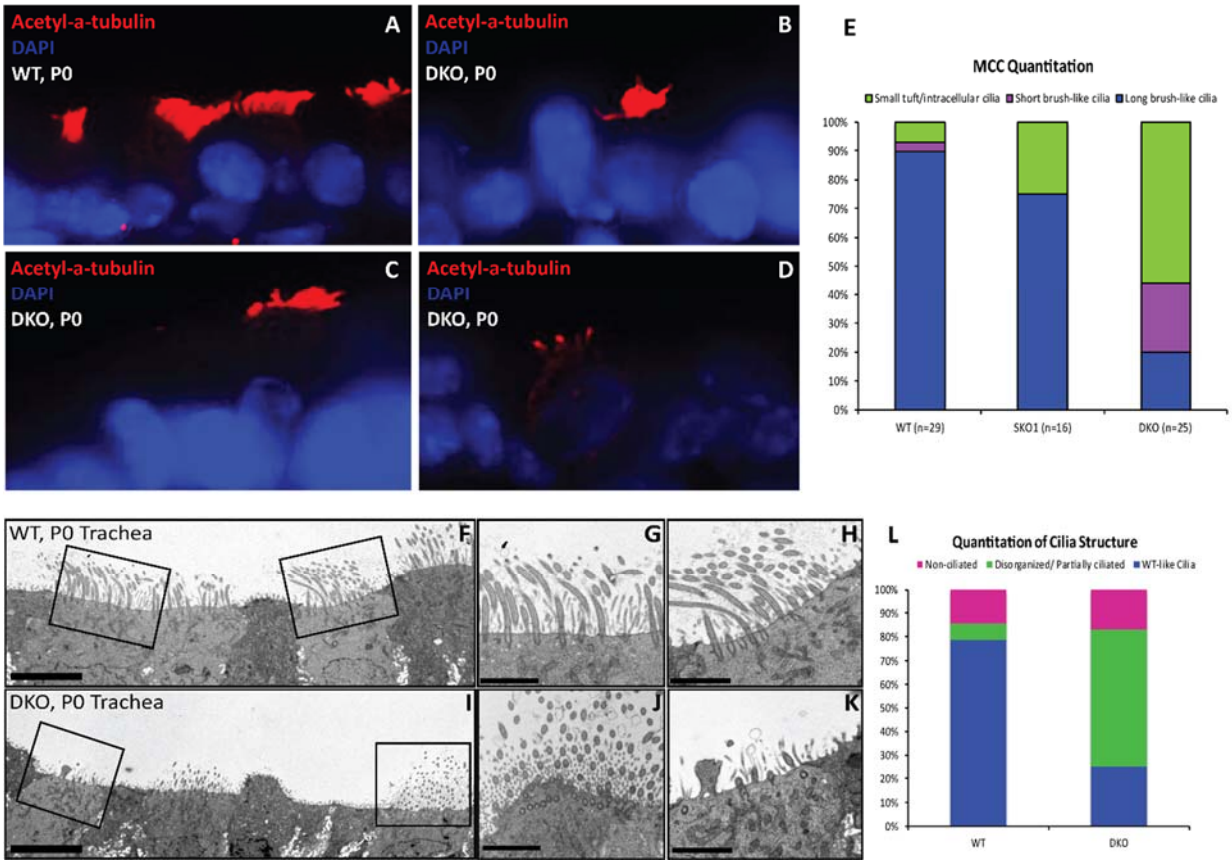

Figure 8: DKOs exhibit impaired ciliogenesis. Immunofluorescence imaging of Acetyl-a-tubulin marking the cilia of MCCs in DKOs and controls illustrates the abnormal, disorganized nature of the cilia structure (A-D). Quantitation of abnormal cilia (E). Transmission Electron Microscopy (TEM) reveals deficiencies of basal body anchoring and angular projection of the axoneme cilia structure causing a partial or disorganized conformation of cilia in DKOs compared with controls (F-K). A-D scale bar 5um, F & I scale bar 5um, and G-H and J-K scale bar 2.5um. Quantitation in E of small, tuft-like, short and long brush-like cilia based on four animals per group**.** Quantitation of "WT" ciliated, disorganized/partially ciliated and non-ciliated cells by TEM (L); WT n=1, DKO n=2.

200ab KO Males	Number of WT Females Set Up with	Pregnancies	Births	Births when Female set up with WT Male
ab KO1	2	0	0	Yes
ab KO2	2	0	0	Yes
ab KO3	2	0	0	Yes
ab KO4	4	0	0	Yes
ab KO5	2	0	0	Yes
ab KO6	4	0	0	Yes
ab KO7	2	0	0	Yes
ab KO8	2	0	0	Yes
ab KO9	2	0	0	Yes

Table 1: *miR-200ab* KO Male fertility rates. *mir-200b/a/429* null males are incapable of generating offspring when place in natural matings (n=9 males; n=22 WT or 200ab$^{+/-}$ females). All females were subsequently set up in natural matings with WT or 200ab$^{+/-}$ males and gave birth to at least one litter. Surprisingly, *mir-200b/429* null males retain their fertility, perhaps due to the presence of *miR-200a*.[112]

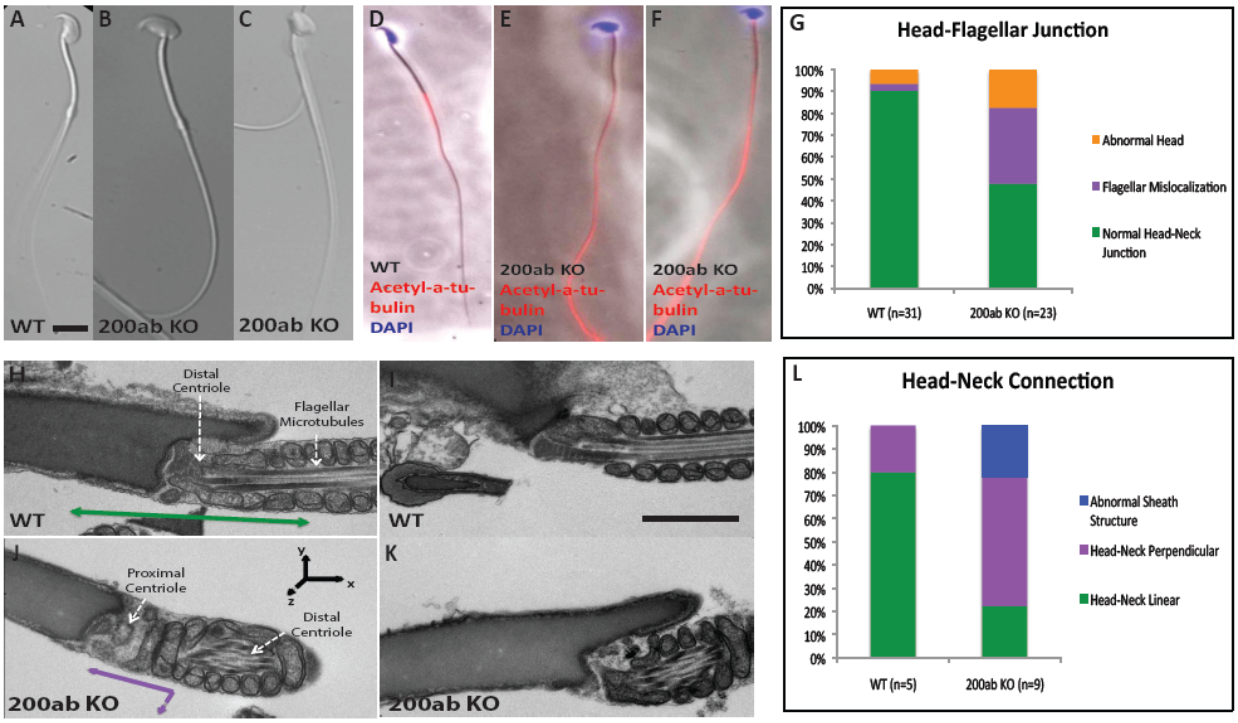

Figure 9: *mir-200b/a/429* KO males exhibit abnormal sperm. Light microscopy of live, miR-200ab KO sperm display abnormal head-flagellum attachment and shape compared with miR-200ab WT (A-C). Immunofluorescence reveals comparable acetyl-a-tubulin staining in WT and miR-200ab KO sperm (D-F). Quantitation of flagellar junction in G (repeated n=3 miR-200ab KO males, all similar ratios). TEM imaging highlights the perpendicular attachment seen in miR-200ab KO males and not in WT counterparts (H-K). Quantitation of head-neck observations (L).

200ab KO Females	Number of WT Males Set Up with	Pregnancies	Births
ab KOF1	1	0	0
ab KOF2	1	0	0
ab KOF3	1	0	0
ab KOF4	1	0	0
ab KOF5	1	0	0

Table 2: *miR-200ab* KO Female fertility rates. *mir-200b/a/429* null females are incapable of becoming pregnant or giving birth to progeny when place in natural matings (n=5 females; n=5 WT males). All males were subsequently set up in natural matings with WT or 200ab$^{+/-}$ females and gave rise to at least one litter. *mir-200b/429* null females are also infertile, despite the presence of *miR-200a*.[112]

Females Crossed	Average Births/ Female	Average Litter Size	Cesarean Section Rate
$200ab^{+/-}$; $c^{-/-}$ Females N=70	1.23	5	23%
$200ab^{+/-}$; $c^{+/+}$ Females N=28	3.97	8	0%
$200ab^{+/+}$; $c^{-/-}$ Females N=24	3.82	7	0%

Table 3: *mir-200ab$^{+/-}$; c$^{-/-}$* females exhibit reduced litter size and require frequent Cesarean section intervention to rescue pups**.** WT, *mir-200ab$^{+/-}$; 200c$^{+/+}$* and *mir-200ab$^{+/+}$; 200c$^{-/-}$* females were never observed to require cesarean section or to miscarry after achieving a full-term pregnancy and tended to have larger litter sizes.

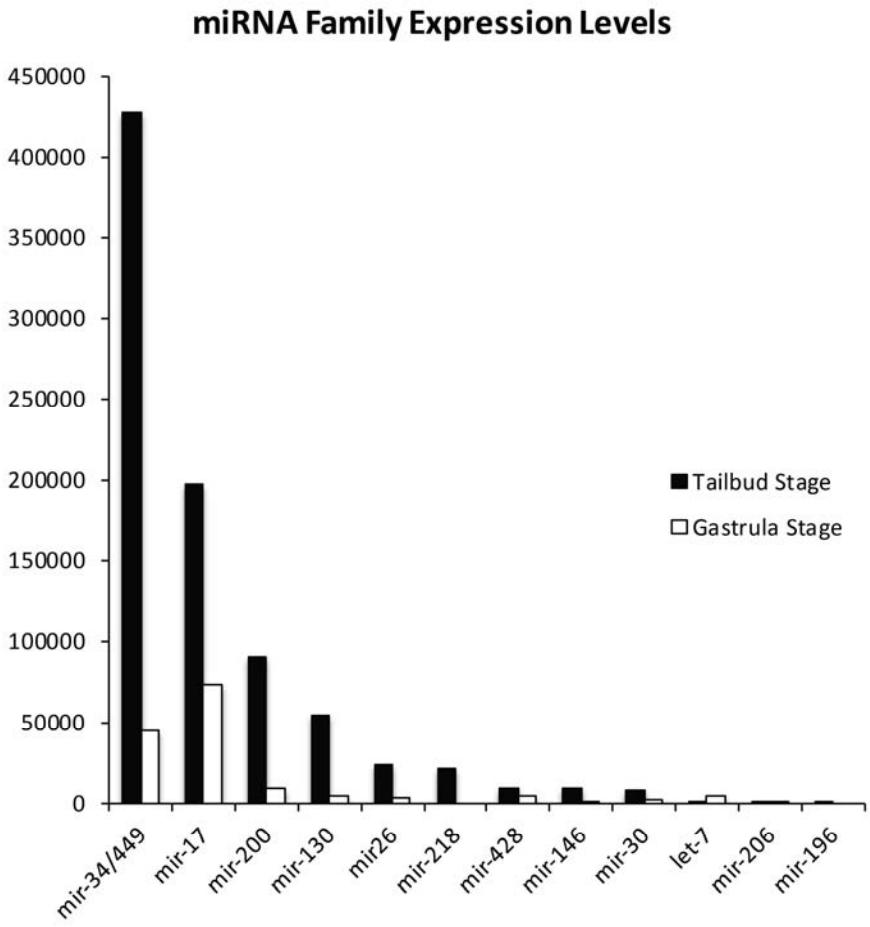

Figure 10. The miR-200 family is the third most enriched miRNA in *X. laevis* epidermis. Mining from published datasets of microRNA microarrays in non-ciliated (gastrula) and ciliated (tailbud) epidermis show enrichment of miR-200.[8]

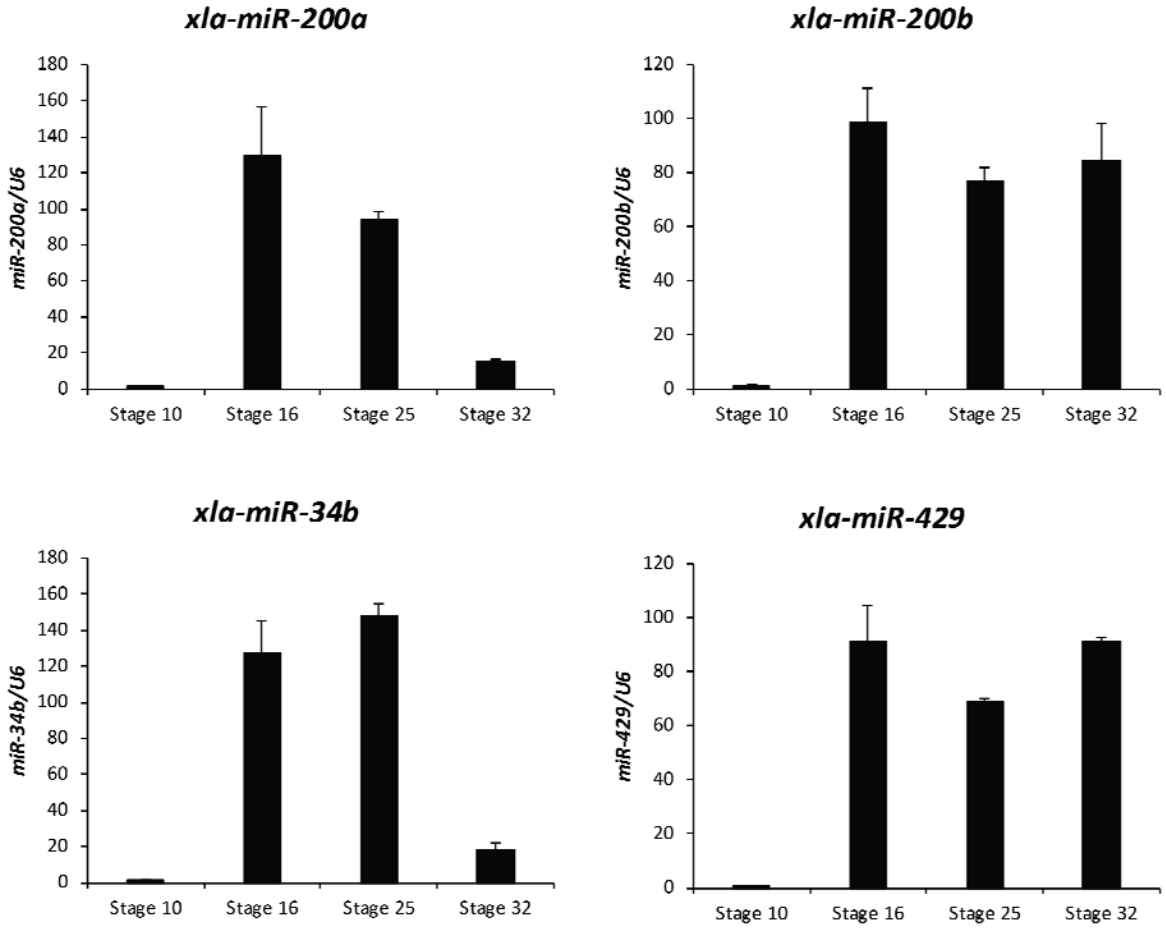

Figure 11. Expression of *miR-200* in developing *X. laevis* epidermal explants. Expression of annotated mir-200 family members are expressed at increasing levels during differentiation of mucociliary development in frogs with the exception of *miR-200a*, which is high in early tailbud stage (25), but decreases in late tailbud stage (32). The *miR-200b* and *miR-429* levels increase and remain high, suggesting that since these miRNAs are transcribed equivalently, *miR-200a* may be turned over more rapidly or *miR-200b* and *miR-429* are more efficiently processed. The *miR-34b* miRNA is a well characterized MCC-specific miRNA characterized as being under the transcriptional control of factors that promote MCC fate.[45,109]

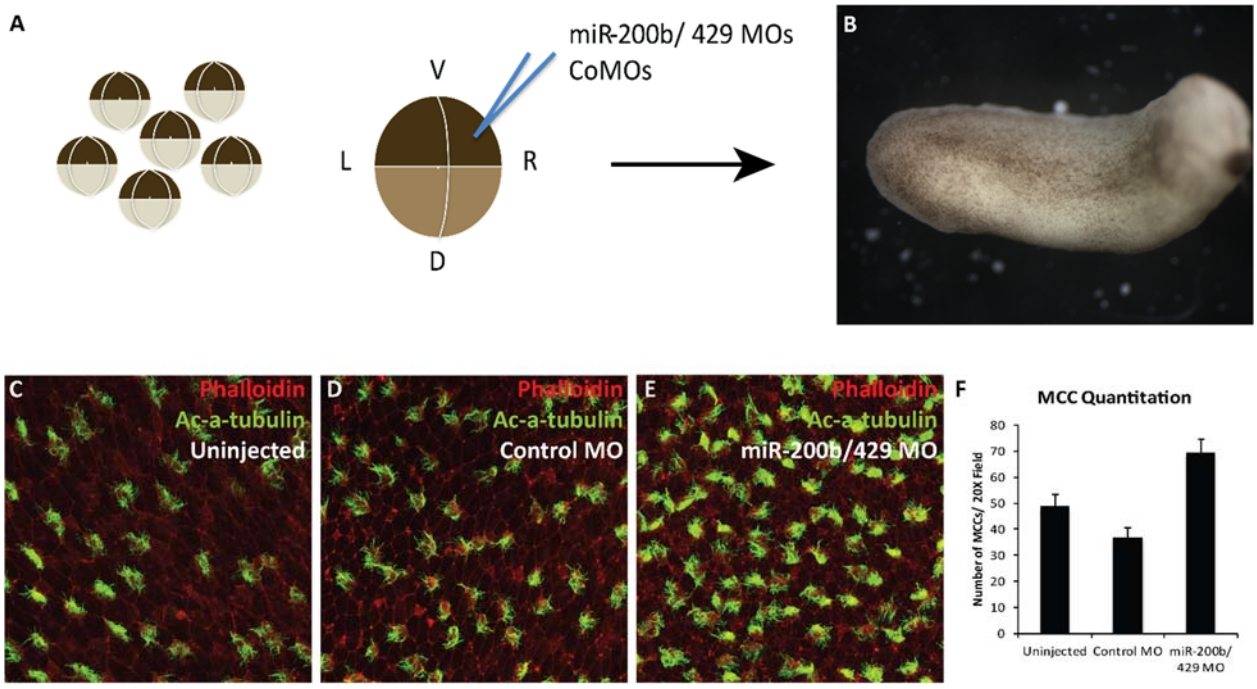

Figure 12. Morpholino knockdown of *miR-200b/ 429* in *X. laevis* embryos affects MCCs. Eight cell stage *X. laevis* embryos were collected and injected in the ventral-right and dorsal-right blastomeres with control or miR-200b/ 429 morpholinos (A), and allowed to develop until tailbud stage (B). Immunofluorescence for cilia marker, acetyl-a-tubulin (MCCs) demonstrated retention of MCC formation, but an increase in MCC numbers (C-F). The experiment was repeated twice with uninjected (n=9), control MO injection (n=8), and miR-200b/ 429 MO injected (n=18) total.

Supplemental Material

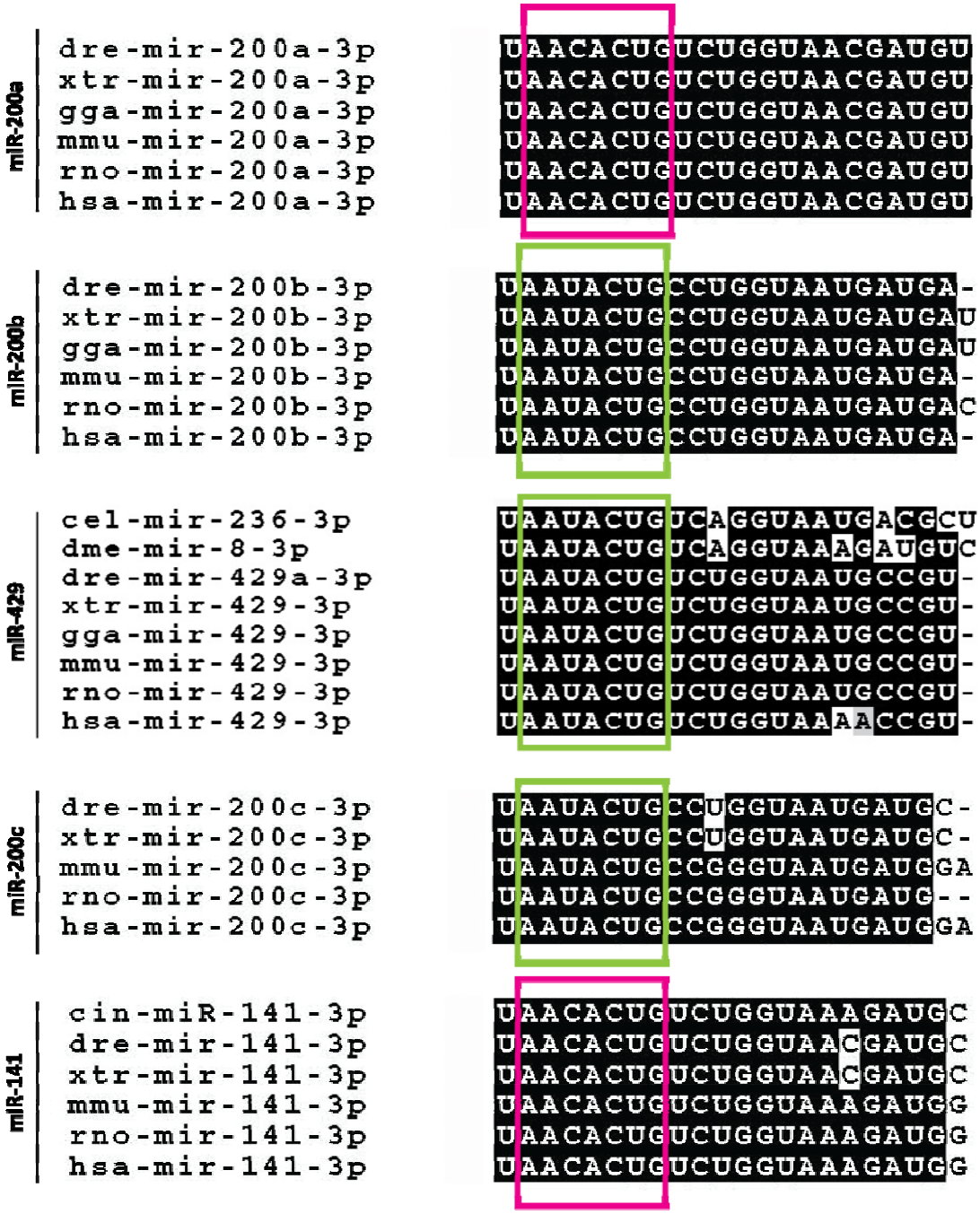

S Figure 1: Multi-species alignment of ancestral miR-200 family members. Seed sequence homology (pink and green boxes) is completely conserved from invertebrates through mammals including humans. Importantly, the other miR-200 family subgroup differs by a single nucleotide in the seed region between invertebrates and vertebrates, highlighting this duplication event during evolution and orthologue formation.

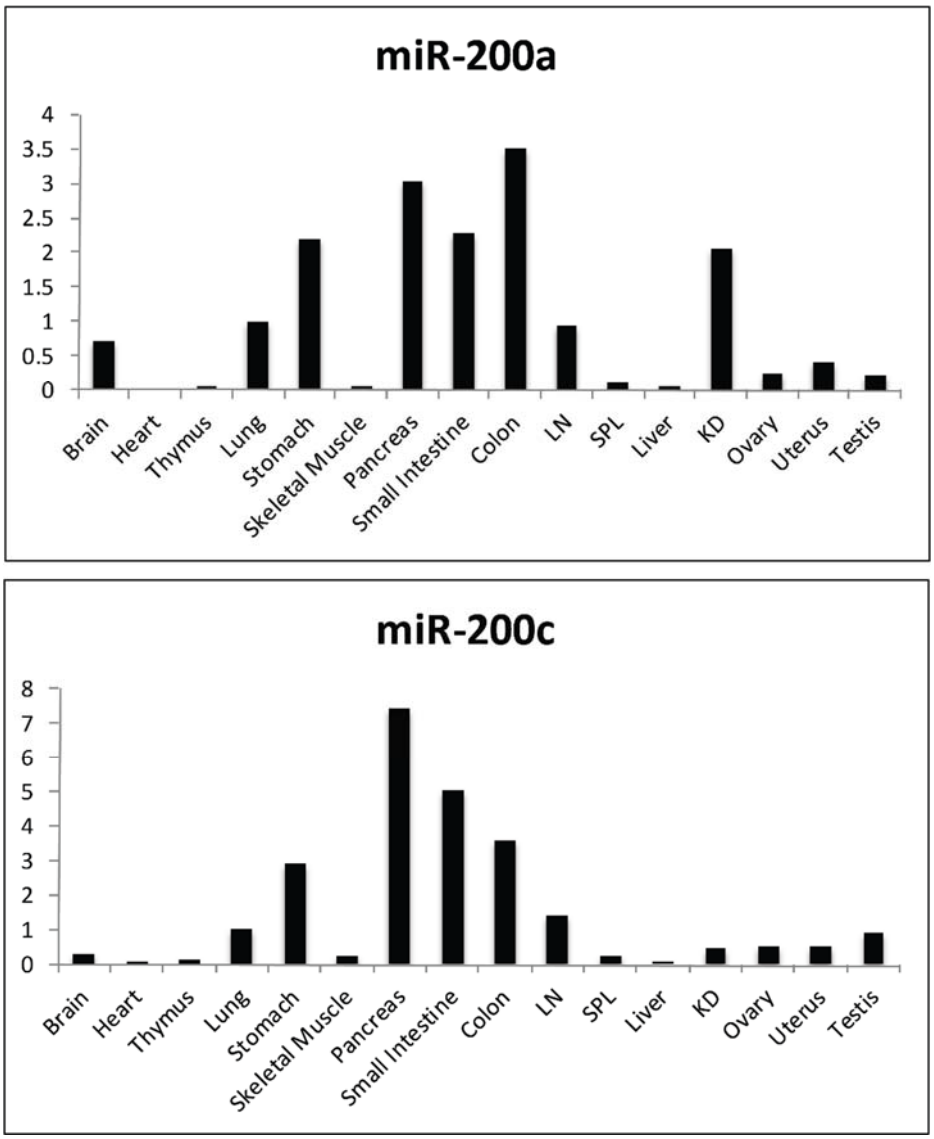

S Figure 2: Expression of miR-200 in adult tissue panel. Expression profiles of miR-200 change slightly in adults, in which both miR-200a and miR-200c show enrichment in epithelial tissues – particularly in the gastrointestinal tract, pancreas kidney, and lung. Of note is the mucosal (GI tract), mucociliary (Lung) and secretory (Pancreas) qualities of these tissues, which may relate to broad miR-200 functional importance in these tissues.

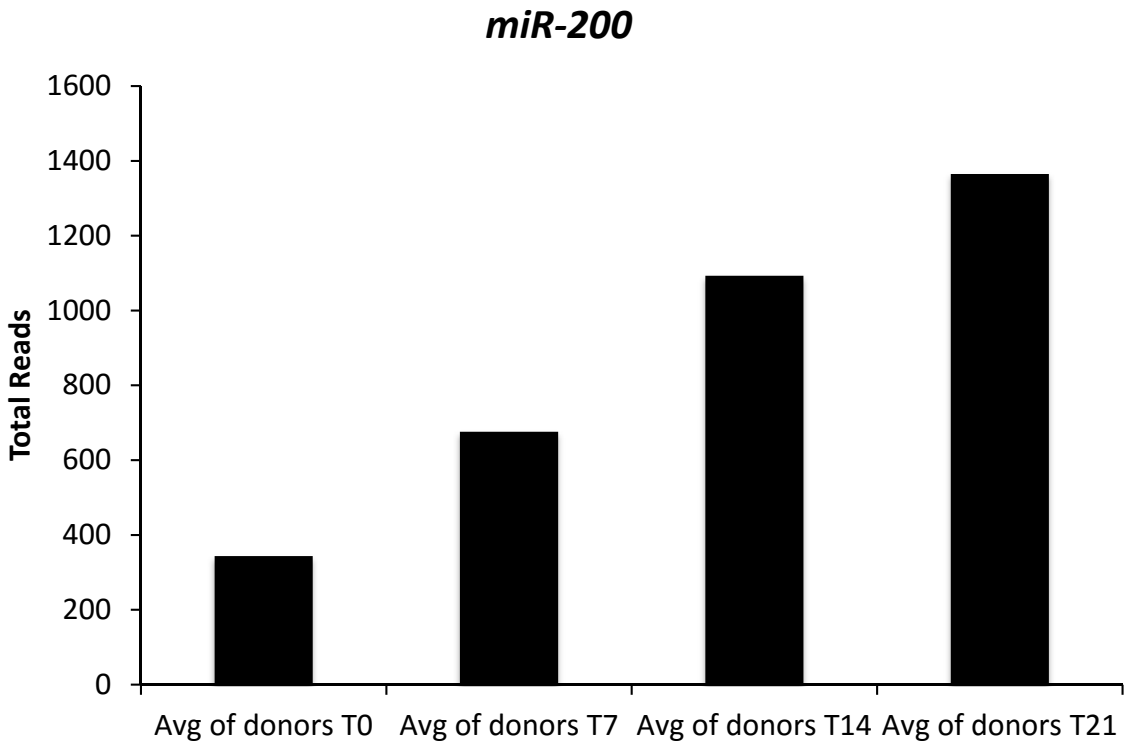

S Figure 3: miR-200 expression is enriched in human ALI culture. Mining from published datasets of microRNA microarrays in non-ciliated (T0) and ciliated (T21) human inferior turbinate, or nasal polyp biopsies, cultured in Air Liquid Interface (ALI) culture conditions shown to support mucociliary development and differentiation show enrichment of miR-200 in mucociliary epithelium.[8,121]

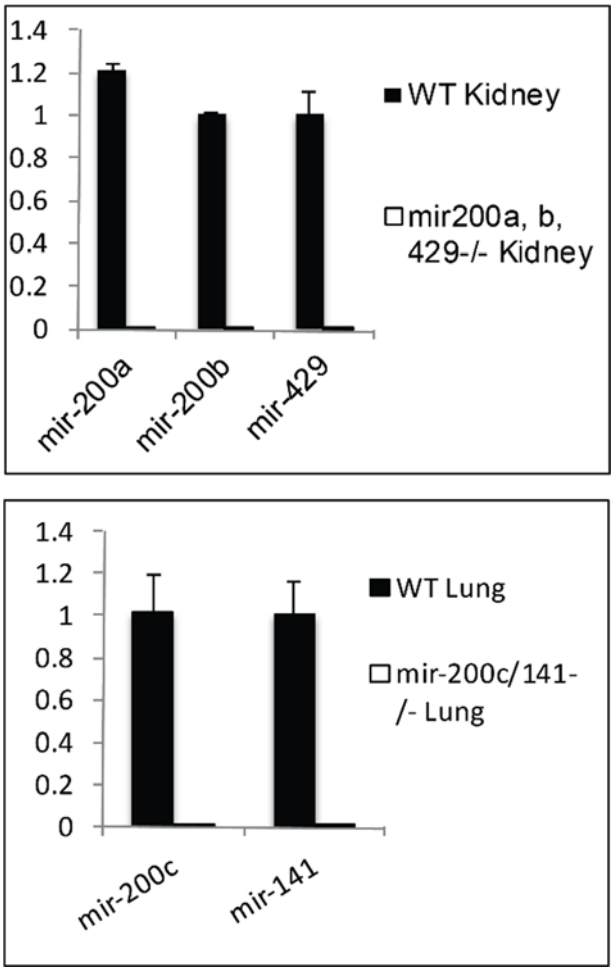

S Figure 4: Sensitivity and Specificity of TaqMan mature microRNA assays. TaqMan Assays were tested for specificity by performing qPCR for *miR-200a*, *miR-200b*, and *miR-429* on WT tissue and *mir-200b/a/429 null* tissue (A). Assays for qPCR of *miR-200c* and *miR-141* were performed on WT tissue and *mir-200c/141 null* tissue (B). All assays could not detect their targets in the null tissues, but easily detected them in tissues known to express miR-200.

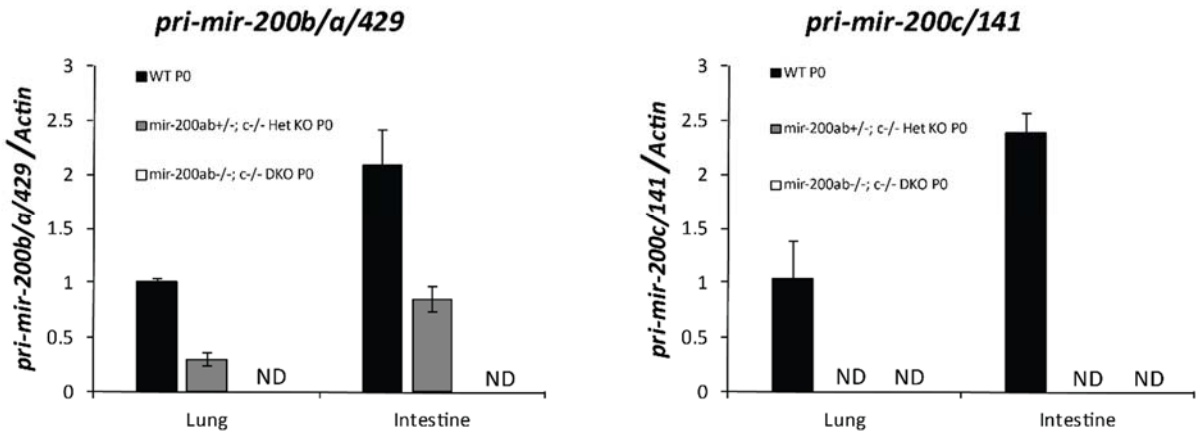

S Figure 5: Primary *mir-200* transcript qPCR. Levels of *pri-mir-200b/a/429* (A) and *mir-200c/141* (B) were specifically detected by TaqMan assays and show enriched expression in Lung and Intestine of WT and to a lesser extent, heterozygous mice, but not in *null* tissues.

Genotype	# Pups	Percentage of Total
mir-200ab $^{+/+}$; *200c* $^{-/-}$ SKO	94	26.4%
mir-200ab $^{+/-}$; *200c* $^{-/-}$ HetKO	184	51.8%
mir-200ab $^{-/-}$; *200c* $^{-/-}$ DKO	77	21.6%

S Table 1: Mendelian Ratio of *mir-200ab*$^{+/-}$; *200c*$^{-/-}$ intercross matings. Normal ratios of single knockout, heterozygous knockout, and double knockout pups were observed (n=70 mothers).

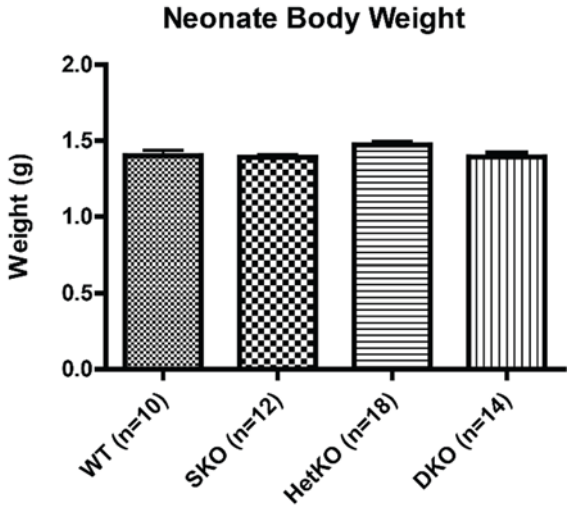

S Figure 6: Body Weight of miR-200 neonates. At birth, all pups were weighed and found to have comparable size and weight between WT controls, SKO and Het KO littermates and DKOs.

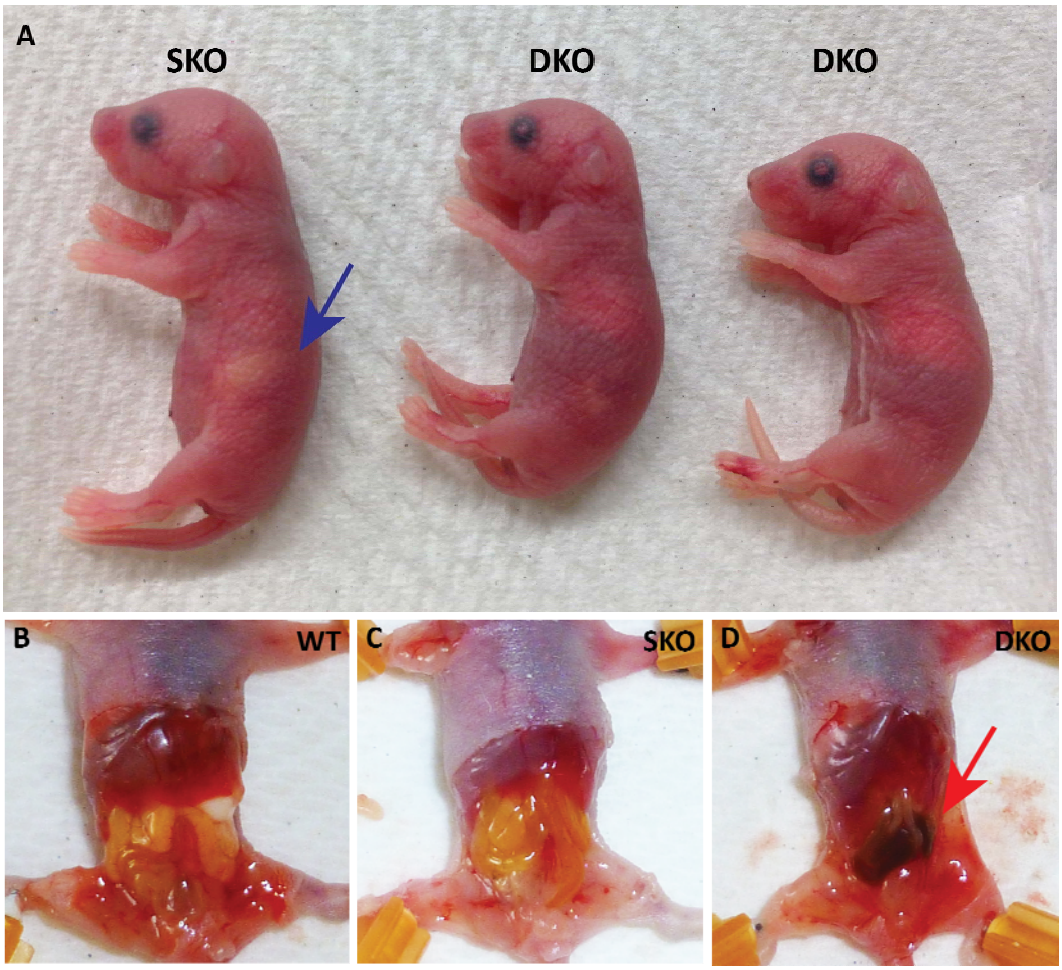

S Figure 7: *miR-200* neonate gut appearance 6 hours post parturition. SKO (and Het KO, not shown) siblings exhibit consistent presence of a milk spot, whereas DKO pups do not, even hours after birth (A, blue arrow). (DKOs are however, capable of latching onto mother). Importantly, all WT and sibling intestines appear healthy, pink and yellow from the milk (B, C), but 53% of DKOs show retention of the black meconium (red arrow) more than 6 hours after birth (D), consistent with a defect known as Meconium Ileus. (WT n=24; SKO n=28, and n=41/77 DKOs)

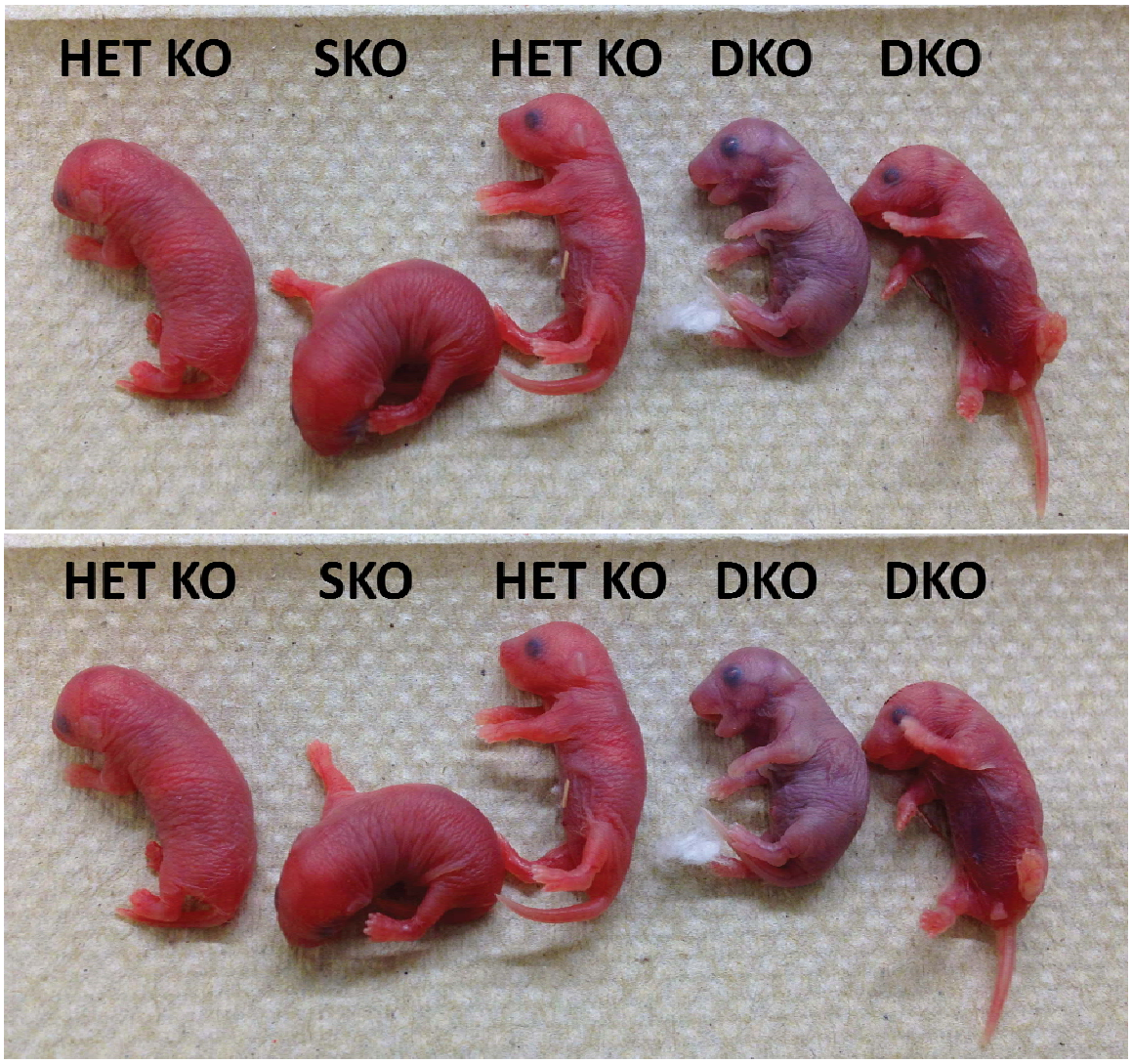

S Figure 8: Terminal DKO pups display cyanotic behavior. Images are stills from a movie taken within hours after birth. DKOs appear blue, and gasping while siblings are pink and move around freely.

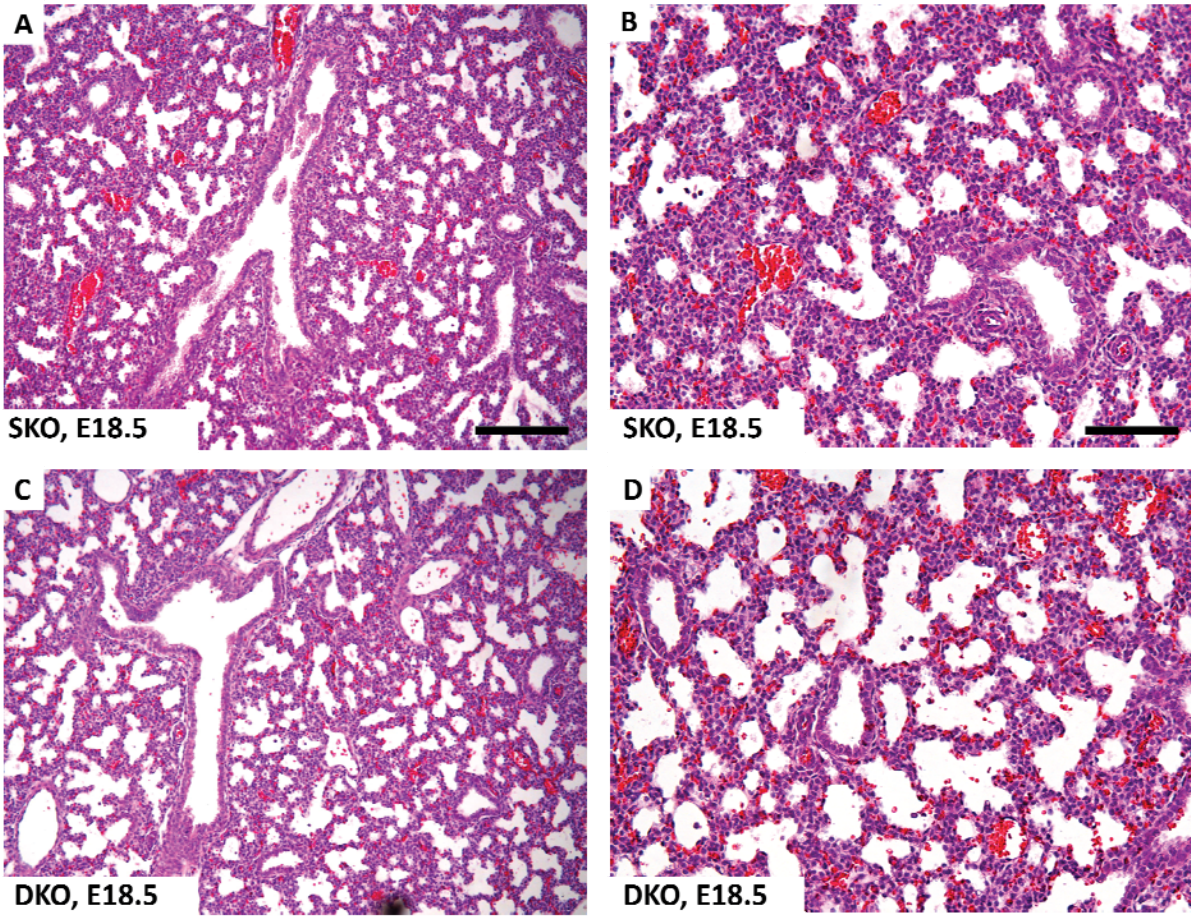

S Figure 9: Pulmonary histology is comparable between SKO and DKO at E18.5. Before birth, the airways are still open and continuous with the fluid-filled amniotic sac, allowing sparse amounts of cellular debris and immune cells to enter into the lungs. H&E staining reveals levels of debris and infiltrating immune cells are similar in the bronchi (A, C) and in the alveoli (B, D) of SKO and DKO siblings (n=3 each).

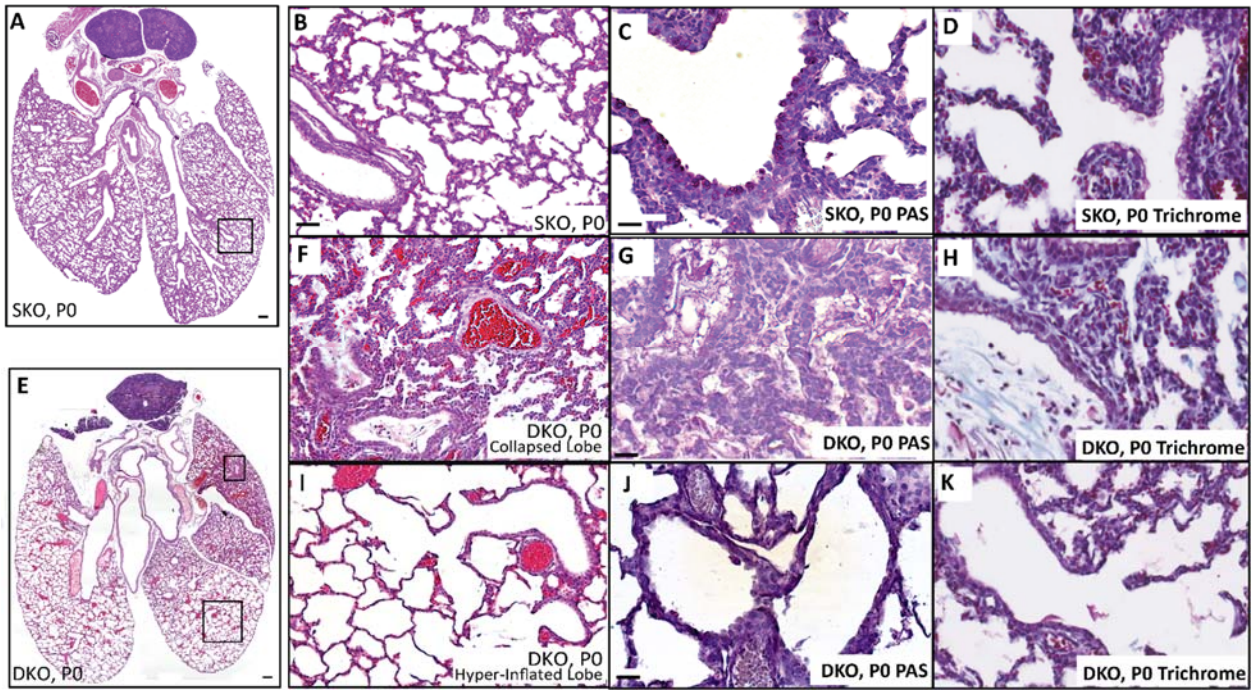

S Figure 10: DKOs exhibit hyperinflation & severe airway obstruction. H&E staining of SKO and DKO siblings illustrate lobe collapse, debris accumulation, and hyperinflation in non-collapsed lobes of DKO (A, B, E, F, I). PAS staining illustrates intracellular mucus in SKO (C) and little of no intracellular mucin in DKOs (G, J) particularly in the collapsed lobe where mucus is pooling in the lumen (G). Collagenous cellular debris shown by Trichrome staining (light blue, D, H, K). A & E whole lungs scale bar 200um; B, F, I scale bar 40um; C-D, G-H, J-K scale bar 20um).

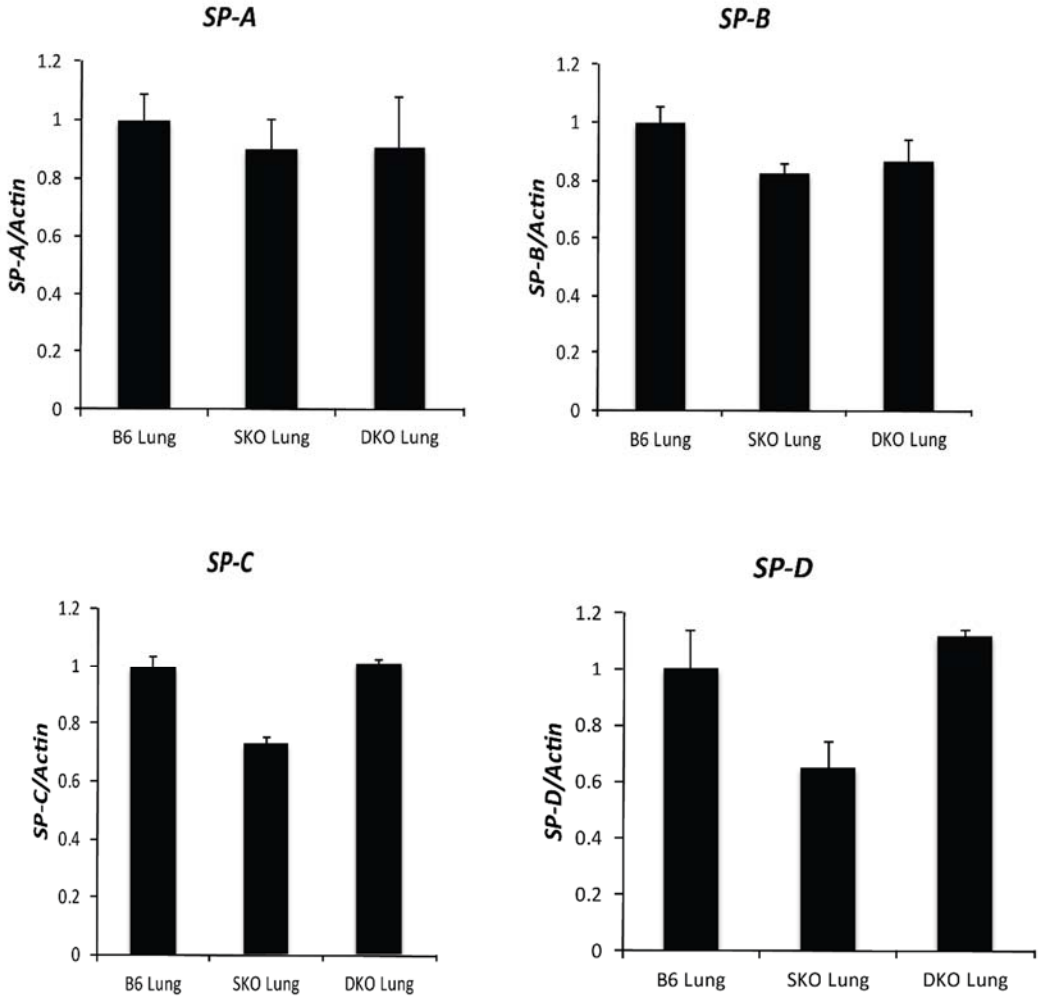

S Figure 11: Surfactant levels appear normal by qPCR. Surfactant is produced by alveolar type two cells (AEC-IIs) and is required for generation of the optimal surface tension necessary for efficient gas exchange. Surfactant proteins A and B appear at comparable levels between WT, SKO and DKO. Interestingly Surfactant proteins- C and D are slightly reduced in SKO siblings, whereas WT and DKO are equivalent. Similarly, no difference in SP-C by immunofluorescence was detected (data not shown).

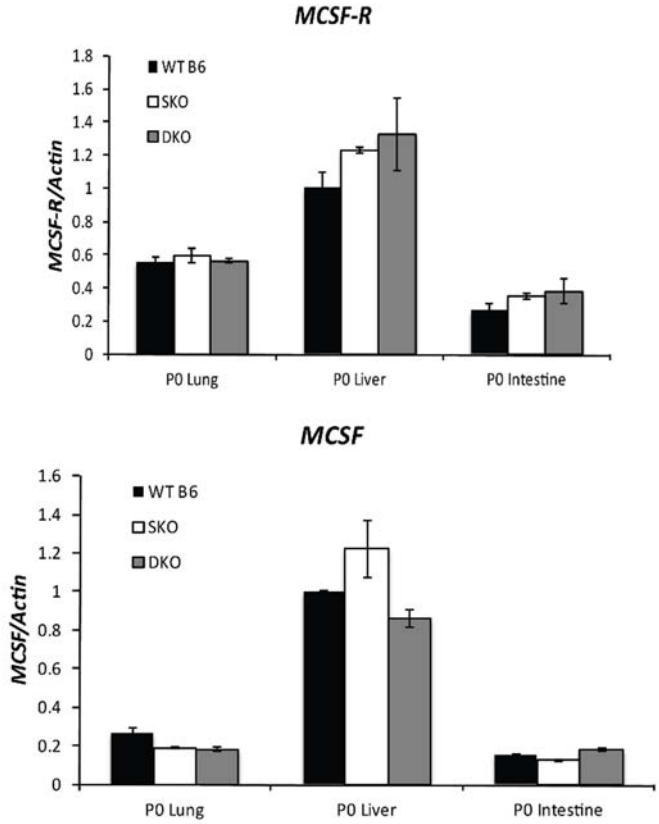

S Figure 12: Macrophage marker and cytokine qPCR. Comparable levels of macrophage-colony stimulating factor (MCSF) and macrophage-colony stimulating factor-receptor (MCSF-R) suggest that macrophage infiltration of the lung does not play a major role in lobe collapse and lethality in DKO pups.

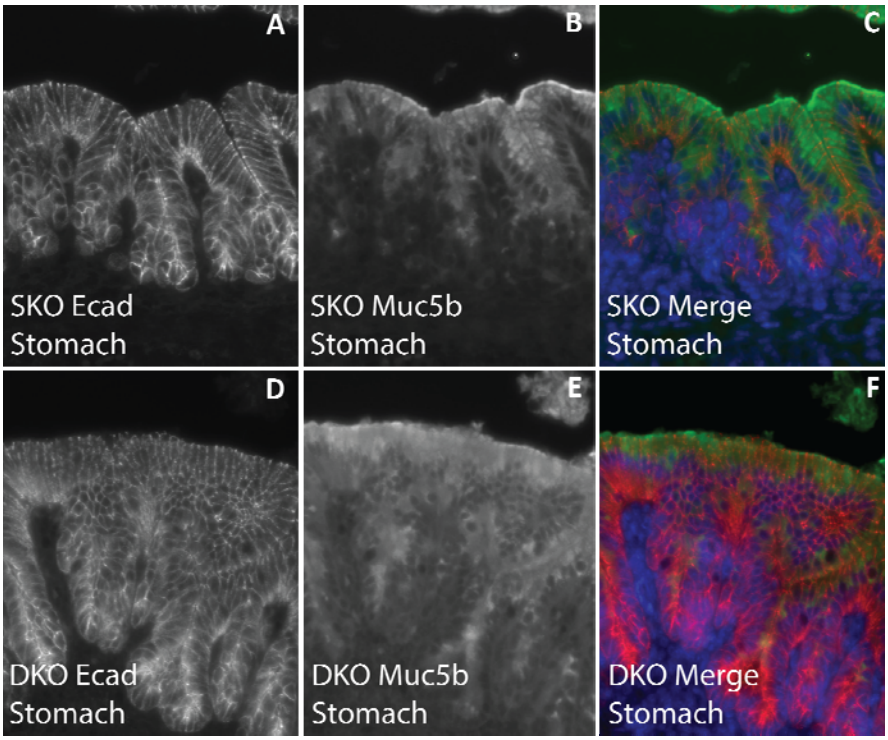

S Figure 13: Mucosal surfaces in the gut. Muc5b^{+} cells stain less intensively in DKOs compared with siblings, but this may perhaps be due to excessive secretion of the mucus. Since Muc5b levels remain constant it suggests that production is not increased, but secretion is perhaps misregulated.

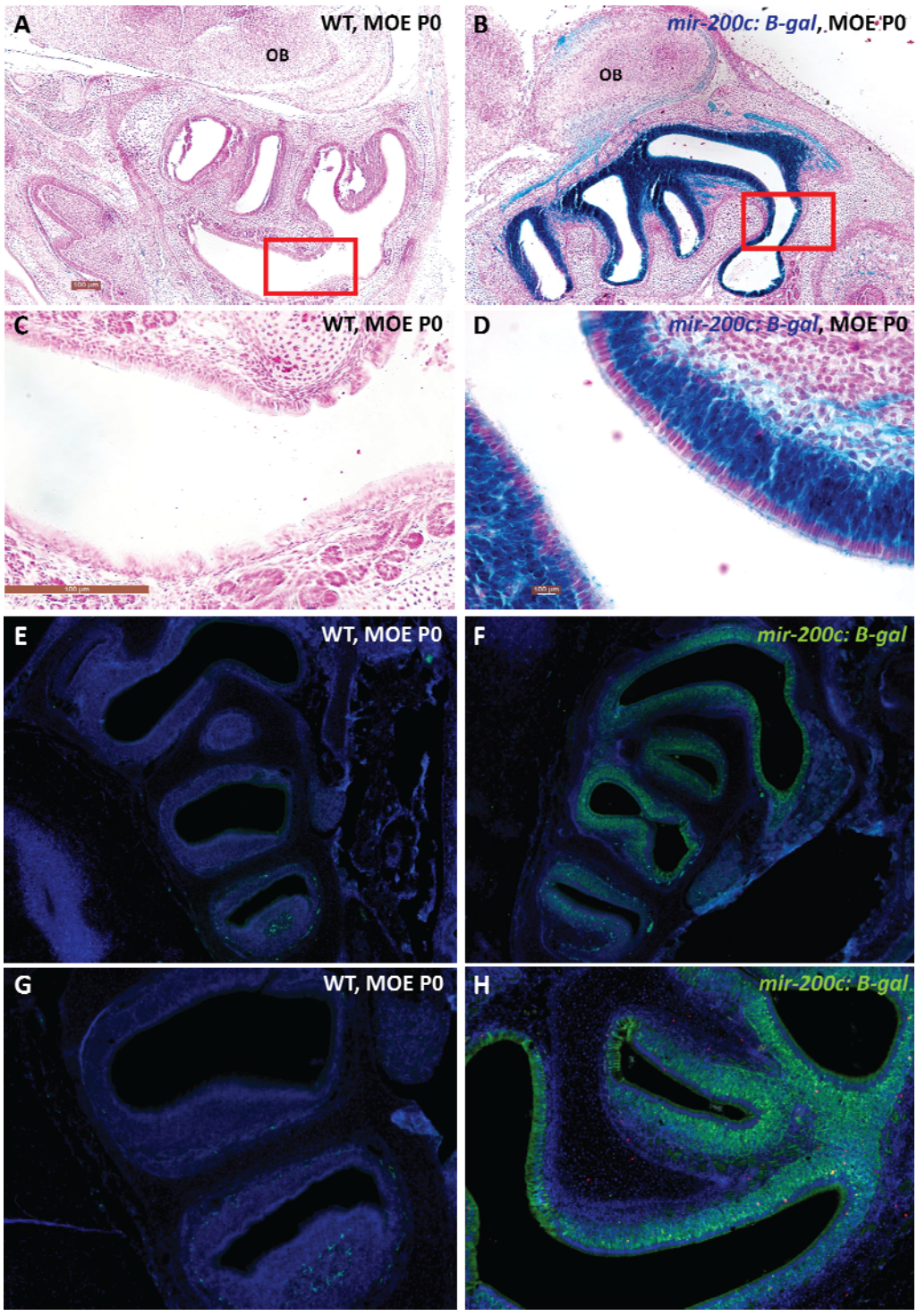

S Figure 14: Olfactory neuroepithelium defects in DKOs. The *mir-200c/141: LacZ* reporter demonstrates high expression in the main olfactory neuroepithelium (MOE) (A-D, blue stain X-gal). Similarly, an anti-beta-galactosidase specific antibody stains the olfactory progenitors and olfactory neurons (E-H, green B-Gal).

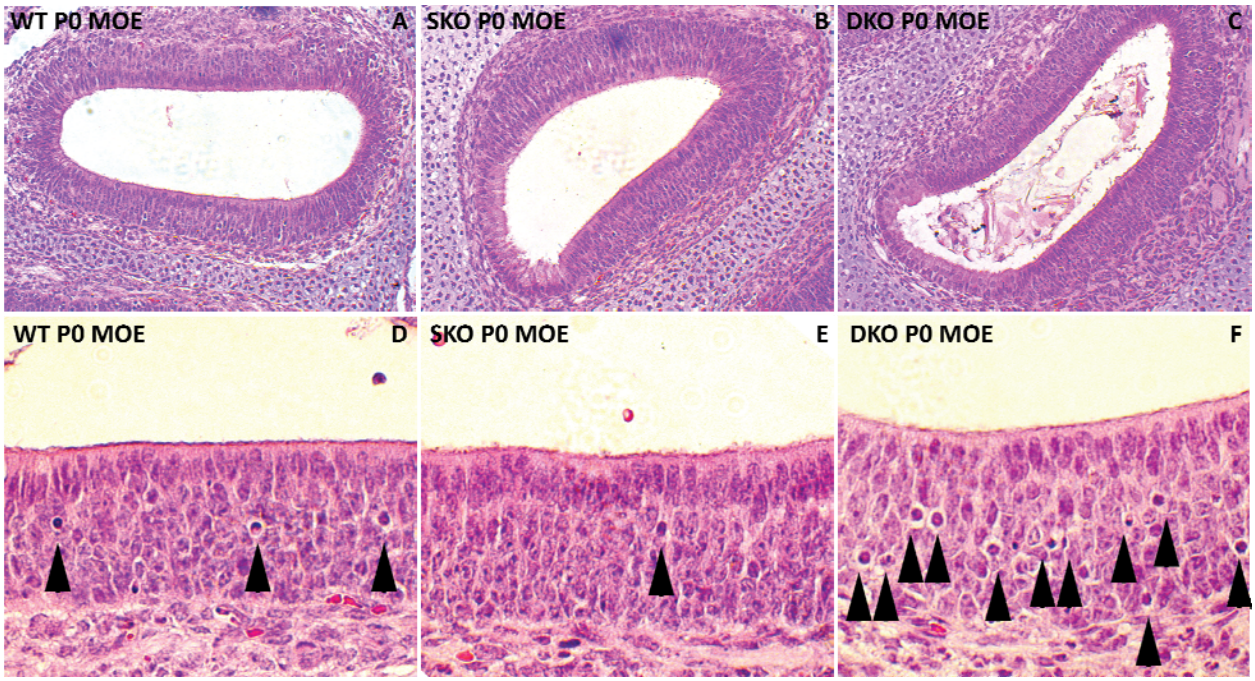

S Figure 15: Olfactory neuroepithelium defects in DKOs. mir-200 DKOs have accumulation of debris in the nasal airways compared with WT and SKO siblings (A-C) as well as enhanced apoptotic death compared with WT and littermates (D-F). H&E staining shows intact WT and SKO main olfactory epithelium, (MOE) (A-B, D-E) and multiple apoptotic foci in DKO MOE (C & F) denoted by black arrows.

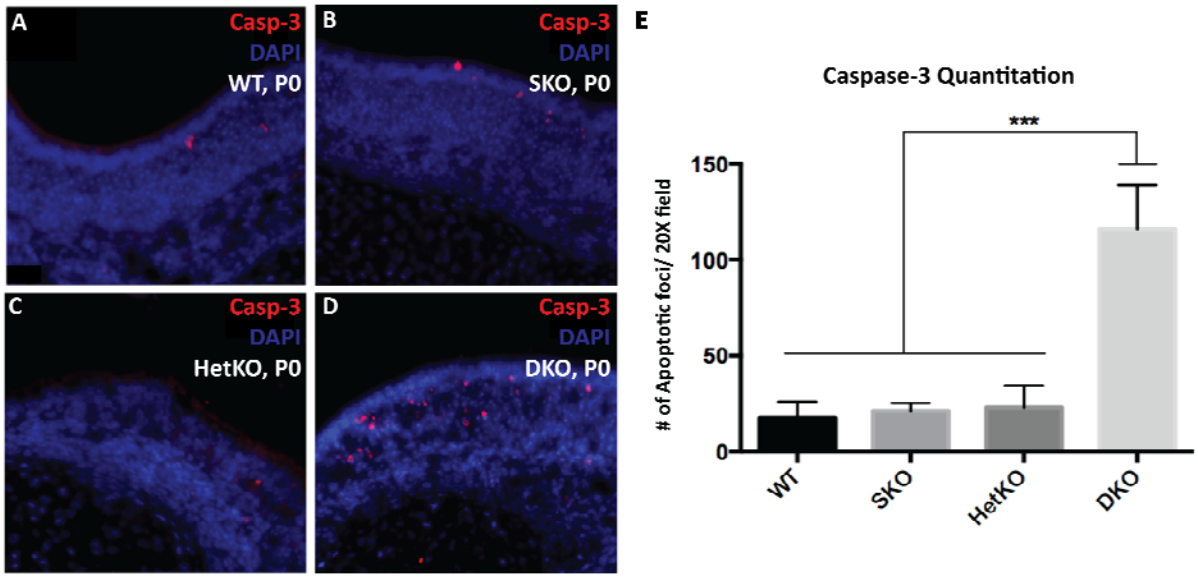

S Figure 16: Main Olfactory Epithelium apoptosis in DKOs. **C**leaved Caspase-3 IF illustrates the increased apoptotic cell number in the DKO compared with WT and siblings (A-D). Caspase-3 quantitation in the MOE of miR-200 DKOs compared with controls (E). Of note: a single copy of the *mir-200ab* locus (in Het KOs) is sufficient to prevent this phenotype. Quantitation performed on n=3 WT, n=4 SKO, n=3 HetKO and n=5 DKOs.

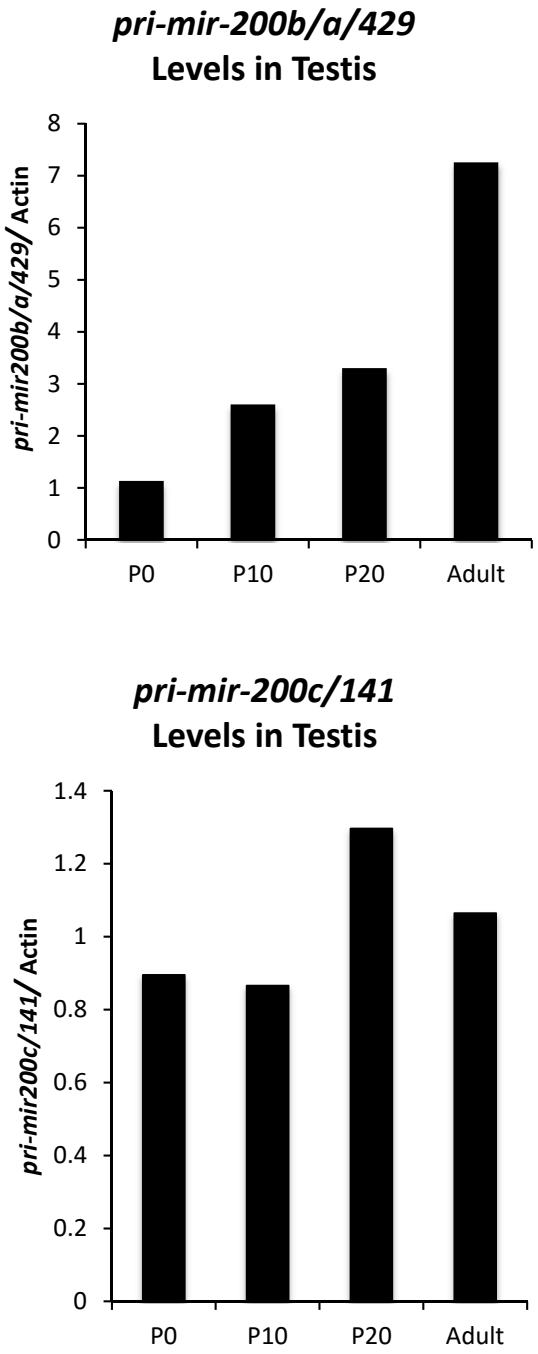

S Figure 17: The mir-200 family shows enrichment in male testis. Expression of the primary transcripts of mir-200 were measured in male WT testis over time for the 200ab and 200c loci. Increasing levels of mir-200 during spermatogenesis suggest there could be an important role for mir-200 that when deficient leads to the infertility we observe in natural matings.

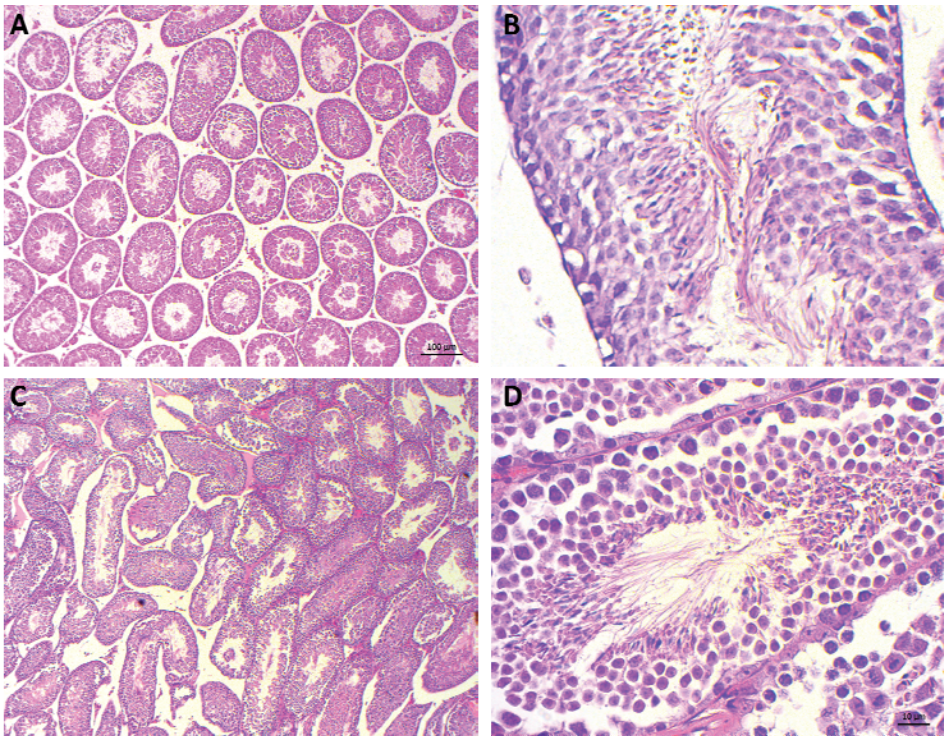

S Figure 18: Histology of mir-200ab KO male testis. WT and mir-200ab KO males exhibit comparable degrees of successful spermatogenesis, supporting the normal sperm counts observed during IVF preparation (data not shown). Defects in orientation of the axoneme are not apparent in the testis at this magnification.

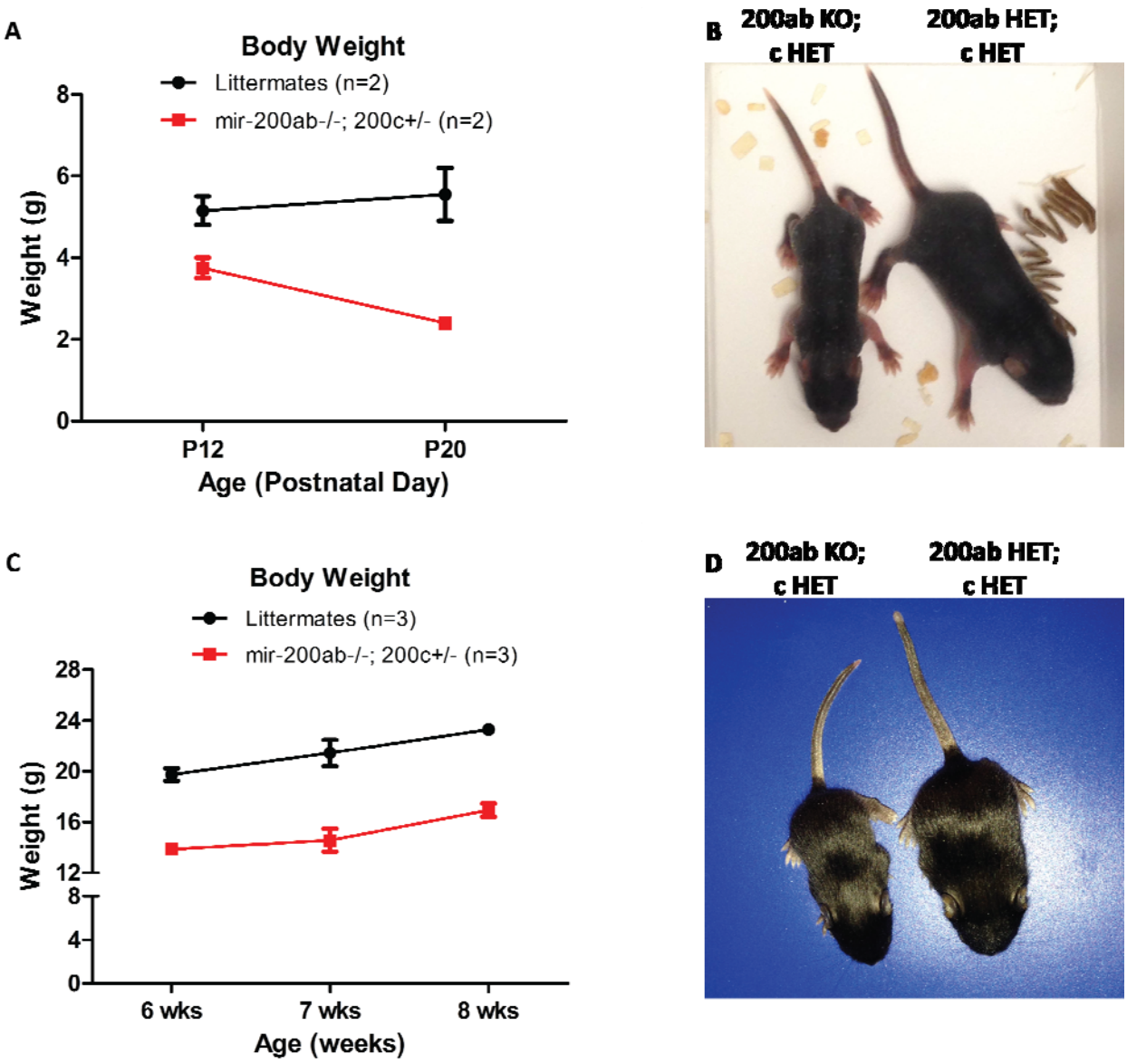

S Figure 19: mir-200ab KO; 200c HET mice exhibit smaller size. Preliminary observations revealed that mir-200ab KO; 200c HET male and female pups were 30% smaller than their siblings (n=5). Weight at early timepoints P12 to P20 showed early differences that increased over time (A) image taken at P12 (B). Animals that survived to adulthood exhibit sustained inability to gain weight like siblings (C), image taken at 4 weeks (D).

References

1. Choi PS, Zakhary L, Choi WY, et al. Members of the miRNA-200 Family Regulate Olfactory Neurogenesis. *Neuron*. 2008;57(1):41-55. doi:10.1016/j.neuron.2007.11.018.

2. Cao H, Wang J, Li X, et al. MicroRNAs play a critical role in tooth development. *J Dent Res*. 2010;89(8):779-784. doi:10.1177/0022034510369304.

3. Cao H, Jheon A, Li X, et al. The Pitx2:miR-200c/141:noggin pathway regulates Bmp signaling and ameloblast differentiation. *Development*. 2013;140(16):3348-3359. doi:10.1242/dev.089193.

4. Park SM, Gaur AB, Lengyel E, Peter ME. The miR-200 family determines the epithelial phenotype of cancer cells by targeting the E-cadherin repressors ZEB1 and ZEB2. *Genes Dev*. 2008;22(7):894-907. doi:10.1101/gad.1640608.

5. Prosser HM, Koike-Yusa H, Cooper JD, Law FC, Bradley A. A resource of vectors and ES cells for targeted deletion of microRNAs in mice. *Nat Biotechnol*. 2011;29(9):840-845. doi:10.1038/nbt.1929.

6. Grubb BR, Boucher RC. Pathophysiology of gene-targeted mouse models for cystic fibrosis. *Physiol Rev*. 1999;79(1):S193-S214.

7. Mullane K, Williams M. Animal models of asthma: Reprise or reboot? *Biochem Pharmacol*. 2014;87(1):131-139. doi:10.1016/j.bcp.2013.06.026.

8. Marcet B, Chevalier B, Luxardi G, et al. Control of vertebrate multiciliogenesis by miR-449 through direct repression of the Delta/Notch pathway. *Nat Cell Biol*. 2011;13(6):693-699. doi:ncb2241 [pii]\r10.1038/ncb2241.

9. Djebali S, Davis CA, Merkel A, et al. Landscape of transcription in human cells. *Nature*. 2012;489(7414):101-108. doi:10.1038/nature11233.

10. Gerstein MB, Kundaje A, Hariharan M, et al. Architecture of the human regulatory network derived from ENCODE data. *Nature*. 2012;489(7414):91-100. doi:10.1038/nature11245.

11. Gerstein MB, Rozowsky J, Yan K-K, et al. Comparative analysis of the transcriptome across distant species. *Nature*. 2014;512:445-448. doi:10.1038/nature13424.

12. Mathelier A, Carbone A. Large scale chromosomal mapping of human microRNA structural clusters. *Nucleic Acids Res*. 2013;41(8):4392-4408. doi:10.1093/nar/gkt112.

13. Lewis BP, Burge CB, Bartel DP. Conserved seed pairing, often flanked by adenosines, indicates that thousands of human genes are microRNA targets. *Cell*. 2005;120(1):15-20. doi:10.1016/j.cell.2004.12.035.

14. Ambros V, Bartel B, Bartel DP, et al. L E T T E R T O THE ED I TO R A uniform system for microRNA annotation. 2003:277-279. doi:10.1261/rna.2183803.One.

15. Griffiths-Jones S. The microRNA Registry. *Nucleic Acids Res*. 2004;32(Database issue):D109-D111. doi:10.1093/nar/gkh023.

16. Kamanu TKK, Radovanovic A, Archer J a C, Bajic VB. Exploration of miRNA families for hypotheses generation. *Sci Rep*. 2013;3:2940. doi:10.1038/srep02940.

17. Berezikov E. Evolution of microRNA diversity and regulation in animals. *Nat Rev Genet*. 2011;12(12):846-860. doi:10.1038/nrg3079.

18. Bagga S, Bracht J, Hunter S, et al. Regulation by let-7 and lin-4 miRNAs results in target mRNA degradation. *Cell*. 2005;122(4):553-563. doi:10.1016/j.cell.2005.07.031.

19. Filipowicz W, Bhattacharyya SN, Sonenberg N. Mechanisms of post-transcriptional regulation by microRNAs: are the answers in sight? *Nat Rev Genet*. 2008;9(2):102-114.

20. Lee RC, Feinbaum RL, Ambros V. The C. elegans heterochronic gene lin-4 encodes small RNAs with antisense complementarity to lin-14. *Cell*. 1993;75(5):843-854. http://www.ncbi.nlm.nih.gov/pubmed/8252621.

21. Wightman B, Ha I, Ruvkun G. Posttranscriptional regulation of the heterochronic gene lin-14 by lin-4 mediates temporal pattern formation in C. elegans. *Cell*. 1993;75(5):855-862. http://www.ncbi.nlm.nih.gov/pubmed/8252622.

22. Slack FJ, Basson M, Liu Z, Ambros V, Horvitz HR, Ruvkun G. The lin-41 RBCC gene acts in the C. elegans heterochronic pathway between the let-7 regulatory RNA and the LIN-29 transcription factor. *Mol Cell*. 2000;5(4):659-669. doi:10.1016/S1097-2765(00)80245-2.

23. Reinhart BJ, Slack FJ, Basson M, et al. The 21-nucleotide let-7 RNA regulates developmental timing in Caenorhabditis elegans. *Nature*. 2000;403(6772):901-906. doi:10.1038/35002607.

24. Pasquinelli a E, Reinhart BJ, Slack F, et al. Conservation of the sequence and temporal expression of let-7 heterochronic regulatory RNA. *Nature*. 2000;408(6808):86-89. doi:10.1038/35040556.

25. Lin SY, Johnson SM, Abraham M, et al. The C. elegans hunchback homolog, hbl-1, controls temporal patterning and is a probable MicroRNA target. *Dev Cell*. 2003;4(5):639-650. doi:10.1016/S1534-5807(03)00124-2.

26. Abrahante JE, Daul AL, Li M, et al. The Caenorhabditis elegans hunchback-like gene lin-57/hbl-1 controls developmental time and is regulated by microRNAs. *Dev Cell*. 2003;4(5):625-637. doi:10.1016/S1534-5807(03)00127-8.

27. Lee Y, Jeon K, Lee JT, Kim S, Kim VN. MicroRNA maturation: Stepwise processing and subcellular localization. *EMBO J*. 2002;21(17):4663-4670. doi:10.1093/emboj/cdf476.

28. Zeng Y, Cullen BR. Sequence requirements for micro RNA processing and function in human cells. *Rna*. 2003;9(1):112. doi:10.1261/rna.2780503.known.

29. Lee Y, Ahn C, Han J, et al. The nuclear RNase III Drosha initiates microRNA processing. *Nature*. 2003;425(6956):415-419. doi:10.1038/nature01957.

30. Lund E, Güttinger S, Calado A, Dahlberg JE KU. Nuclear Export of Microrna Precursors. *Science (80-)*. 2004;303(5654):95-98. doi:10.1126/science.1090599.

31. Hutvágner G, McLachlan J, Pasquinelli AE, Bálint E, Tuschl T, Zamore PD. A cellular function for the RNA-interference enzyme Dicer in the maturation of the let-7 small temporal RNA. *Science*. 2001;293(5531):834-838. doi:10.1126/science.1062961.

32. Bernstein E, Caudy a a, Hammond SM, Hannon GJ. Role for a bidentate ribonuclease in the initiation step of RNA interference. *Nature*. 2001;409(6818):363-366. doi:10.1038/35053110.

33. Ketting RF, Fischer SEJ, Bernstein E, Sijen T, Hannon GJ, Plasterk RH a. Dicer functions in RNA interference and in synthesis of small RNA involved in developmental timing in C. elegans. *Genes Dev*. 2001;(516):2654-2659. doi:10.1101/gad.927801.2654.

34. Elbashir SM, Elbashir SM, Lendeckel W, Lendeckel W, Tuschl T, Tuschl T. RNA interference is mediated 1- and 22-nucleotide RNAs. *Genes Dev*. 2001;15:188-200. doi:10.1101/gad.862301.vents.

35. Grishok A, Pasquinelli a E, Conte D, et al. Genes and mechanisms related to RNA interference regulate expression of the small temporal RNAs that control C. elegans developmental timing. *Cell*. 2001;106(1):23-34. http://www.ncbi.nlm.nih.gov/pubmed/11461699.

36. Hutvágner G, Zamore PD. A microRNA in a Multiple- Turnover RNAi Enzyme Complex. *Science (80-)*. 2002;297(September):2056-2060. doi:10.1126/science.1073827.

37. Llave C, Xie Z, Kasschau KD, Carrington JC. Cleavage of Scarecrow-like mRNA Targets Directed by a Class of Arabidopsis miRNA. 2002;297(September):2053-2056. doi:10.1126/science.1076311.

38. Doench JG, Petersen CP, Sharp PA. siRNAs can function as miRNAs. *Genes Dev*. 2003;17(4):438-442. doi:10.1101/gad.1064703.

39. Okamura K, Ishizuka A, Siomi H, Siomi MC. Distinct roles for Argonaute proteins in small RNA-directed RNA cleavage pathways. *Genes Dev*. 2004;18(14):1655-1666. doi:10.1101/gad.1210204.

40. Kozomara A, Griffiths-Jones S. MiRBase: Annotating high confidence microRNAs using deep sequencing data. *Nucleic Acids Res*. 2014;42(D1):68-73. doi:10.1093/nar/gkt1181.

41. Miska EA, Alvarez-Saavedra E, Abbott AL, et al. Most Caenorhabditis elegans microRNAs are individually not essential for development or viability. *PLoS Genet*. 2007;3(12):2395-2403. doi:10.1371/journal.pgen.0030215.

42. Park CY, Choi YS, McManus MT. Analysis of microRNA knockouts in mice. *Hum Mol Genet*. 2010;19(R2):1-7. doi:10.1093/hmg/ddq367.

43. Park CY, Jeker LT, Carver-moore K, et al. A resource for the conditional ablation of microRNAs in the mouse. *Cell Rep*. 2012;1(4):385-391. doi:10.1016/j.celrep.2012.02.008.A.

44. Marson A, Levine SS, Cole MF, et al. Connecting microRNA Genes to the Core Transcriptional Regulatory Circuitry of Embryonic Stem Cells. *Cell*. 2008;134(3):521-533. doi:10.1016/j.cell.2008.07.020.

45. Song R, Walentek P, Sponer N, et al. miR-34/449 miRNAs are required for motile ciliogenesis by repressing cp110. *Nature*. 2014;510(7503):115-120. doi:10.1038/nature13413.

46. Liu N, Bezprozvannaya S, Williams AH, et al. microRNA-133a regulates cardiomyocyte proliferation and suppresses smooth muscle gene expression in the heart. *Genes Dev*. 2008;22(23):3242-3254. doi:10.1101/gad.1738708.

47. Ventura A, Young AG, Winslow MM, et al. Targeted deletion reveals essential and overlapping functions of the miR-17 through 92 family of miRNA clusters. *Cell*. 2008;132(5):875-886. doi:10.1016/j.cell.2008.02.019.

48. de Pontual L, Yao E, Callier P, et al. Germline deletion of the miR-17∼92 cluster causes skeletal and growth defects in humans. *Nat Genet*. 2011;43(10):1026-1030. doi:10.1038/ng.915.

49. He L, Thomson JM, Hemann MT, et al. A microRNA polycistron as a potential human oncogene. *Nature*. 2005;435(7043):828-833. doi:10.1038/nature03552.

50. Mu P, Han Y-C, Betel D, et al. Genetic dissection of the miR-17 92 cluster of microRNAs in Myc-induced B-cell lymphomas. *Genes Dev*. 2009;23(646):2806-2811. doi:10.1101/gad.1872909.

51. Olive V, Bennett MJ, Walker JC, et al. miR-19 is a key oncogenic component of mir-17-92. *Genes Dev*. 2009;23(24):2839-2849. doi:10.1101/gad.1861409.

52. Olive V, Sabio E, Bennett MJ, et al. A component of the mir-17-92 polycistronic oncomir promotes oncogene-dependent apoptosis. *Elife*. 2013;2013(2):1-24. doi:10.7554/eLife.00822.001.

53. Burk U, Schubert J, Wellner U, et al. A reciprocal repression between ZEB1 and members of the miR-200 family promotes EMT and invasion in cancer cells. *EMBO Rep*. 2008;9(6):582-589. doi:10.1038/embor.2008.74.

54. Spaderna S, Schmalhofer O, Wahlbuhl M, et al. The transcriptional repressor ZEB1 promotes metastasis and loss of cell polarity in cancer. *Cancer Res*. 2008;68(2):537-544. doi:10.1158/0008-5472.CAN-07-5682.

55. Christoffersen NR, Silahtaroglu A, Orom UA, Kauppinen S, Lund AH. miR-200b mediates post-transcriptional repression of ZFHX1B. *RNA*. 2007;13(8):1172-1178. doi:10.1261/rna.586807.

56. Hurteau GJ, Carlson JA, Spivack SD, Brock GJ. Overexpression of the MicroRNA hsa-miR-200c leads to reduced expression of transcription factor 8 and increased expression of E-cadherin. *Cancer Res*. 2007;67(17):7972-7976. doi:10.1158/0008-5472.CAN-07-1058.

57. Gaur A, Jewell DA, Liang Y, et al. Characterization of microRNA expression levels and their biological correlates in human cancer cell lines. *Cancer Res*. 2007;67(6):2456-2468. doi:10.1158/0008-5472.CAN-06-2698.

58. Gibbons DL, Lin W, Creighton CJ, et al. Contextual extracellular cues promote tumor cell EMT and metastasis by regulating miR-200 family expression. *Genes Dev*. 2009;23(18):2140-2151. doi:10.1101/gad.1820209.

59. Li J, Li X, Ren S, et al. MiR-200c overexpression is associated with better efficacy of EGFR-TKIs in non-small cell lung cancer patients with EGFR wild-type. *Oncotarget*. 2014;5(17):7902-7916. doi:10.18632/oncotarget.2302.

60. Pecot C V, Rupaimoole R, Yang D, et al. Tumour angiogenesis regulation by the miR-200 family. *Nat Commun*. 2013;4:2427. doi:10.1038/ncomms3427.

61. Tejero R, Navarro A, Campayo M, et al. MiR-141 and miR-200c as markers of overall survival in early stage non-small cell lung cancer adenocarcinoma. *PLoS One*. 2014;9(7):1-9. doi:10.1371/journal.pone.0101899.

62. Zhang H, Sun F, Li S. Serum miR-200c expression level as a prognostic biomarker for gastric cancer. 2015;14(4):15913-15920.

63. Chan YC, Khanna S, Roy S, Sen CK. MiR-200b targets Ets-1 and is down-regulated by hypoxia to induce angiogenic response of endothelial cells. *J Biol Chem*. 2011;286(3):2047-2056. doi:10.1074/jbc.M110.158790.

64. Korpal M, Ell BJ, Buffa FM, et al. Direct targeting of Sec23a by miR-200s influences cancer cell secretome and promotes metastatic colonization. *Nat Med*. 2011;17(9):1101-1108. doi:10.1038/nm.2401.

65. Tang X, Hou Y, Yang G, et al. Stromal miR-200s contribute to breast cancer cell invasion through CAF activation and ECM remodeling. *Cell Death Differ*. 2015:1-14. doi:10.1038/cdd.2015.78.

66. Li Y, Zhang Z. Potential microRNA-mediated oncogenic intercellular communication revealed by pan-cancer analysis. *Sci Rep*. 2014;4:7097. doi:10.1038/srep07097.

67. Keely PJ. Mechanisms by which the extracellular matrix and integrin signaling act to regulate the switch between tumor suppression and tumor promotion. *J Mammary Gland Biol Neoplasia*. 2011;16(3):205-219. doi:10.1007/s10911-011-9226-0.

68. Chen J, Jiang CC, Jin L, Zhang XD. Regulation of PD-L1: A novel role of pro-survival signalling in cancer. *Ann Oncol*. 2015;(December 2015):1-18. doi:10.1093/annonc/mdv615.

69. Chen LL, Gibbons DL, Goswami S, et al. Metastasis is regulated via microRNA-200/ZEB1 axis control of tumour cell PD-L1 expression and intratumoral immunosuppression. *Nat Commun*. 2014;5:5241. doi:10.1038/ncomms6241.

70. Wang G, Guo X, Hong W, et al. Critical regulation of miR-200 / ZEB2 pathway in Oct4 / Sox2-induced mesenchymal-to-epithelial transition and induced pluripotent stem cell generation. *Proc Natl Acad Sci U S A*. 2013;110(8):2858-2863. doi:10.1073/pnas.1212769110/-/DCSupplemental.www.pnas.org/cgi/doi/10.1073/pnas.1212769110.

71. Samavarchi-Tehrani P, Golipour A, David L, et al. Functional genomics reveals a BMP-Driven mesenchymal-to-Epithelial transition in the initiation of somatic cell reprogramming. *Cell Stem Cell*. 2010;7(1):64-77. doi:10.1016/j.stem.2010.04.015.

72. Kang Y, Siegel PM, Shu W, et al. A multigenic program mediating breast cancer metastasis to bone. *Cancer Cell*. 2003;3(6):537-549. http://www.ncbi.nlm.nih.gov/pubmed/12842083.

73. Mamoori A, Gopalan V, Anthony Smith R, King-Yin Lam A. Modulatory roles of microRNAs in the regulation of different signalling pathways in large bowel cancer stem cells. *Biol Cell*. 2015:51-64. doi:10.1111/boc.201500062.

74. Pichler M, Ress a L, Winter E, et al. MiR-200a regulates epithelial to mesenchymal transition-related gene expression and determines prognosis in colorectal cancer patients. *Br J Cancer*. 2014;110(6):1614-1621. doi:10.1038/bjc.2014.51.

75. Finlay-Schultz J, Cittelly DM, Hendricks P, et al. Progesterone downregulation of miR-141 contributes to expansion of stem-like breast cancer cells through maintenance of progesterone receptor and Stat5a. *Oncogene*. 2014;34(September):25241899. doi:10.1038/onc.2014.298.

76. Shin JO, Lee JM, Cho KW, et al. MiR-200b is involved in Tgf-?? signaling to regulate mammalian palate development. *Histochem Cell Biol*. 2012;137(1):67-78. doi:10.1007/s00418-011-0876-1.

77. Rock JR, Randell SH, Hogan BLM. Airway basal stem cells: a perspective on their roles in epithelial homeostasis and remodeling. *Dis Model Mech*. 2010;3(9-10):545-556. doi:10.1242/dmm.006031.

78. Morrisey EE, Hogan BLM. Preparing for the First Breath: Genetic and Cellular Mechanisms in Lung Development. *Dev Cell*. 2010;18(1):8-23. doi:10.1016/j.devcel.2009.12.010.

79. Hogan BLM, Barkauskas CE, Chapman HA, et al. Repair and regeneration of the respiratory system: Complexity, plasticity, and mechanisms of lung stem cell function. *Cell Stem Cell*. 2014;15(2):123-138. doi:10.1016/j.stem.2014.07.012.

80. Metzger RJ, Klein OD, Martin GR, Krasnow MA. The branching programme of mouse lung development. *Nature*. 2008;453(7196):745-750. doi:10.1038/nature07005.

81. Jain L, Eaton DC. Physiology of fetal lung fluid clearance and the effect of labor. *Semin Perinatol*. 2006;30(1):34-43. doi:10.1053/j.semperi.2006.01.006.

82. Francis RJB, Chatterjee B, Loges NT, Zentgraf H, Omran H, Lo CW. Initiation and maturation of cilia-generated flow in newborn and postnatal mouse airway. *Am J Physiol Lung Cell Mol Physiol*. 2009;296(6):L1067-L1075. doi:10.1152/ajplung.00001.2009.

83. Association AL. *Trends in Asthma Morbidity and Mortality*. Vol 12.; 2010. doi:10.2188/jea.12.217.

84. Kung TT, Jones H, Adams III GK, et al. Characterization of a Murine Model of Allergic Pulmonary Inflammation. In: *International Archives of Allergy and Immunology*. Vol 105. ; 1994:83-90. doi:10.1159/000236807.

85. Woodruff PG, Modrek B, Choy DF, et al. T-helper type 2-driven inflammation defines major subphenotypes of asthma. *Am J Respir Crit Care Med*. 2009;180(5):388-395. doi:10.1164/rccm.200903-0392OC.

86. Escobar MA, Grosfeld JL, Burdick JJ, et al. Surgical considerations in cystic fibrosis: A 32-year evaluation of outcomes. *Surgery*. 2005;138(4):560-572. doi:10.1016/j.surg.2005.06.049.

87. Farrell PM, Rosenstein BJ, White TB, et al. Guidelines for diagnosis of cystic fibrosis in newborns through older adults: Cystic Fibrosis Foundation consensus report. *J Pediatr*. 2008;153(2):S4-S14. doi:S0022-3476(08)00398-3 [pii]\r10.1016/j.jpeds.2008.05.005.

88. Cystic Fibrosis Foundation. Cystic Fibrosis Foundation. www.cff.org. Published 2015.

89. Vertex Pharmaceuticals Inc. CF Source. https://www.cfsource.com/symptoms/. Published 2015.

90. Knowles M, Gatzy J, Boucher R. Increased Bioelectric Potential Across Respiratory Epithelia in Cystic Fibrosis. *N Engl J Med*. 1981;305(25):1489-1495. doi:10.1056/NEJM199401273300403.

91. Knowles MR, Stutts MJ, Spock A, Fischer N, Gatzy JT, Boucher RC. Abnormal Ion Permeation through Cystic Fibrosis. *Sciencer*. 1983;221(4615):1067-1070. http://www.jstor.org/stable/1691539.

92. Best JA, Quinton PM. Salivary secretion assay for drug efficacy for cystic fibrosis in mice. *Exp Physiol*. 2005;90(2):189-193. doi:10.1113/expphysiol.2004.028720.

93. O'Neal WK, Hasty P, McCray PB, et al. A severe phenotype in mice with a duplication of exon 3 in the cystic fibrosis locus. *Hum Mol Genet*. 1993;2(10):1561-1569. http://www.ncbi.nlm.nih.gov/pubmed/7505691.

94. Hasty P, O'Neal WK, Liu KQ, et al. Severe phenotype in mice with termination mutation in exon 2 of cystic fibrosis gene. *Somat Cell Mol Genet*. 1995;21(3):177-187. doi:10.1007/BF02254769.

95. Delaney SJ, Alton EW, Smith SN, et al. Cystic fibrosis mice carrying the missense mutation G551D replicate human genotype-phenotype correlations. *EMBO J*. 1996;15(5):955-963. http://www.pubmedcentral.nih.gov/articlerender.fcgi?artid=449990&tool=pmcentrez&rendertype=abstract.

96. Mall M, Grubb BR, Harkema JR, O'Neal WK, Boucher RC. Increased airway epithelial Na+ absorption produces cystic fibrosis-like lung disease in mice. *Nat Med*. 2004;10(5):487-493. doi:10.1038/nm1028.

97. Livraghi A, Grubb BR, Hudson EJ, et al. Airway and lung pathology due to mucosal surface dehydration in {beta}-epithelial Na+ channel-overexpressing mice: role of TNF-{alpha} and IL-4R{alpha} signaling, influence of neonatal development, and limited efficacy of glucocorticoid treatment. *J Immunol*. 2009;182(7):4357-4367. doi:10.4049/jimmunol.0802557.

98. Nakanishi a, Morita S, Iwashita H, et al. Role of gob-5 in mucus overproduction and airway hyperresponsiveness in asthma. *Proc Natl Acad Sci U S A*. 2001;98(9):5175-5180. doi:10.1073/pnas.081510898.

99. Roy MG, Livraghi-Butrico A, Fletcher A a, et al. Muc5b is required for airway defence. *Nature*. 2014;505(7483):412-416. doi:10.1038/nature12807.

100. Ordoñez CL, Khashayar R, Wong HH, et al. Mild and moderate asthma is associated with airway goblet cell hyperplasia and abnormalities in mucin gene expression. *Am J Respir Crit Care Med*. 2001;163(2):517-523. doi:10.1164/ajrccm.163.2.2004039.

101. Innes AL, Woodruff PG, Ferrando RE, et al. Epithelial mucin stores are increased in the large airways of smokers with airflow obstruction. *Chest*. 2006;130(4):1102-1108. doi:10.1378/chest.130.4.1102.

102. Thornton DJ, Rousseau K, McGuckin M a. Structure and function of the polymeric mucins in airways mucus. *Annu Rev Physiol*. 2008;70:459-486. doi:10.1146/annurev.physiol.70.113006.100702.

103. J.V. F, B.F. D. Medical progress: Airway mucus function and dysfunction. *N Engl J Med*. 2010;363(23):2233-2247. http://www.embase.com/search/results?subaction=viewrecord&from=export&id=L360087147.

104. Lazarowski ER, Boucher RC. Purinergic receptors in airway epithelia. *Curr Opin Pharmacol*. 2009;9(3):262-267. doi:10.1016/j.coph.2009.02.004.

105. Adler KB, Tuvim MJ, Dickey BF. Regulated mucin secretion from airway epithelial cells. *Front Endocrinol (Lausanne)*. 2013;4(SEP):1-9. doi:10.3389/fendo.2013.00129.

106. Davis CW, Lazarowski E. Coupling of airway ciliary activity and mucin secretion to mechanical stresses by purinergic signaling. *Respir Physiol Neurobiol*. 2008;163(1-3):208-213. doi:10.1016/j.resp.2008.05.015.

107. Tarran R, Button B, Boucher RC. Regulation of Normal and Cystic Fibrosis Airway Surface Liquid Volume By Phasic Shear Stress. *Annu Rev Physiol*. 2006;68(1):543-561. doi:10.1146/annurev.physiol.68.072304.112754.

108. Krapf D, Ruan YC, Wertheimer E V., et al. cSrc is necessary for epididymal development and is incorporated into sperm during epididymal transit. *Dev Biol*. 2012;369(1):43-53. doi:10.1016/j.ydbio.2012.06.017.

109. Walentek P, Bogusch S, Thumberger T, et al. A novel serotonin-secreting cell type regulates ciliary motility in the mucociliary epidermis of Xenopus tadpoles. *Development*. 2014;141(7):1526-1533. doi:10.1242/dev.102343.

110. Sive HL, Grainger RM, Harland RM. Early Development of Xenopus laevis. *Cold Spring Harb Lab Press*. 2000.

111. Olive V, Minella AC, He L. Outside the coding genome, mammalian microRNAs confer structural and functional complexity. *Sci Signal*. 2015;8(368):1-15. doi:10.1126/scisignal.2005813.

112. Hasuwa, Hidetoshi; Ueda, Jun; Ikawa, Masahito; Okabe M. Hasuwa et al., 2013 Science -mir-200b□429 essential for female fertility.pdf. *Science (80-)*. 2013;341.

113. Kuma A, Hatano M, Matsui M, et al. The role of autophagy during the early neonatal starvation period. *Nature*. 2004;432(7020):1032-1036. doi:nature03029 [pii]\r10.1038/nature03029.

114. Cohn L. Mucus in chronic airway diseases: Sorting out the sticky details. *J Clin Invest*. 2006;116(2):306-308. doi:10.1172/JCI27690.

115. Brabletz S, Brabletz T. The ZEB/miR-200 feedback loop--a motor of cellular plasticity in development and cancer? *EMBO Rep*. 2010;11(9):670-677. doi:10.1038/embor.2010.117.

116. Fliegauf M, Benzing T, Omran H. When cilia go bad: cilia defects and ciliopathies. *Nat Rev Mol Cell Biol*. 2007;8(11):880-893. doi:10.1038/nrm2278.

117. Satir P, Christensen ST. Overview of structure and function of mammalian cilia. *Annu Rev Physiol*. 2007;69:377-400. doi:10.1146/annurev.physiol.69.040705.141236.

118. Saare M, Rekker K, Laisk-Podar T, et al. High-throughput sequencing approach uncovers the miRNome of peritoneal endometriotic lesions and adjacent healthy tissues. *PLoS One*. 2014;9(11). doi:10.1371/journal.pone.0112630.

119. Teves ME, Zhang Z, Costanzo RM, et al. Sperm-associated antigen-17 gene is essential for motile cilia function and neonatal survival. *Am J Respir Cell Mol Biol*. 2013;48(6):765-772. doi:10.1165/rcmb.2012-0362OC.

120. Evans CM, Raclawska DS, Ttofali F, et al. The polymeric mucin Muc5ac is required for allergic airway hyperreactivity. *Nat Commun*. 2015;6(May 2014):6281. doi:10.1038/ncomms7281.

121. Vladar EK, Brody SL. *Analysis of Ciliogenesis in Primary Culture Mouse Tracheal Epithelial Cells*. Vol 525. 1st ed. Elsevier Inc.; 2013. doi:10.1016/B978-0-12-397944-5.00014-6.